The Structure and Dynamics of Compounds Related to Fast Ionic Conductors

A thesis

Submitted for the degree of

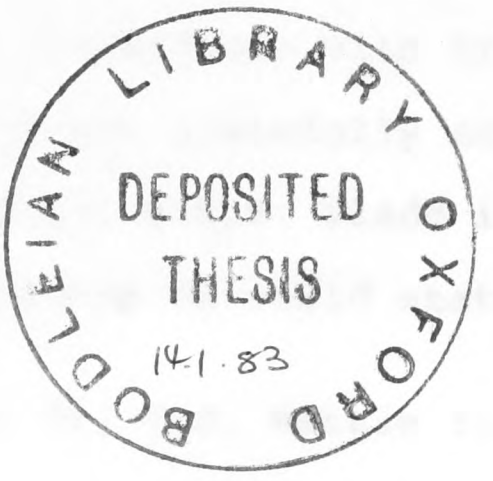
Doctor of Philosophy

to the Board of the

Faculty of Physical Sciences

in the

University of Oxford



A.N. FITCH

St. Catherine's College

Hilary 1982

ACKNOWLEDGEMENTS

It is a pleasure to thank my supervisor Dr. B.E.F. Fender for his encouragement, guidance and insight during the course of this work, both at Oxford and the ILL.

My thanks also go to Dr. P.J. Bendall, with whom I enjoyed many interesting discussions, for instructing me in the art of profile refinement, and for the use of his multipattern refinement program.

I am indebted to Dr. A.F. Wright for his valuable help with the work on the proton conducting systems, and also Dr. A.T. Howe who provided the samples and some interesting ideas. I thank Dr. A.W. Hewat who acted as local contact on D1A for the studies on uranium chloride systems. Some useful discussions with Dr. C. Riekel on the nature of intercalation compounds are gratefully acknowledged, as is the valuable assistance of Dr. R.C.T. Slade in connection with both the practice and interpretation of solid state pulsed NMR.

I should like to thank Dr. P.D. Battle for some helpful suggestions, particularly concerning the redimensioning of the Rietveld program, and I acknowledge the financial support of the ILL for the post of CTT for one year, during which this thesis was written.

Finally, I should like to thank everyone else, too numerous to mention individually, who by means of their companionship, practical help or experience, or simply by being there, contributed to this work and the production of this thesis.

CONTENTS

Page

Chapter 1. Aims of Research 1

Chapter 2. Theory of Neutron Scattering and Pulsed Solid State NMR 5

2.1. Introduction to Neutron Scattering 5

2.2. Scattering of Neutrons by a Single Fixed Nucleus 6

2.3. Scattering from Many Nuclei - Coherent and Incoherent Scattering 7

2.4. Nuclear Bragg Scattering 9

2.5. Powder Neutron Diffraction 11

2.6. Profile Analysis 14

2.7. Developements since Rietveld 17

2.8. Refinement of Diffraction Profiles Containing More than One Pattern 21

2.9. Fourier Techniques 24

2.10. Theory of NMR and Relaxtion Times 25

2.11. Motion in Solids and Relaxtion 28

Chapter 3. Instrumentation 31

3.1. Powder Neutron Diffractometers 31

3.2. D1A 33

3.3. NMR Spectrometer 36

Chapter 4. Structural Studies on $DUO_2AsO_4.4D_2O$ and $LiUO_2AsO_4.4D_2O$ 40

4.1. Introduction 40

$HUO_2AsO_4.4H_2O$ 40

$LiUO_2AsO_4.4H_2O$ 45

4.2. Sample Preparation and Experimental 46

4.3. Structural Refinements and Discussion 47

$DUO_2AsO_4.4D_2O$ at 305K 47

$DUO_2AsO_4.4D_2O$ at low temperature 55

$LiUO_2AsO_4.4D_2O$ at 294K 75

Page

Chapter 5. Structural Studies on A_2UCl_6 Compounds 83

5.1. Introduction 83

5.2. Experimental 96

5.3. Data Analysis and Discussion 99

Na_2UCl_6 99

Li_2UCl_6 107

K_2UCl_6 120

5.4. Conclusions 126

Chapter 6. An NMR Study of Titanium Rich $TiS_2(NH_3)$ 130

6.1. Introduction 130

6.2. Sample Preparation and Characterisation 141

6.3. NMR Studies 146

6.4. Results and Discussion 147

Chapter 7. Conclusions and Suggestions for Further Research 153

Bibliography 158

Abstract

CHAPTER 1

AIMS OF RESEARCH

In this thesis we investigate the structure or dynamics of a number of compounds which are chemically and structurally related to, or are themselves, good ionic conductors.

For the structural studies, powder neutron diffraction is employed and the complex overlapping powder patterns are analysed by the method of profile analysis. Neutron diffraction is well suited for studies on ionic conductors which often contain light mobile ions in an array or network of heavier ions which dominate the X-ray diffraction pattern. Powders allow the quick and efficient investigation of structures where there is already considerable structural knowledge from previous X-ray studies. Neutron diffrac tion also allows easy access to a wide range of temperatures which may have a marked effect on the observed conductivity as the result of structural phase changes. In this respect, profile analysis allows the investigation of structures in which we have only very little prior knowledge, for, in certain circumstances and for certain compounds, single crystals may not be readily available. The structure refinements we attempt here make use of new programs for profile analysis which enable more than one phase to be simultaneously refined. We also make use of an enlarged version of this program which can accommodate up to 300 structural parameters and 3000 overlapping reflections.

The first class of structures we have investigated is based on $HUO_2AsO_4.4H_2O$, (HUAs), which contains essentially two dimensional

layers of water constrained between layers of uranyl and arsenate ions. At room temperature HUAs (isostructural with HUP, $HUO_2PO_4.4H_2O$) shows very high proton conductivity parallel with the water layers, and has been the subject of considerable recent interest. Single crystal X-ray diffraction on HUP has located the positions of the heavy atoms and indicates that there is hydrogen disorder over a number of available hydrogen bond sites within the water layers. Neutron diffraction should allow determination of this hydrogen distribution and may suggest how this is related to the observed conductivity. At 301K HUAs transforms to a low temperature non-conducting antiferroelectric phase which is presumably associated with ordering of the hydrogen ions. The structure, which is of low symmetry, poses a testing problem for profile refinement techniques, which we examine in detail in order to judge how far these techniques may be applied for this type of problem. Certain of the hydrogen ions in HUAs may be replaced by a variety of cations to form related compounds with modified conductivities which may reflect changes in the water layers. We would like to understand the relationship between such compounds, their structures, and their conductivities, and as a preliminary investigation of such compounds we examine $LiUO_2AsO_4.4D_2O$. These detailed structural studies can be expected to provide models for the interpretation of the dynamics of water and proton mobilities which can be studied by NMR and incoherent quasielastic neutron scattering.

The second class of structures investigated involves alkali metal uranium chlorides. Large halide ions may often form the basis of a number of good ionic conductors,eg AgI or $SrCl_2$ which

conduct at high temperature by dynamic catonic disorder, and lattice defect migration mechanisms respectively. Na_2UBr_6 has been shown to be a good ionic conductor at elevated temperature, and contains rather discrete $[UBr_6]$ octahedra which perform marked molecular librations, which may lead to the dynamic creation of conduction pathways for a mobile sodium ion. In this investigation we have explored how the molecular nature of the octahedra responds to the variation of the light cation in such compounds by structural studies at room temperature on the series A_2UCl_6, A = Li, Na or K. Again, because of the difficulty in preparing pure compounds, the multipattern profile refinement program is valuable.

The correlation between the structural information and the need for models for interpretation of dynamical behaviour was noted earlier. The structures of the layered dichalcogenide intercalation compounds are quite well determined, and the nature of ammonia in $TaS_2(NH_3)$ has been studied by both NMR and quasi-elastic neutron scattering. The pulsed NMR studies are relatively simple to perform, although the interpretation is not always straightforward. Electrochemical studies on $LiTiS_2$ and $NaTiS_2$ (which are both very good ionic conductors) indicate that the ionic mobility depends most sharply on the precise stoichiometry of the TiS_2 host, decreasing by two orders of magnitude for a 2% excess of titanium. The equivalent ammonia intercalation compound $TiS_2(NH_3)$ also shows high ammonia diffusion between the TiS_2 layers and also performs molecular spinning and reorientation. In some aspects this system resembles that of HUAs since both have an arrangement of molecules (water or ammonia) confined in

a region of reduced dimensionality. In the latter case however, the forces between the molecule and the confining layers are much less and the ammonia resembles more a two dimensional liquid. In this study we examine whether the mobility of the ammonia molecule is sensitive, like its lithium analogue, to small changes in the stoichiometry of the lamellar host, which must reflect the nature of these forces. To do this we have performed a series of measurements of the NMR proton spin-lattice relaxation time T_1 as a function of temperature on three different samples of $TiS_2(NH_3)$, with an excess of titanium ranging from 0.1 - 2.0%.

CHAPTER 2

THEORY OF NEUTRON SCATTERING AND PULSED SOLID STATE NMR

The theory of neutron scattering has been described in detail by several authors, eg Marshall and Lovesey (1971), Bacon (1975), Lomer and Low (1965), Squires (1978), and Windsor (1973) upon whom some of the text presented here is based.

A good introduction to the theory of solid state pulsed NMR may be found in the text by Farrar and Becker (1971).

2.1. Introduction to Neutron Scattering

The source of neutrons for the neutron scattering experiments described in this thesis is the high flux reactor at the ILL (Grenoble). **Neutrons** emerge from the reactor in thermal equilibrium with the D_2O moderator and therefore have a Maxwellian distribution of velocities. When neutrons are scattered by an atomic nucleus, the nuclear forces which cause the scattering operate over a range of about 10^{-14} - 10^{-15}m. The wavelength of a thermal neutron is of the order 10^{-10}m and is therefore much larger than the range of the nuclear forces. In these circumstances the scattering is isotropic.

For any scattering process, the direction of the scattered neutrons may be described, in polar coordinates, in terms of the polar angle θ and the azimuthal angle ϕ. The differential cross-section is defined by :

$$\frac{d\sigma}{d\Omega} = \frac{\text{number of neutrons scattered per second into a small solid angle } d\Omega \text{ in the direction } \theta,\phi}{N_I \, d\Omega} \qquad 2.1$$

where $d\Omega = \sin\theta d\theta\, d\phi$ and N_I is the flux of incident neutrons per unit area per second.

The total scattering cross-section is defined by

$$\sigma_{tot} = \frac{\text{(total number of neutrons scattered per second)}}{N_I} . \qquad 2.2$$

$$\text{Clearly, } \sigma_{tot} = \int_{\text{all directions}} \left(\frac{d\sigma}{d\Omega}\right) d\Omega \qquad 2.3$$

2.2. Scattering of Neutrons by a Single Fixed Nucleus

If a plane wave of neutrons described by the wavefunction

$$\psi_{in} = \exp(ikz), \qquad 2.4$$

where k is defined by $k = 2\pi/\lambda$ and is the magnitude of the wave-vector $\vec{k}$, and the z-axis is taken along the direction of $\vec{k}$, is incident upon a single atomic nucleus fixed at the origin, the scattered wave will be spherically symmetric. The wavefunction of the scattered neutrons at the point $\vec{r}$ may be written in the form

$$\psi_{sc} = -(b/r)\ \exp(ikr) \qquad 2.5$$

where b is defined as the scattering length and is a complex quantity with the dimensions of length. In most cases, the imaginary part of the scattering length is very small and we may ignore it. The imaginary component, however, becomes important for nuclei which have a high coefficient of absorption for neutrons, eg ^{113}Cd, ^{157}Gd or ^{10}B.

The resultant neutron wavefunction after scattering is therefore

$$\psi = \exp(ikz) - (b/r)\ \exp(ikr) \quad . \qquad 2.6$$

We may readily calculate the differential cross section $d\sigma/d\Omega$ for scattering from a single fixed nucleus. If v is the velocity

of the neutrons (the same before and after scattering for an elastic process), the number of neutrons passing through the small area dS per second is

$$v dS |\psi_{sc}|^2 = v dS b^2/r^2 = v b^2 d\Omega \ . \qquad 2.7$$

The flux of incident neutrons is

$$N_I = v|\psi_{in}|^2 = v, \qquad 2.8$$

$$\text{so that } \frac{d\sigma}{d\Omega} = \frac{v b^2 \ d\Omega}{N_I d\Omega} = b^2. \qquad 2.9$$

From equation 2.3 we may then write

$$\sigma_{tot} = 4\pi b^2. \qquad 2.10$$

2.3. Scattering from Many Nuclei - Coherent and Incoherent Scattering

Consider the scattering from two fixed nuclei with positions $\vec{r}_1$ and $\vec{r}_2$ and separated by a vector $\vec{r}$. If $\vec{k}$ and $\vec{k}'$ are the wave vectors for the incident and scattered radiation (where k = k' for an elastic process) the phase difference between the scattered waves

$$\phi = (2\pi/\lambda)\ (\vec{r}.\vec{k}' - \vec{r}.\vec{k}) = (2\pi/\lambda)\ \vec{r}.(\vec{k}'-\vec{k}) = \vec{Q}.\vec{r}. \qquad 2.11$$

The resultant amplitude is the sum of the amplitude from each nucleus, allowing for the phase difference,

$$\text{ie} \quad b_{r_1} + b_{r_2} \exp(i\vec{Q}.\vec{r}).$$

For a whole assembly of stationary nuclei at various positions $\vec{R}$, with scattering length b_R (where b_R may vary irregularly from

isotope to isotope, or indeed, from one nucleus to another of the same isotope if there is non-zero nuclear spin and hence a magnetic interaction with the neutron magnetic moment), the phase of the scattered radiation is $\exp(i\vec{Q}.\vec{R})$ and the differential cross-section is

$$\frac{d\sigma}{d\Omega} = \sum_R |b_R \exp(i\vec{Q}.\vec{R})|^2 = \sum_{R,R'} b_R b_{R'} [\exp i\vec{Q}.(\vec{R}-\vec{R}')]$$

$$= \sum_R b_R^2 + \sum'_{R,R'} b_R b_{R'} \exp[i\vec{Q}.(\vec{R}-\vec{R}')] \qquad 2.12$$

where Σ' indicates a summation not including $R = R'$. The first term in equation 2.12 is $N\langle b_R^2\rangle$ where N is the number of nuclei and the brackets $\langle\rangle$ denote the average value. There is no correlation between b_R and $b_{R'}$, so that $\langle b_R b_{R'}\rangle = \langle b_R\rangle\langle b_{R'}\rangle = \langle b_R\rangle^2$, and the second term may be written

$$N\langle b_R\rangle^2 \sum_{R,R'} \exp[i\vec{Q}.(\vec{R}-\vec{R}')]$$

$$= -N\langle b_R\rangle^2 + N\langle b_R\rangle^2 \exp[i\vec{Q}.(\vec{R}-\vec{R}')].$$

Thus

$$\frac{d\sigma}{d\Omega} = N(\langle b^2\rangle - \langle b\rangle^2) + N\langle b\rangle^2 |\Sigma \exp(i\vec{Q}.\vec{R})|^2 . \qquad 2.13$$

The term $N(\langle b^2\rangle - \langle b\rangle^2)$ in equation 2.13 can also be written as $N\langle (b-\langle b\rangle)^2\rangle$, showing that it depends on the mean square deviation of the scattering lengths from their average value. It is known as the incoherent scattering cross-section, and (ignoring the effects of thermal motion) gives rise to an isotropic background to the coherent scattering represented by the remaining term

$$N\langle b\rangle^2 |\sum_R \exp(i\vec{Q}.\vec{R})|^2 .$$

The coherent scattering takes into account interference effects arising from the phase differences in the scattered radiation due to the relative displacements of the various nuclei in the assembly, and therefore contains information concerning the structural relationships between different atoms.

2.4. Nuclear Bragg Scattering

In a crystal, in which the atoms lie in a regular periodic three dimensional array, we can replace the position vector of a particular nucleus $\vec{R}$ by the sum of two vectors $\vec{n} + \vec{\rho}$. $\vec{n}$ is the lattice vector and refers to a particular unit cell, and $\vec{\rho}$ is the position of an atom within a cell. By relating $\vec{n}$ to the basis vectors of the unit cell, and $\vec{Q}$ to the reciprocal lattice basis vectors, it can be shown that the coherent part of the elastic cross-section is

$$\frac{d\sigma}{d\Omega} = N_o \frac{(2\pi)^3}{V} \sum_{\tau} \delta(\vec{Q}-\vec{\tau}) \times |F_\tau|^2 \qquad 2.14$$

with $F_\tau = \sum_{\rho} b_\rho \exp(i\vec{\tau}.\vec{\rho})$.

Here N_o is the total number of cells, each of volume V, and $\vec{\tau}$ defines a reciprocal lattice point. F_τ is known as the structure factor per unit cell. The delta function $\delta(\vec{Q}-\vec{\tau})$ indicates that the scattering is limited to values of the scattering vector $\vec{Q}$ equal to the set of the reciprocal lattice vectors $\vec{\tau}$. With $Q = 4\pi\sin\theta/\lambda$, and the distances $|\vec{\tau}| = 2\pi/d$ inversely proportional to the plane spacing d of the various Bragg reflecting planes, scattering can only occur at angles given by the Bragg equation

$$\lambda = 2d\sin\theta. \qquad 2.15$$

The atoms in a real crystal are not stationary, as we have so far assumed, but vibrate about their mean lattice points. It is necessary to introduce a term therefore into the structure factor expression to allow for this. We may write the structure factor for a reflection, with Miller indices hkl, F_{hkl}, as

$$F_{hkl} = \sum_{\rho} b_{\rho} \exp 2\pi i(hx + ky + lz) \exp(-W_{\rho}) \qquad 2.16$$

where the summation is over all the atoms in a unit cell and the term $\exp(-W_{\rho})$ is the general expression for the temperature factor.

An often valid (or necessary) approximation considers that an atom in a crystal vibrates both harmonically and isotropically. We may then write the temperature factor as

$T = \exp(-\frac{1}{2} Q^2 \langle u^2 \rangle)$ where $\langle u^2 \rangle$ is the mean square displacement of the atom from its mean position. Thus

$$T = \exp[-(8\pi^2 \sin^2\theta_{hkl}/\lambda^2) \langle u^2 \rangle]$$

$$\text{or } T = \exp(-B \sin^2\theta_{hkl}/\lambda^2) = \exp[-B/4(2\sin\theta_{hkl}/\lambda)^2] =$$

$$\exp[-B/4(1/d_{hkl})^2] \qquad 2.17$$

where $B = 8\pi^2 \langle u^2 \rangle$ and is the isotropic temperature factor quoted in this work (in $\mathring{A}^2$). More generally, though, there is no reason to suppose that the thermal displacements are the same in all directions and we must allow for anisotropic thermal motion. If we approximate this anisotropic motion as ellipsoidal, we may write the temperature factor in the form of a 3 x 3 symmetric tensor. The six independent elements B_{ij} are the temperature factor coefficients and we may write

$$T = \exp\left[-\tfrac{1}{4}\left(B_{11}h^2a^{*2}+B_{22}k^2b^{*2}+B_{33}l^2c^{*2}+2B_{12}hka^*b^*+2B_{13}hla^*c^*+2B_{23}klb^*c^*\right)\right]$$

where a^*,b^* and c^* are the magnitudes of the basic vectors of the reciprocal cell, and $B_{ij} = 8\pi^2 \langle u_{ij}^2 \rangle$.
The values that may be taken by the various B_{ij} are restricted so that the 3 x 3 tensor transforms according to the point symmetry of the atom to which it refers. These relationships have been tabulated by Peterse and Palm (1966) (and also Willis and Pryor, 1975, p 105) for the special positions of all the space groups in their standard settings.

2.5. Powder Neutron Diffraction

The simplest method of satisfying the Bragg conditions is to use a powdered sample in which will always be found a few crystallites with the required orientation. The scattering, at fixed wavelength, comes out in a series of cones, called Debye-Scherrer cones, which are successively crossed by the detector as it moves to higher scattering angles. The scattering cross-section integrated over a complete cone is

$$\sigma(\tau) = \frac{4\pi^3 No}{k^2 V} \frac{Z_\tau}{\tau} |F_\tau|^2 \qquad 2.18$$

where Z_τ is the number of equivalent reflecting planes associated with $\vec{\tau}$. The actual quantity measured in an experiment is the integrated intensity I_{hkl}. The conversion from $\sigma(\tau)$ to I_{hkl} involves certain instrumental and geometric factors, since the detector only passes through a fraction of the Debye-Scherrer cone,

$$\text{ie} \quad I_{hkl} = \sigma(\tau) \frac{l_s}{2\pi r_o \sin 2\theta_{hkl}} \qquad 2.19$$

where l_s is the height of a cylindrical sample, whose axis is normal to the incident beam, and r_o is the distance to the detector from the sample. The sample is uniformly bathed in neutrons and absorption is neglected. Information is invariably lost using a powder, where there is overlap of reflections which are either coincident, or very close together in 2θ. This problem is particularly marked at high angle where there is often a high density of reflections, which are considerably broader than those found at lower angles.

With single crystal samples, there is no difficulty in separating the nuclear Bragg reflections which occur from the various planes of the crystal, as scattering can only occur for a specific plane when the sample is correctly aligned with $\vec{\tau}$ parallel to $\vec{Q}$. Single crystal studies are in general more powerful and direct, because they examine quite separately the neutrons which have traversed the crystal in specific directions. In the powder method, all this directional information, containing in particular information concerning the symmetry of the structure,is lost. Much higher count rates are achieved in single crystal studies since all the diffracted radiation for a given reflection is directed towards the detector, rather than spread out over a cone. This method, though, is more time consuming due to the need for careful positioning of the sample and the detector to measure each of the many reflections that can occur from a complex structure. This is an important consideration when using the relatively weak sources in neutron diffraction. Single crystal diffraction studies have therefore been used routinely for the solving of crystal structures, and are one of the most powerful tools available to increase our

understanding of the solid state.

Nevertheless, in many circumstances, powder studies are of great value. Single crystals may be impossible to grow to the correct size, or may fracture or form domains when a structural phase transition is investigated. The relatively large single crystals required for neutron diffraction (as compared with X-rays where the source of radiation is much more intense) may lead to problems with secondary extinction which is usually absent in powder work. If integrated Bragg intensities are required in a single crystal study, a high proportion of the time is spent off the centre of the peaks, measuring the base and background regions, and more time is spent reorienting the crystal for each Bragg peak. Measurements on powders are much quicker, making the technique attractive for studying the effects on a structure of changes in temperature or pressure, etc. Neutron powder studies may be very useful for locating the positions of light atoms, eg hydrogen or lithium, when combined with single crystal X-ray diffraction by which the structure of the heavy atoms has already been determined.

One great advantage of powder neutron diffraction, as compared with the equivalent X-ray powder studies, is that the data may be more readily analysed by the method of profile analysis, because we have an accurate knowledge of the Gaussian peak shape function. For X-rays, the peak shape is much less easy to define and is often described as Lorentzian, or modified Lorentzian, though none of these is completely satisfactory. There are however great efforts to extend profile refinement to a wider range of X-ray problems (Young, Mackie and Von Dreele, 1977; Immirzi, 1980; Waltersson, Werner and Wilhelm, 1977).

In a powder pattern, the individual integrated intensity of the various Bragg peaks may be lost due to the overlap of adjacent peaks, yet the very complexity of the overlapping powder pattern means that it still contains much structural information. Rietveld (1967, 1969) chose to forget about separating the individual Bragg intensities and instead concentrate on the detailed shape of the powder pattern against which the various structural models can be refined to give the best fit.

2.6. Profile Analysis

Rietveld (1967, 1969) showed that each Bragg reflection of a neutron powder pattern from a steady state source can be described by a Gaussian peak $Y_{i,k}$ whose full width at half height H_k depends upon three parameters,

$$\text{ie} \quad H_k^2 = U \tan^2 \theta_k + V \tan \theta_k + W. \qquad 2.20$$

The Gaussian

$$Y_{i,k} = P_k \exp -b_k (2\theta_i - 2\theta_k)^2, \qquad 2.21$$

with $b_k = 4\ln 2/H_k^2$, is arbitrarily cut off at a distance $1.5H_k$ at either side of its centre $2\theta_k$ where its intensity becomes very small. The values of $2\theta_k$ are obtained from the lattice parameters, known wavelength, and zeropoint. The values of P_k are calculated from the various structural parameters,

$$\text{ie} \quad P_k = t\, F_k^2\, j_k\, L_k \frac{2\sqrt{\ln 2}}{H_k\sqrt{\pi}} \qquad 2.22$$

where t is the counter step, F_k the structure factor, j_k the multiplicity and L_k the Lorentz factor. The procedure is followed in two stages. In the first stage, the so-called "profile

preparation" program corrects the observed counts for the contribution due to the background, by subtracting values of the background intensity which are obtained by linear interpolation between supplied estimates obtained from regions between the Bragg peaks. The positions and range of all the Bragg peaks are calculated from the supplied values of the lattice parameters, zeropoint, wavelength and halfwidth parameters. The weight to be assigned to each profile point is calculated as

$$w_i \propto 1/\sigma^2 \approx 1/y_i(\text{obs}).$$

In the second stage, the "profile refinement" program uses the method of least squares to adjust the values of the various instrumental and structural parameters (including anisotropic temperature factors, Hewat, 1973) to minimise the function

$$\chi^2 = \sum_i w_i |y_i(\text{obs}) - (1/c)\ y_i(\text{calc})|^2 \qquad 2.23$$

where $y_i(\text{obs})$, $y_i(\text{calc})$ and c are the observed intensity at the position $2\theta_i$, the calculated intensity, and a scale factor respectively, and hence obtain the best fit between the observed and calculated profiles. The use of least squares techniques in crystallography has been described by Rollett (1965, 1970), Hamilton (1964), and Cruickshank (1959, 1970). In crystallographic problems the observations are not linear functions of the various parameters which are not independent of each other. In this case the program calculates the various shifts that must be applied to each parameter for a better fit and the process is iterated. Allowance is made for peak asymmetry at low angles by including a semi-empirical correction, and also for preferred orientation of plate-like samples by assuming that the distribution of the orientations of the crystallites is a Gaussian

centred on a single preferred orientation direction. Full details of these corrections may be found in Rietveld's papers.

At the end of each cycle of least squares refinement, the program prints out the new parameters, their estimated standard deviations (esd's) and a series of R factors, by which we may judge the goodness of the fit. The esd of an independent parameter χ_p is calculated according to the formula

$$\sigma(\chi_p) = [M_{pp}^{-1} \Sigma_i w_i (cy_i(obs) - y_i(calc))^2/(N-P+C)]^{1/2} \quad 2.24$$

where M_{pp}^{-1} is the diagonal element of the inverted normal matrix corresponding to the p^{th} parameter. The quantity (N-P+C) is the number of degrees of freedom, where N is the number of statistically independent observations, P the number of least squares parameters, and C the number of constraint functions.

Three R factors are produced :

the profile R factor -

$$R_p = 100\Sigma_i |y_i(obs) - (1/c)y_i(calc)|/\Sigma_i y_i(obs) \ ;$$

the weighted profile R factor -

$$R_{wp} = 100[\Sigma_i \ w_i(y_i(obs) - (1/c)y_i(calc))^2/\Sigma_i \ w_i(y_i(obs))^2]^{1/2} \ ;$$

and an R factor based on estimates of the integrated intensities of the observed Bragg peaks -

$$R_I = 100 \ \Sigma_k |I_k(obs) - (1/c)I_k(calc)|/\Sigma_k \ I_k(obs).$$

There is also an expected R factor

$$R_E = 100[(N-P+C)/\Sigma_i \ w_i(y_i(obs))^2]^{1/2},$$

which we might expect to obtain were differences between the observed and calculated profiles only statistical in origin. It is commonly held that a structure is "solved" if the value of $R_{wp} < 2R_E$. This criterion, although a useful guide, is without a

theoretical basis and should be used only with extreme caution, for misleading results may otherwise be obtained.

2.7. Developments since Rietveld

Since Rietveld's original papers, there have been improvements to both the instrumentation and the methods of data processing for powder neutron diffraction. Some of these have had a profound effect, others were rather more experimental, and some have yet to see their true potential realised. Some examples are discussed in a general review of neutron profile analysis by Cheetham and Taylor (1977).

(i) Instrumentation : The advent of high flux reactors, focussing monochromators, banks of high efficiency counters, multidetectors, and the electronics to cope with a high rate of data acquisition has meant that a greater priority can now be given to instrumental resolution. With good resolution, and high effective flux, the amount of information stored in the profile pattern is greatly increased, allowing the refinement of bigger and more complicated structures, with unit cell volumes as high as 2177 $\mathring{A}^3$ in the case of $Ti_2 Nb_{10} O_{29}$ (Von Dreele and Cheetham, 1974), and possibly higher. With the development of the new pulse sources using time of flight (TOF) methods with backscattering geometry, better resolution to much higher values of $\sin\theta/\lambda$ will be achieved. These sources also provide the opportunity for high resolution patterns to be collected in perhaps a few seconds, opening the way for kinetic studies on a large number of systems.

(ii) Constrained refinement : As well as the linear and quadratic "strict" constraints between atomic parameters as required by space group symmetry or chemical composition etc, which were permitted in the original Rietveld program, Cheetham and Taylor (1977) report the introduction of flexible "chemical" constraints

(Waser, 1963) to the procedure. There are as yet no reports of their application to profile refinement problems. Pawley (1972) has discussed generally the merits of constrained refinement in crystallography, and has used his program EDINP to apply strict constraints to preserve the molecular geometry in the refinement of the crystal structures of p-$C_6H_4Br_2$ and p-$C_6F_4Br_2$. The orientation of the molecule in the monoclinic unit cell was determined by allowing the three Euler angles to vary (Pawley, Mackenzie and Dietrich, 1977). In a subsequent paper, Bacon, Lisher and Pawley (1979) applied thermal constraints to the molecular motion of α-Resorcinol with the rigid-body methods of TL, TLX and TLS, and compared these to the unconstrained refinement to assess the applicability of these models. They concluded that their development will prove a powerful tool in future powder refinement analyses of organic materials.

(iii) Background : Estimation of the true neutron background below the Bragg reflections is a very difficult problem, particularly at high angle where instrumental resolution is lowest and peak density is at a maximum. The normal procedure of linear interpolation between regions containing no peaks may be impossible, since such regions may no longer exist. To a large extent this problem limits the accuracy to which reliable temperature parameters can be obtained from powder diffraction work. Sabine and Clarke (1977) introduced a method whereby, after subtraction of the contribution from the instrumental background and the sample-can (a blank run), the true sample background is obtained by summing the incoherent scattering due to isot opic disorder and nuclear spin effects, the paramagnetic scattering, and any diffuse scattering arising from random substitutional atomic defects. The

least squares refinement then compares the total observed pattern with the calculated profile. This method ignores thermal diffuse scattering (TDS) and so is only suitable for low temperature data. The program EDINP (Pawley, 1980) incorporates a refineable background which is the sum of a flat component and a rising component related to the size of the overall temperature factor. This function is also unsuitable for TDS. Immirzi (1980) has introduced a purely empirical background function which consists of straight sections and refineable bumps which appears to be quite successful in describing the diffuse background of an X-ray study on semi-amorphous isotactic polypropylene.

(iv) Refined parameters and esd's : Sakata and Cooper (1979) have made a detailed comparison between the methodology of Rietveld and refinement by integrated intensities. They point out that, although in profile refinement each data point is considered to be an independent observation, the points of a single Bragg peak are not structurally independent, for between them they provide only <u>one</u> structurally related observation. Moreover, in profile refinement, fitting is to the individual measurements, whereas for intensity refinement the structure is fitted to the complete integrated intensity, and there is no reason to assume that the weighting schemes employed for the two methods give the same statistical bias, resulting in different error distributions. The problem of the estimation of the background means that the contribution to the weighting scheme from uncertainties in the background is often very difficult to assess. This can lead in profile analysis to the overestimation of the relative weights of the points furthest from the centre of a profile peak. (In fact

Sakata and Cooper assume that the background uncertainty, a major contribution to the true uncertainty in weaker regions of the profile, is ignored. This is now less common. We ourselves use the weighting scheme $w_i = 1/(y_i(obs)+B_i)$ where $y_i(obs)$ is the value of the profile point i before subtraction of the estimated background B_i).

Due to the differing statistical characteristics of the weighting schemes used in the minimisation functions for profile analysis and integrated intensity refinement (in the absence of zero background), the two methods may lead to slightly different sets of structural parameters. In addition, the correlation between data points within a single Bragg peak means that their errors may also be correlated. These errors depend quite separately upon both the refined values of the structural parameters and the profile parameters. The esd's are calculated from the overall pattern of errors whereas the errors on the structural parameters depend solely on the fit to the Bragg intensities. The Bragg intensities are often considerably less well determined than the overall fit to the shape of the peaks, which leads to a serious underestimation of the esd's calculated for structural parameters from profile refinement. For the examples they quote, Sakata and Cooper show that this can range from a factor of 2 to 5, and suggest that a complete reassessment of the profile refinement technique is necessary.

Prince (1981), however, has argued that if a pattern of well resolved peaks is adequately described by a crystallographic model, as determined by the usual well established statistical tests, the estimates of the parameters or their standard deviations will not

be significanlty different, in a statistical sense, whether the method of refinement uses peak profiles or integrated intensities. Differences between these estimates that exceed the differences expected, because of the greater precision of the profile method in estimating the intensity of a peak in the presence of background, are not due to incorrect computation in the profile method, but to the failure of a model to fit adequately the particular data set. If the model does not fit, esd's cannot be evaluated by statistical means. When peaks overlap, there are also correlations because there needs to be some procedure for decomposing the composite peak to estimate the individual values of the reflections contained in it. This is automatically done in profile refinement. Prince recommends that a refineable background function should always be included as part of the model, to account for correlations between temperature parameters and the background, which become more important as the pattern becomes increasingly less well resolved.

(v) Multi-pattern refinement : Recently, the Rietveld program has been modified to refine a profile containing overlapping peaks from more than one pattern. Due to the importance of this method with respect to this thesis, it is discussed separately in the next Section.

2.8. Refinement of Diffraction Profiles Containing more than one Pattern

One advantage of neutrons over X-rays in powder diffraction is the ease with which data can be collected over a wide range of temperatures and pressures. In such applications, more than one diffraction pattern can occur in the observed profile, eg from

sample cans built to withstand high temperatures and pressures, or from material, eg MgO, deliberately added to the sample to hinder sintering or preferred orientation. Occasionally we might observe peaks from small amounts of impurities, or unreacted starting materials, particularly when the stoichiometric limits of a compound are narrow. Small quantities of impurity may be poor X-ray scatterers, as compared the major component, and escape detection in, say, Debye-Scherrer photographs of the sample, and yet be excellent neutron scatterers.

Where the diffraction pattern covers most of the angular range examined, overlap between the various patterns is unavoidable. If it is not possible to collect data from each minor phase independently, under identical experimental conditions to the original experiment, the usual practice has been to exclude these regions of data to which the minor phase contributes intensity. This is a rather inelegant process, and in some cases may be impractical where peaks of key interest may be cut from the pattern. Furthermore, the range of any regions excluded from refinement must be very carefully chosen, as the program extrapolates in its calculation of "observed" intensities. Thus, if a single profile point at the edge of an excluded region contributes to a reflection within that region, the program may extrapolate an unrealistic value of the observed intensity from this point, and this may lead to an unstable refinement. This is particularly so in the analysis of data from low resolution instruments at high 2θ values, where peak overlap is most severe.

Bendall (1980), Thomas and Bendall (1978) and Bendall and Thomas (1980) have described modifications to the Rietveld program

which allow refinement of a complete profile containing up to three separate patterns. One of the major problems encountered involves the relative amounts of each component to be refined. Two simple methods may be used. Firstly, the scale factors for all the patterns may be set to the same arbitrary value, and the occupation numbers of the atoms of the constituent patterns refined subject to the normal constraints of stoichiometry. Alternatively, the scale factors for all the patterns may be set to a single refined value, but the occupation numbers of one of the patterns are kept fixed, the others being refined again subject to the constraints of stoichiometry. This method allows the application of "strict" constraints to the occupancies of the pattern with the fixed occupation numbers,eg when an atom is disordered over a number of partially occupied sites, the sum of whose occupancies must conform to the chemically determined value. It is generally hoped that these two methods for accounting for the relative amounts of the components should be sufficient to encompass the majority of multi-component systems.

If, however, two or more components have disordered structures which require the use of "strict" constraints, and assuming that this does not attempt to extract from the data more information than it is reliably equipped to give, it is necessary to refine the scale factors of each of the patterns independently. Such an analysis must account for the discrepancies between observed and calculated intensities at a profile point on the correct scale. The use of a minimisation function of the form of equation 2.23 is inappropriate if there is more than one scale factor. The alternative function, appropriate for multipattern data is

$$\chi^2 = \frac{\Sigma_i\, w_i \sum_{l=1}^{np} \left(y_{il}(obs) - (1/c_l)\, y_{il}(calc)\right)^2}{\Sigma_i\, w_i (y_i(obs))^2} \qquad 2.25$$

where the inner summation runs over the (np) patterns.

We present in this thesis the first successful applications of this technique to some real crystallographic problems.

2.9. Fourier Techniques

Fourier summations are an integral part of crystal structure analysis because they relate the scattering density at any point (x,y,z) in the unit cell to the diffracted intensities by a mathematical relationship of the type

$$\rho(xyz) = 1/V\ \Sigma F_{hkl}\ \exp(-2\pi i(hx+ky+lz)), \qquad 2.26$$

where V is the unit cell volume and the summation is over all the reflections in the diffraction pattern. The structure factor F_{hkl} is expressed by

$$F_{hkl} = \sum_j b_j \exp(2\pi i(hx_j+ky_j+lz_j))$$

$$= \sum_j b_j(\cos(hx_j+ky_j+lz_j) + i\sin(hx_j+ky_j+lz_j)) \qquad 2.27$$

where the summation is over the j atoms of effective scattering power b_j.

The complex quantity F_{hkl} is related to its magnitude by

$$F_{hkl} = |F_{hkl}|\ \exp(2\pi i\ \phi_{hkl}) \qquad 2.28$$

where ϕ_{hkl} is the phase angle of the reflection (hkl), so that equation 2.26 may be written as

$$\rho(xyz) = 1/V\ \Sigma|F_{hkl}|\exp(-2\pi i(hx+ky+lz-\phi_{hkl})). \qquad 2.29$$

Thus the density of scattering material may be calculated from the observed structure factors using phases derived from a trial structural model.

In profile refinement, however, often no direct estimate of the observed structure factor is available due to the overlap of adjacent reflections. The observed structure factor is approximated by partitioning the profile intensity at each point in the profile amongst the contributing reflections according to the relative magnitudes of the peak shape function, the multiplicity, the Lorentz factor, and the squared calculated structure factor. This estimate is therefore biased towards the trial model for the structure. Thus, for the best results, the trial model should be such that there is already a reasonably good fit between the observed and calculated profiles. Nevertheless, Fourier techniques are of great help in analysing powder diffraction data, for they may give a valuable insight into the relationship between the various atoms in a structure, or reveal the fallacy of certain misleading assumptions which can impede an otherwise potentially successful refinement.

2.10. Theory of NMR and Relaxation Times

A nucleus with non zero angular momentum (ie $I>0$) possesses a magnetic moment $\vec{\mu} = \gamma h \vec{I}$, where γ is the gyromagnetic ratio which is characteristic of a particular nucleus. In a magnetic field $\vec{B}_o$, applied by convention along the z-axis, the magnetic moment precesses about the field direction with a frequency $\omega_o = \gamma B_o$ (the Larmor frequency). In a rotating frame of reference with angular velocity $-\omega\vec{k}$, the magnetic moment in the static field $B_o\vec{k}$ satisfies the equation

$$\frac{d\vec{\mu}}{dt} = \gamma\vec{\mu} \times (B_o - \omega/\gamma)\vec{k}. \qquad 2.30$$

When the frame of reference is rotating at the Larmor frequency, the apparent field seen by the nucleus $(B_o - \omega/\gamma)$ is zero and the moment is stationary in the rotating frame. The theories and models of NMR studies become much simpler both conceptually and mathematically when referred to this rotating frame of axes x',y',z', where z' is the same as the laboratory frame z.

If the oscillating magnetic field of a pulse of radio frequency electromagnetic radiation $B_1\cos(\omega t)$ is applied orthogonally to the static field B_o, the effective field in the rotating frame is given by

$$\vec{B}_{eff} = (B_o - \omega/\gamma)\vec{k} + B_1\vec{i}. \qquad 2.31$$

At resonance, when the frequency of the applied radiation $\omega = \omega_o$, then $\vec{B}_{eff} = B_1\vec{i}$ and the moment precesses in the y'z' plane, ie about x'.

For an ensemble of nuclei, we must consider the net magnetisation of the sample $\vec{M}$, ie the sum of the individual moments, all of which, when at equilibrium in the static field $\vec{B}_o$, have components along the field direction z,but a random distribution of phases in the xy plane. Hence $M_x = M_y = 0$, and

$$\vec{M}_z = \sum_i \gamma\hbar\vec{I}_i. \qquad 2.32$$

$\vec{M}$ precesses about the applied field at the Larmor frequency in exactly the same manner as the individual moments. Application of a pulse of RF radiation B_1 at resonance causes $\vec{M}$ to rotate in the x'z' plane towards x'. The angle through which $\vec{M}$ is rotated by a given pulse depends on the strength of the signal,

B_1, and the length of time for which it is applied, t, ie $\theta = \gamma B_1 t$. By choosing pulses of suitable strength and duration, we may rotate $\vec{M}$ by 90° so that it lies along the x' axes, or by 180°, reversing the original direction of magnetisation, along -z'. The processes by which the magnetisation returns to its equilibrium state following the application of a pulse is known as relaxation. After a 90° pulse, the magnetisation $\vec{M}$ is left precessing in the x'y' plane. The individual spins lose coherence, which reduces M_x and M_y with a characteristic time T_2, and is termed spin-spin relaxation. The return to equilibrium in the z direction, as a result of energy exchanges with the rest of the system, is characterised by the spin-lattice relaxation time T_1. Bloch (1946) assumed that relaxation was a first order process which could be described by an exponential with a characteristic relaxation time. In the rotating frame we may write

$$\frac{dM_z}{dt} = (M_z^{eq} - M_z)/T_1$$
$$\frac{dM_x}{dt} = \frac{-M_x}{T_2} \quad ; \quad \frac{dM_y}{dt} = \frac{-M_y}{T_2} \; . \qquad 2.33$$

When the free induction decay (FID) is non-exponential, T_2 is <u>defined</u> as the time taken for M_x to fall to M_x/e. When T_2 becomes long (ms range), magnetic field inhomogeneities result in different precession rates and consequent loss of spin coherence. The Carr-Purcell-Meiboom-Gill (CPMG) pulse sequence (Carr and Purcell, 1954; Meiboom and Gill, 1958) may be used to average this effect to zero.

The relaxation phenomenon requires that the components of $\vec{M}$ be changed. This is brought about by fluctuations in the local

fields $\vec{B}_L$ experienced by the nuclear spins. The torque exerted by $\vec{B}_L$ on $\vec{M}$ is $\vec{B}_L \times \vec{M}$. It follows from the properties of vector products that, in the rotating frame, components $\vec{B}_{Lx}$ and $\vec{B}_{Ly}$ will lead to relaxation in both the x'y' plane (T_2 processes) and along z' (T_1 processes), whereas $\vec{B}_{Lz}$ can only cause relaxation in the x'y' plane (T_2). Viewed from the laboratory frame, this implies that zero frequency processes can only affect T_2, whereas processes occurring at the Larmor frequency are important for both T_1 and T_2. The limiting value of T_2 is always T_1, as thermal equilibrium is reattained. The local fields may become time dependent, and thus fluctuate at the required frequencies, as a result of molecular motions.

2.11. Motion in Solids and Relaxation

Static fields of the order 1 kiloGauss (kG) are typically used to study relaxation in solids where ω_o is conveniently in the radio-frequency range. In such fields $B_{eff} >> B_L$ and the system can be treated in terms of weak collisions with many molecular jumps in a relaxation period.

The basic treatment of relaxation in this weak field case is that of Bloembergen, Purcell and Pound, (BPP), (1948). The spins are treated as taking part in translational and/or reorientational Brownian motion. The formulae deduced for a homonuclear system are

$$1/T_1 = 1/3\ CM_2\gamma^2(J(\omega_o) + 4J(2\omega_o))$$
$$1/T_2 = 1/6\ CM_2\gamma^2(3J(0) + 5J(\omega_o) + 2J(2\omega_o)), \qquad 2.34$$

where C is that part of the second moment M_2 removed by the motion.

M_2 is calculable from the crystal structure (van Vleck, 1948), or is determined experimentally at low temperatures when T_2 reaches the rigid lattice limit. The spectral density $J(\omega)$ is given by

$$J(\omega) = \int K(\tau) \exp(i\omega\tau)\, d\tau.$$

$K(\tau)$ is the two particle correlation function which is generally assumed to be exponential with $K(\tau) = K(0) \exp(-\tau/\tau_c)$ with τ_c chosen such that for times less than τ_c the motion is considered small.

The properties of the BPP model for a simple diffusional process are shown qualitatively for log(relaxation times) v $1/T$ in Fig. 2.1. The minimum in T_1 occurs when $\omega_o\tau_c = 0.616$. When the motion conforms to Arrhenius type behaviour, the slopes for T_1 either side of the minimum, and for T_2, are given by E_A/R.

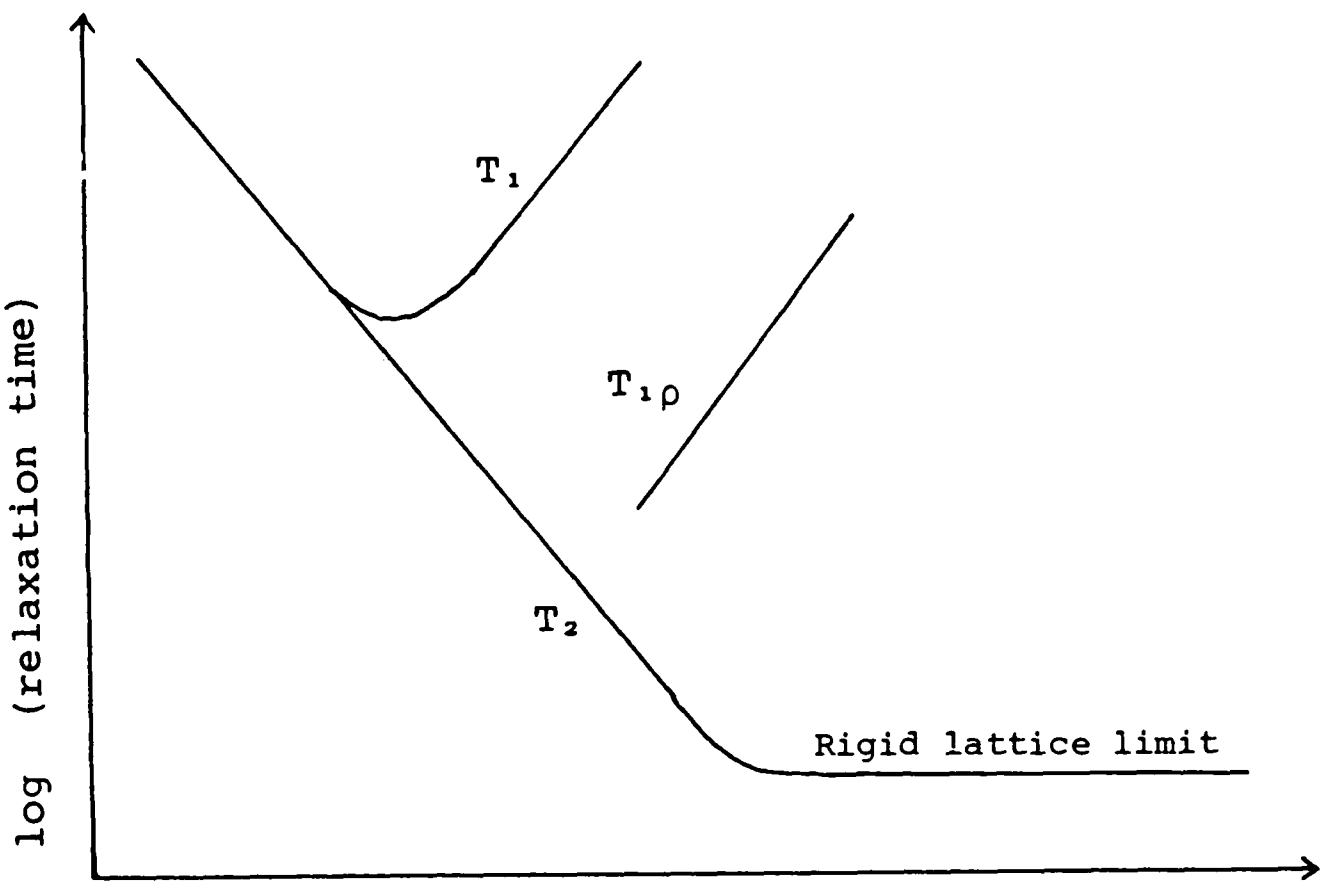


Fig. 2.1. The variation of relaxation time with temperature as predicted by the BPP model. The relaxation time $T_{1\rho}$ is the spin-lattice relaxation time in the rotating frame (Hartman and Hahn, 1962) and is sensitive to motions of lower frequency than ω_o.

CHAPTER 3

INSTRUMENTATION

3.1. Powder Neutron Diffractometers

Conventional two-axis diffractometers used for powder neutron diffraction differ widely in their characteristics. These may be varied to optimise the measurement of those features which are of greatest importance for the particular type of system under investigation. The factors which govern the choice of any particular instrument are the effective flux at the sample, the accessible wavelengths, the angular range and the resolution. For the analysis of a complex crystal structure we require very good resolution, since this increases the amount of information contained in the overlapping peak profile. For simpler systems, of known symmetry, at high temperatures, perhaps approaching the sample's melting point, resolution is of less importance and high flux is required to minimise the effects of sintering, or to improve the statistics of a pattern which may be considerably weakened by the effects of high temperature factors.

It is important to maintain the simple geometry of the conventional diffractometer, for the profile refinement technique requires a precise knowledge of the peak shape function. The sample is a cylinder of low absorbing material, the incident radiation is selected from a white beam by a crystal monochromator having an effective Gaussian mosaic spread, and the line shape, being a convolution of a number of nearly Gaussian distributions, approaches even more closely the ideal Gaussian shape. Thus we may not use

the focussing techniques of X-ray camera systems to obtain improved resolution, for this would lead to a more complicated line profile. Hewat (1975) has discussed in depth the relationship between the various factors to be considered in the design of a powder diffractometer.

The resolution of an instrument is dependent upon the definition of the incident energy spectrum by the monochromator, and the collimation of the incident and scattered beams. For most diffractometers, three sets of collimators are employed; between the source and the monochromator; the monochromator and the sample; and the sample and the detector. If the angular divergences of these collimators are designated as α_1, α_2 and α_3 respectively, and that of the monochromator crystal as a result of mosaic spread β, then the full width at half height H_k of a diffraction peak at angle θ may be described as a function of α_1, α_2, α_3, β and θ_M, the monochromator angle (Bacon, 1975). The integrated line intensity of the Bragg peak is given by

$$L = \alpha_1 \alpha_2 \alpha_3 \beta / (\alpha_1^2 + \alpha_2^2 + 4\beta^2)^{1/2} \qquad 3.1$$

and the maximum resolution will occur where $\tan\theta \approx \tan\theta_M$ at which H_k is approximately $(\alpha_1^2 + \alpha_2^2)^{1/2}$. At higher angles the resolution decreases rapidly.

The effective flux is dependent both on the number of incident neutrons, and the efficiency of the detector system. The incident flux may be increased by decreasing the instrumental resolution and by the design of the monochromator. The counting efficiency may be increased by using arrays of counters covering an extended

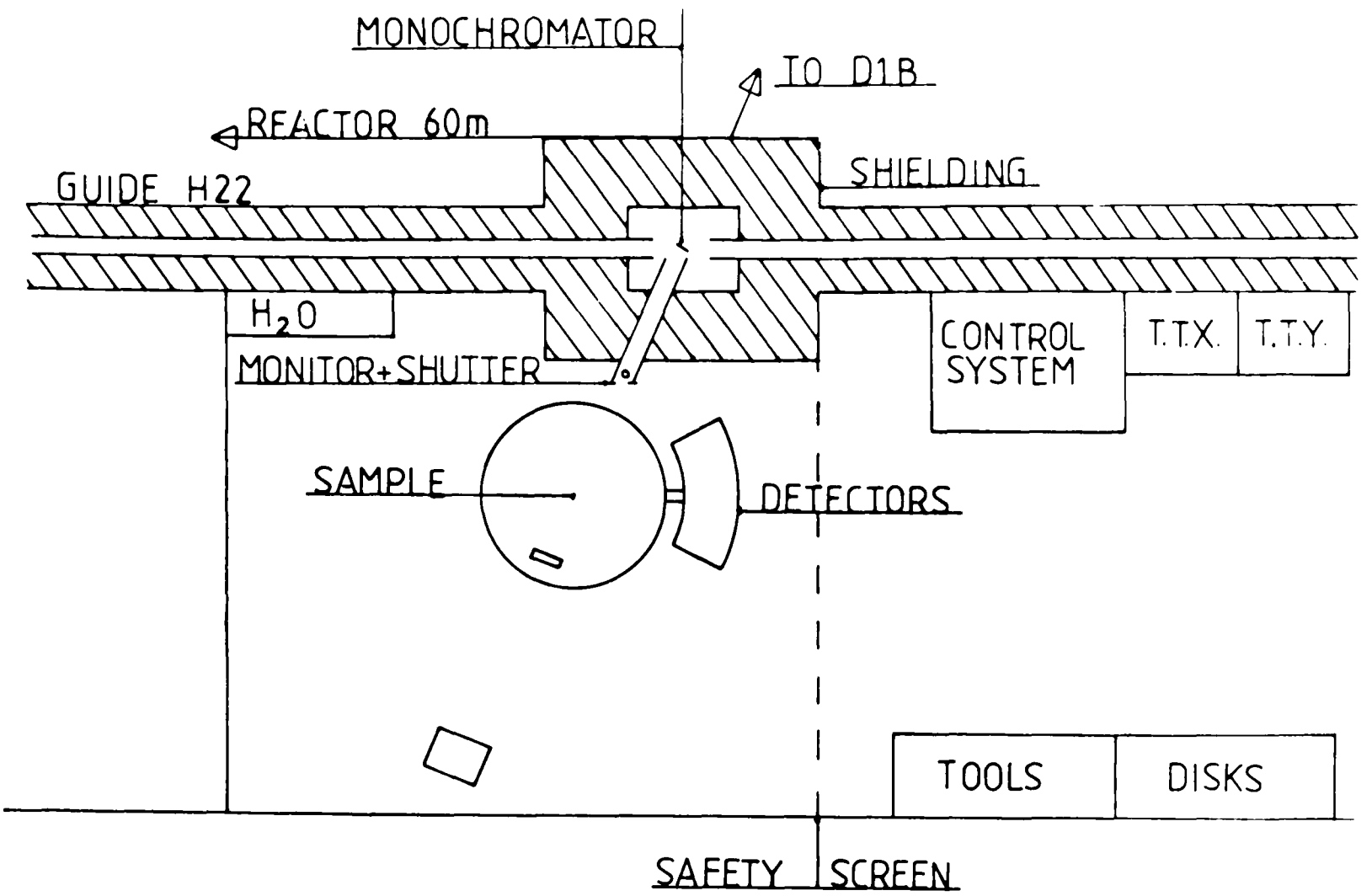
angular range, instead of just one.

3.2. D1A

The diffractometer D1A is situated at the end of the thermal guide tube H22, 60m from the reactor core in the neutron guide hall at the ILL. The guide tube transmits about 50% of thermal neutrons within a small solid angle (11' x 11' for 1.4 Å neutrons) which provides the α_1 collimation in the horizontal plane. An anisotropically squashed germanium monochromator, with a take-off angle of $2\theta_M = 122°$ and using the hhl (all odd) Bragg reflections, focusses the beam from 150mm high onto only 15mm giving an effective ten-fold increase in intensity at the sample position. The instrument is shown schematically in Fig. 3.1. Good resolution may be achieved up to $2\theta = 160°$, with the sample monochromator distance of 1500mm allowing the detector to enter into this back-scattering region. Rotation of the monochromator provides neutron wavelengths in the region 1.0 - 5.7 Å.

The detector system, Fig. 3.2, employs a bank of ten high pressure (5 atm) ^{3}He counters, each of dimensions 50mm diameter x 100mm long. At 1.4 Å their efficiency is greater than 90%. The ten counters are separated by angles of 6° to fill an overall angle of 60°. The counters are collimated by Söller slits, with blades made of 25 μm aluminised mylar foil coated on each side by 25 μm of gadolinium oxide paint. Their useful cross section is 100mm high x 20mm wide with a divergence of 10' horizontal and 6.6° vertical. They have a transmission of 96%. The instrument resolution is

$$\Delta d/d = 2 \times 10^{-3} \text{ at } 2\theta = 120°.$$



GENERAL LAYOUT OF D1A.

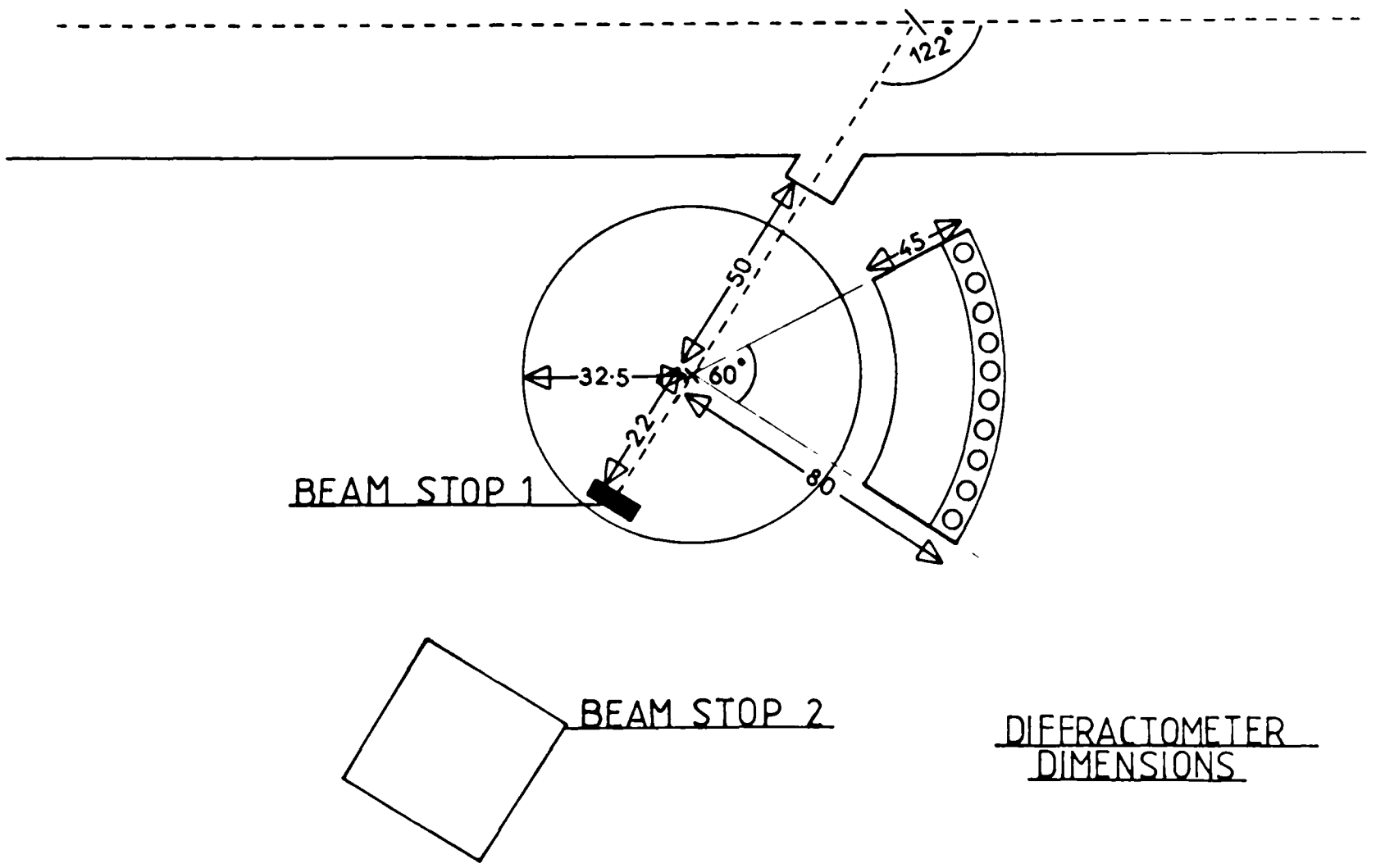


Fig. 3.1. Schematic representation of the high resolution powder diffractometer D1A at ILL (Grenoble), from the user manual, S. Heathman, ILL Report, 1981.

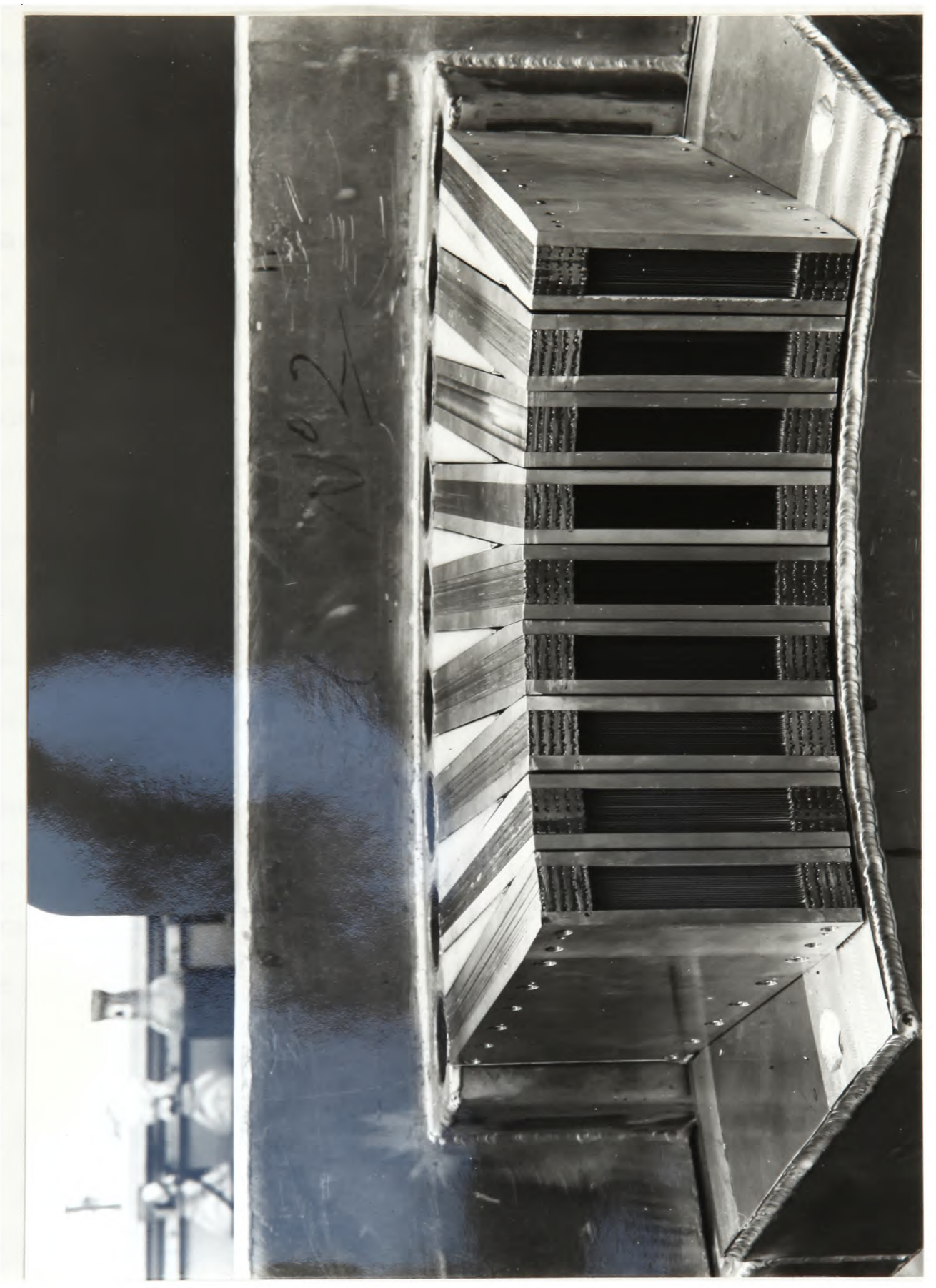


Fig. 3.2. The counter bank on D1A, during construction.

The counters are usually stepped by 0.05° from low to high 2θ. The counting time at each point is controlled by selecting a suitable monitor count. The step, monitor, and data acquisition are controlled by the instrument's dedicated Plessey Micro 1 computer, which stores the counts from each counter on a disc before they are transferred to the ILL main PDP10 computer. The counts from each counter may then be summed over their appropriate angular ranges using the interactive computer program POWDER (Hewat, 1978) which applies the corrections necessary to account for small differences in counter efficiencies and displacements. For convenience, so that all parts of the summed profile are on the same scale independent of the number of counters contributing to a particular point, the program calculates the mean number of counts per counter, and we weight each point in the profile refinement program according to the number of counters n contributing to that point, ie $w_i \approx n/\bar{y}_i(obs)$ (Hewat and Bailey, 1976).

The instrument has a selection of ancillary equipment including a standard cryostat (1.5K - 300K), a furnace (to 1000°C), pressure cells (up to 30 kbar) and a 15 kGauss electromagnet, for the study of neutron magnetic scattering. A photograph of the instrument is shown in Fig. 3.3.

3.3. NMR Spectrometer

Solid state NMR measurements in this work were made using a variable frequency Bruker SXP pulse spectrometer and ancillary Datalab data accumulation electronic equipment. A block diagram of the set up is shown in Fig. 3.4.

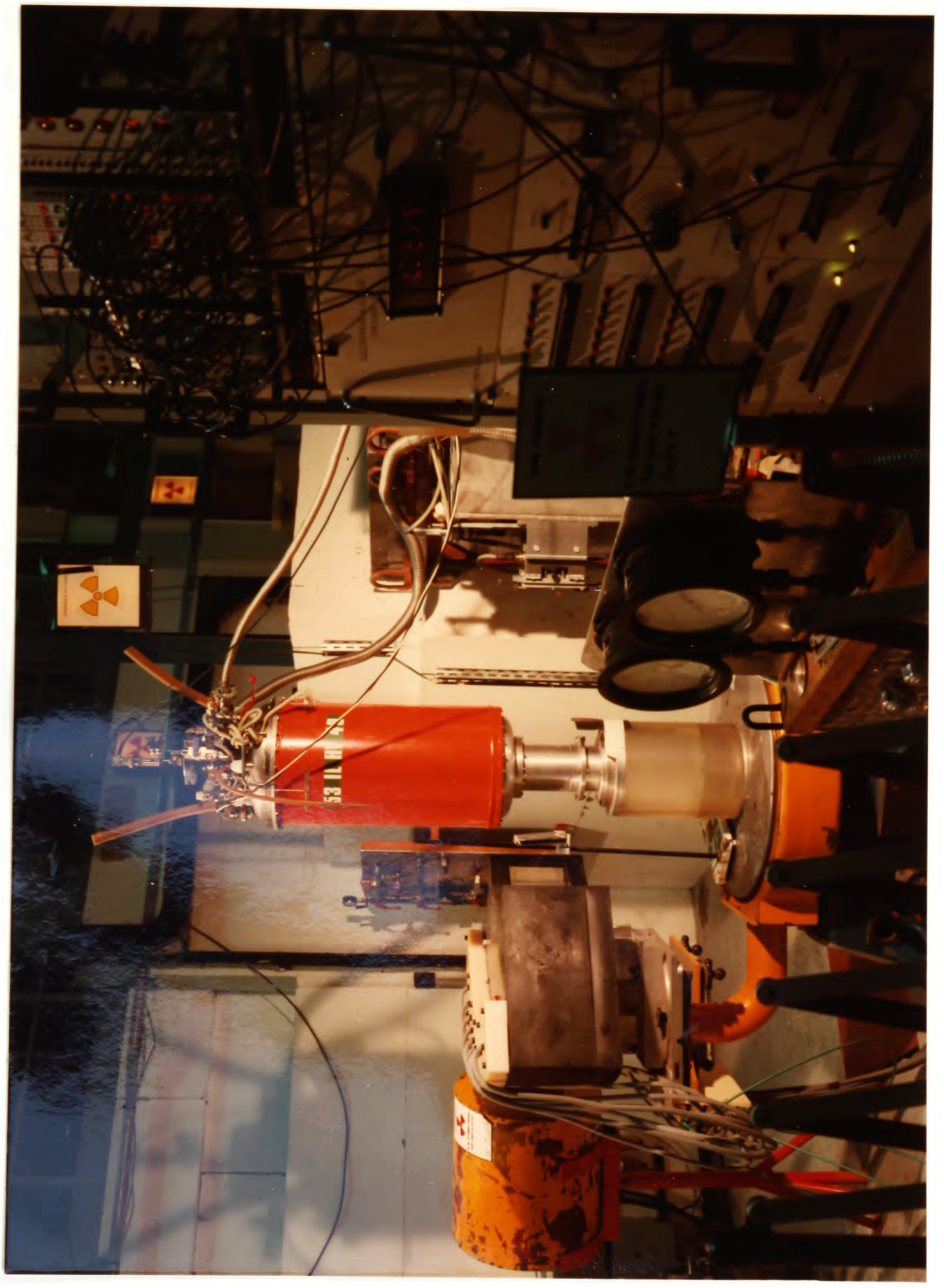


Fig. 3.3. View of D1A with its standard cryostat in place. The counter bank is at low scattering angle.

The central component in the spectrometer is a 1 MHz crystal oscillator, which controls the timing and triggers for the pulse sequence generator and (via a frequency synthesiser) the RF of the pulses themselves. Only when a trigger opens the gating circuits does the RF pass to the probe.

The probe consists of a single coil transmitter and receiver. The receiver pre-amplifier is largely protected from the saturating effect of the high power transmission pulses by an automatic pulse limiter.

All signals pass, after amplification and phase-sensitive detection, to a transient recorder which is interfaced to a data averager. For a given pulse sequence and repeat time set using the pulse programmer, the averager arms the transient recorder to store the signal when triggered. After a single recording sweep the data is transferred to the averager and the transient recorder is ready to be triggered again after a delay of at least 6 x T_1, when the system has returned to thermal equilibrium. Output from the averager can be monitored on an oscilloscope or on an X-Y pen recorder. Use of the data averager increases the signal-to-noise ratio by a factor of $\sqrt{N}$ for N sweeps (assuming a Gaussian noise distribution) and facilitates use of data direct from the spectrometer.

Samples in the spectrometer can be cooled below room temperature in a stream of cold nitrogen from a liquid nitrogen reservoir, or heated by means of hot air. Care must be taken not to condense water vapour from the air around the sample when cooling. Thermal equilibration of the sample takes at least an hour.

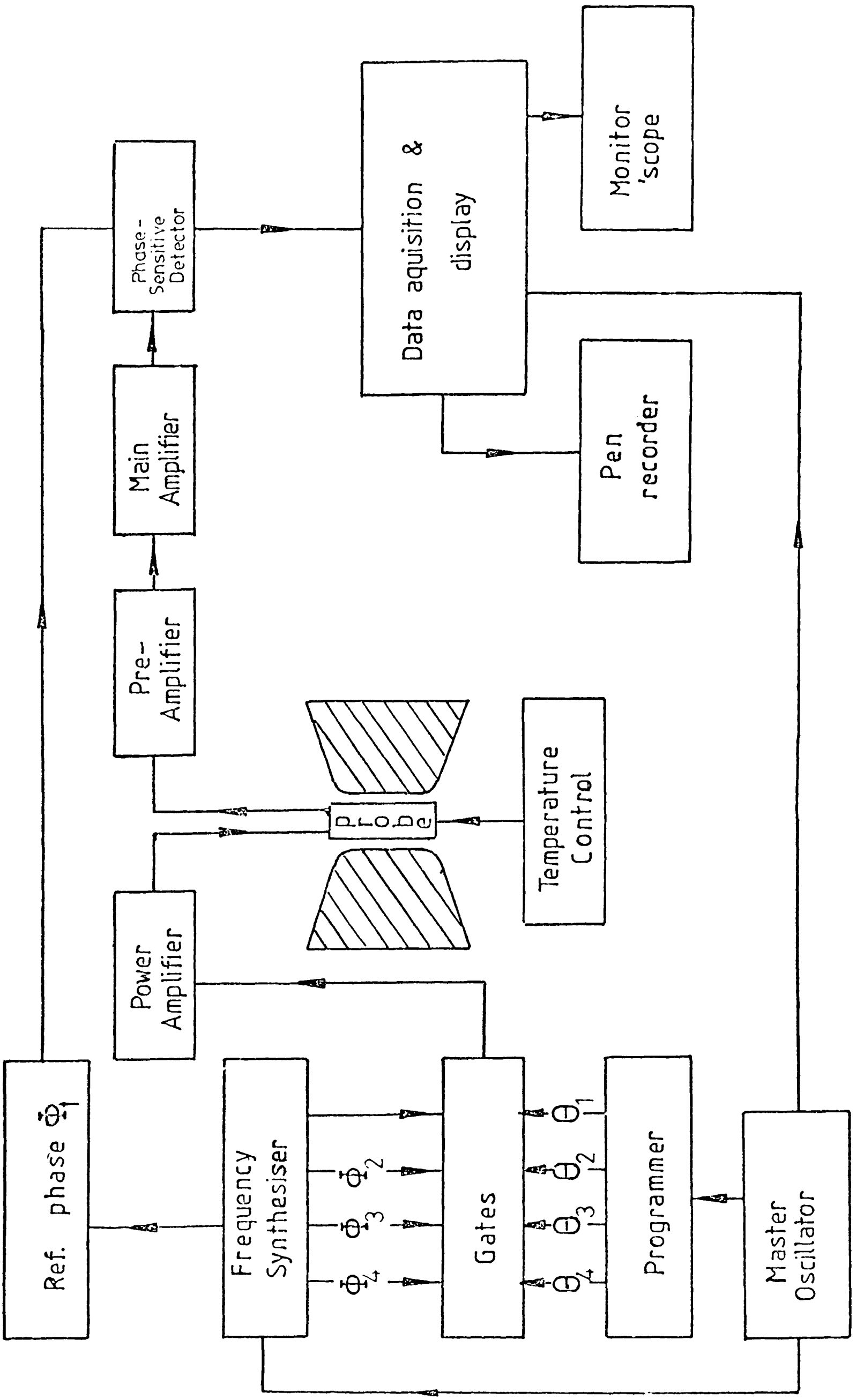


Fig. 3.4. Block diagram of the set up of the NMR spectrometer and data aquisition equipment.

CHAPTER 4

STRUCTURAL STUDIES ON $DUO_2AsO_4.4D_2O$ AND $LiUO_2AsO_4.4D_2O$

4.1. Introduction

$HUO_2AsO_4.4H_2O$

There exists a large class of structurally related layer type synthetic and naturally occurring compounds of general formula $A^{z+}_{1/z}\ (UO_2\ XO_4).nH_2O$, where A^{z+} may be almost any monovalent or divalent cation, X is P or As, and n varies from 0 to 5. The structure type was first described by Beintema (1938), and subsequently various members have been studied in more detail by other workers. Single crystal X-ray studies on $NH_4(UO_2AsO_4).3H_2O$ and $K(UO_2AsO_4).3H_2O$ have been reported by Ross and Evans (1964), and on $Ba(UO_2PO_4)_2.8H_2O$ by Nuffield and Milne (1953). Weigel and Hoffmann (1976) tabulate a large quantity of structural and TGA data for various compounds studied by themselves and other authors.

Of particular interest, and the subject of many recent studies, have been the isostructural compounds $HUO_2PO_4.4H_2O$, (HUP), and $HUO_2AsO_4.4H_2O$, (HUAs), which show very high proton conductivities at room temperature. In a series of papers (Shilton and Howe, 1977, Howe and Shilton, 1979, 1980b) it is shown by measurements on single crystals of HUP, and on pressed pellets of HUAs, that proton conductivity is a bulk property of the crystals, and shows a marked anisotropy. At 290K and 310K respectively, HUP and HUAs have proton conductivities of 0.6 $ohm^{-1}\ m^{-1}$ parallel to the layers with an activation energy for conduction of about

31 ± 1 kJ mole^{-1}. In the direction perpendicular to the layers the conductivity falls by a factor of at least a hundred. Measurement of T_1 and T_2 by ^1H pulsed NMR (Childs, Halstead, Howe and Shilton, 1978) indicated the occurance of rapid hydrogen diffusion with an activation energy of 20 ± 1 kJ mole^{-1}.

Morosin (1978a) has performed a single crystal X-ray diffraction study on HUP at room temperature and located the positions of all the atoms except the hydrogens. HUP crystallises in space group P4/ncc with Z = 4 and a = 6.995(2), c = 17.491 (4) Å. The structure is shown in Fig. 4.1 and consists of two dimensional networks of water molecules, grouped into squares also containing the remaining H^+ ion, which alternate with layers of UO_2^{2+} and PO_4^{3-} ions. These water molecule networks are located about z = 1/4 and z = 3/4. The UO_2^{2+} ion is linear by symmetry along the c-axis and the uranium atom is co-ordinated equitorially by four coplanar oxygen atoms of four different PO_4^{3-} groups. The hydrogen bond network connects both the water molecules to each other and also to the PO_4^{3-} ions. In each two dimensional water network each water molecule participates in 4 hydrogen bonds, so there are more hydrogen bond sites than available hydrogen ions (for every 4 oxygens there are 9 hydrogens to be distributed over 10 sites). The conductivity mechanism must depend on how these hydrogens are distributed over the available sites.

Both the conductivity and NMR measurements show that HUP and HUAs undergo a transition, the former at 274K and the latter at 301K, to a poorly conducting low temperature phase. For

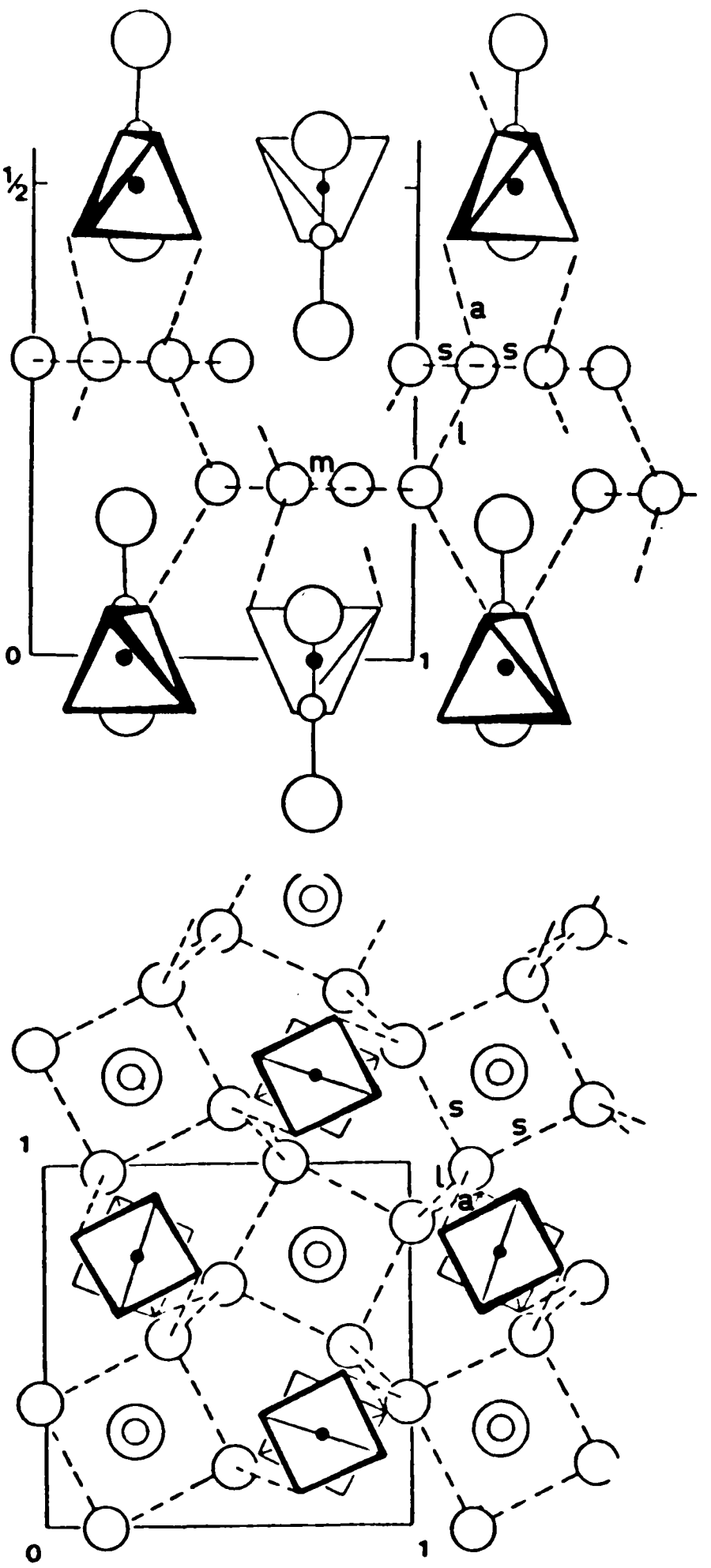


Fig. 4.1. Projection of HUP structure along [100],top, and [001], bottom. Large open circles, uranyl oxygens; medium open circles, water oxygens; open and solid small circles, U and P, respectively. There are three types of hydrogen bond: (s), between water molecules within a square; (a), to the phosphate oxygen; and (l), linking adjacent water squares. The unfilled octahedral site m may contain smaller cations in some structurally related materials (Morosin, 1978 a,b).

HUAs this coincides with the paraelectric to antiferroelectric transition observed by de Benyacar and de Dussel (1975).

Using X-ray powder diffraction, differential scanning calorimetry (DSC), and infra-red spectroscopy, Shilton and Howe (1980) have investigated the nature of these transitions. At 305K, they confirm that HUAs crystallises in space group P4/ncc with $a = 7.150(2)$ and $c = 17.613(5)$ Å. On cooling to 293K, they observe a change to orthorhombic symmetry with $a = 7.128(2)$, $b = 7.168(2)$ and $c = 17.613(5)$ Å. At 260K HUP is also orthorhombic with $a = 6.966(5)$, $b = 7.004(5)$ and $c = 17.43(1)$ Å.

Below their transition temperatures, the crystals appear as two sets of anisotropic domains oriented at approximately 90° to each other with domain walls parallel with (110) of the original tetragonal cell. The enthalpy of the transition, from DSC, has an upper limit of 0.5 kJ per mole of water. IR spectroscopy gave clear evidence for the presence of H_3O^+ ions in both compounds above and below the transitions, and down to 80K. The occurrence of peaks in the region 2200-2300 cm^{-1} is compatible with the presence of $[H_5O_2]^+$ ions, which has also been suggested due to the short hydrogen bond in HUP (2.56 Å) linking adjacent water squares. A definite assignment, however, was not possible due to the presence of water bands in this region.

Thus it has been established that the paraelectric-antiferroelectric transition observed in HUAs is accompanied by a displacive transition resulting in orthorhombic symmetry. A similar transition occurs for HUP, though whether HUP becomes antiferroelectric has yet to be confirmed. That the ordering responsible for the

antiferroelectricity is mainly due to changes in the water behaviour is indicated by the large changes in proton conductivity and NMR relaxation times. The possibility that this is due to "freezing" of the water between layers can be ruled out due to the small size of the enthalpy of transition. (For ice it is 4.8 kJ $mole^{-1}$). Hence the water network is essentially solid above and below the transition in accordance with the activation energy of 20 kJ $mole^{-1}$ for the spin-spin and spin-lattice relaxation times at room temperature. Only a small change in lattice dimensions occurs, and this also indicates a small change in water behaviour rather than a drastic reorganisation, probably involving ordering of the hydrogen bond network, which would inhibit proton conductivity.

de Benyacar and de Dussel (1978), from detailed observations of the domain and subdomain structure of HUAs below the transition temperature, suggest that the antiferroelectric phase must crystalise in point groups 1, $\bar{1}$, 2 or 222. Shilton and Howe (1979), as a result of their observed orthorhombic unit cell, have proposed an ordered hydrogen bonded structure based on the original sized unit cell consistent with 222 in space group $P2_12_12$, which is a sub group of P4/ncc. In a paraelectric to antiferroelectric transition a multiple unit cell usually results (Zheludev, 1971). If, however, the paraelectric structure contains an even number of equivalent "molecules", this may not be necessary in order to realise the superstructure characteristic of an antiferroelectric phase (Känzig, 1957).

$LiUO_2AsO_4.4H_2O$

The "acidic" proton of HUP or HUAs may be easily replaced by another cation to produce closely related compounds. Weigel and Hoffmann (1976) tabulate the unit cell dimensions for a large number of these substituted analogues, although the cation positions for very few of them are known. Ross and Evans (1964) show that in $KUO_2AsO_4.3H_2O$ and $NH_4UO_2AsO_4.3H_2O$, the potassium or ammonium ion simply substitutes randomly for an H_3O^+ ion in the basic HUP structure. The additional hydrogen atom introduced by the NH_4^+ ion completely fills the available sites, thus removing the proton site vacancies required for proton conduction. The situation is very similar with the potassium ion, which reduces the number of available hydrogen bond sites; those remaining (24 on average in the unit cell) are completely filled. The conductivity in the compounds is accordingly three orders of magnitude less than in HUP or HUAs (Johnson, Shilton and Howe, 1981). For structures containing smaller sized ions, eg $Cu(UO_2PO_4)_2.8H_2O$ (Ross, Evans and Appleman, 1964), the unfilled oxygen octahedron labelled m in Fig. 4.1 (ie formed from two uranyl oxygen atoms above and below the plane of four water oxygens) is occupied on an alternating basis. This, it is postulated, removes the need for in-square hydrogen bonding and again all the available sites are fully occupied. No difinitive studies, however, have yet been done to determine exactly the hydrogen bonding arrangements in any of these compounds.

$LiUO_2AsO_4.4H_2O$ is reported by Weigel and Hoffmann to be tetragonal, $a = 7.13(2)$, $c = 9.21(6)$ Å. Conductivity measurements on the

phosphate analogue $LiUO_2PO_4.4H_2O$ by Johnson et al (1981) show that the room temperature conductivity of this compound is several thousand times smaller than that found for HUP, ie 1×10^{-4} ohm^{-1} m^{-1}. The arsenate is similarly a poor conductor (A.T. Howe, personal communication). There appears to be no other information in the literature. We should like to understand the structural constraints acting upon these types of compounds, and how this is related to the observed conductivities and hydrogen bond systems. Perhaps surprising is the observation that $NaUO_2PO_4.3H_2O$ shows relatively high conductivity (1×10^{-2} ohm^{-1} m^{-1}) which has been interpreted in terms of the mobility of the sodium ion.

4.2. Sample Preparation and Experimental

The samples, 8.61g of $DUO_2AsO_4.4D_2O$ and 4.18g of $LiUO_2AsO_4.4D_2O$, were prepared by Dr. M.G. Shilton and supplied by Dr. A.T. Howe.

$HUO_2AsO_4.4H_2O$ was first prepared as described by Howe and Shilton (1980a) by precipitation from a mixture of solutions containing equimolar proportions of uranyl nitrate and H_3AsO_4 at room temperature. The precipitate was washed in distilled water and allowed to dry in air.

Deuteration was effected by submerging the sample for three days in 99.8% D_2O. Excess water was removed by vacuum to a predetermined weight corresponding to $4D_2O \pm 1\%$. This was performed twice. Lumps of DUAs were loaded into a standard thin walled 16mm diameter vanadium sample can without further grinding to encourage a random orientation amongst the plate-like crystallites. The can was sealed with PTFE tape and a rubber washer.

The makers estimated that the equilibrium water content of the sample was 4.0, with minimum free water, and a deuterium content of about 99.6 ± 0.1%.

$LiUO_2AsO_4.4D_2O$ was prepared by stirring DUAs with a large excess of 4M $LiNO_3$ solution for about a day. The lithium substituted compound is less soluble and is formed preferentially. The sample was loaded into a 16mm vanadium can, in a similar manner to DUAs. In this case the D_2O content of the sample is less certain, and is estimated to be in the region 3.5 - 4.0 (Weigel and Hoffmann,1976).

The samples were run on D1A (ILL, Grenoble) at a wavelength of 1.9094 Å (reflection from <115> of the Ge monochromator), calibrated by a nickel standard. DUAs was studied at 305K, 250K and 4K and $LiUO_2AsO_4.4D_2O$ at 294 K. For the low temperature runs on DUAs, the sample was contained in the instrument's standard cryostat. Each run took about 24 hours.

4.3. Structure Refinements and Discussion

The scattering lengths used in the following refinements are $U = 0.85 \times 10^{-12}$cm, $As = 0.64 \times 10^{-12}$cm, $O = 0.58 \times 10^{-12}$cm, $D = 0.667 \times 10^{-12}$cm, $Li = 0.214 \times 10^{-12}$cm (Bacon 1975). In DUAs, deuterium atoms nominally contribute 45% of the coherent scattering of the sample. For the comparative X-ray study, they would contribute 4% at $\sin\theta = 0$ and 0.7% at $\sin\theta/\lambda = 0.5$ A^{-1} (ie at $2\theta \approx 145°$ for $\lambda = 1.909$ Å).

$DUO_2AsO_4.4D_2O$ (DUAs) at 305K

The structure of DUAs at 305K was refined in space group P4/ncc, with the origin at $\bar{1}$, using the atomic parameters obtained from the HUP single crystal study as starting parameters for the heavy

atoms. The deuterium atoms were allowed to occupy the available hydrogen bonding sites in what was considered to be a reasonable manner.

In earlier papers, Howe and Shilton (eg 1979) assumed that the two possible (though crystallographically distinct) hydrogen sites between water molecule oxygens within a square would both be randomly occupied with hydrogen atoms, because both sites have similar chemical environments. A Fourier map, however, based on observed intensities clearly indicates that only one of these sites is occupied, Fig. 4.2. The hydrogen bonding within a square is therefore ordered in a particular sense. Refinement of the occupancy of this site H(1) indicates that it is only 3/4 occupied, ie 12 hydrogen atoms are statistically distributed over the 16 available positions in the unit cell.

The hydrogen atoms H(2) directed towards the oxygen of an AsO_4^{3-} group are linked to the oxygen of a water molecule in agreement with the IR data. These sites are fully occupied with 16 hydrogens per unit cell. The remaining 8 hydrogens in the unit cell, making 36 in all, are in the inter-square linking position. An observed Fourier map, Fig. 4.3, shows that these hydrogens H(3) may be associated with a single maximum in scattering density situated midway between, but not collinear with, the two oxygen atoms of two water molecules in neighbouring squares. This site is at the special crystallographic position 8f ($\bar{x}$ x 1/4) which lies on a two-fold axis of symmetry.

Thus the final refinement involved a total of 54 atomic parameters, including the scale factor and the scattering length of deuterium, and 8 instrumental parameters, ie 2 lattice parameters, 3 halfwidth parameters, the zero point, asymmetry and preferred orientation

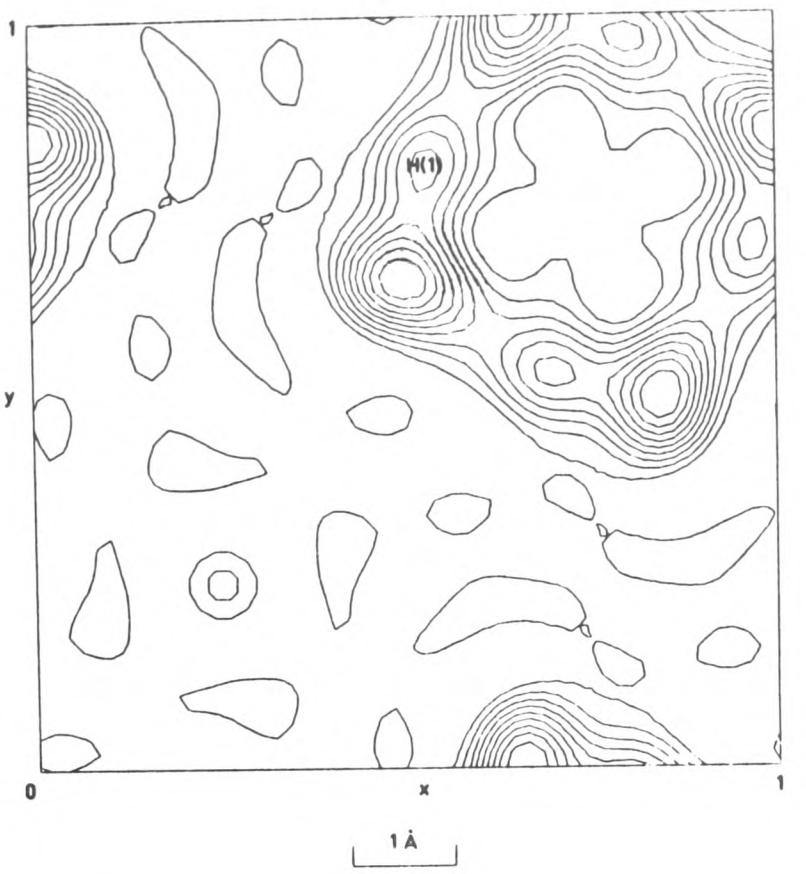


Fig. 4.2. Fourier section based on observed intensities and calculated phases, for $DUO_2AsO_4.4D_2O$ at 305K, parallel to the x,y plane at z = 0.19 through the plane of the water layer. The occupancy of a single hydrogen bond site H(1) is clearly visible.

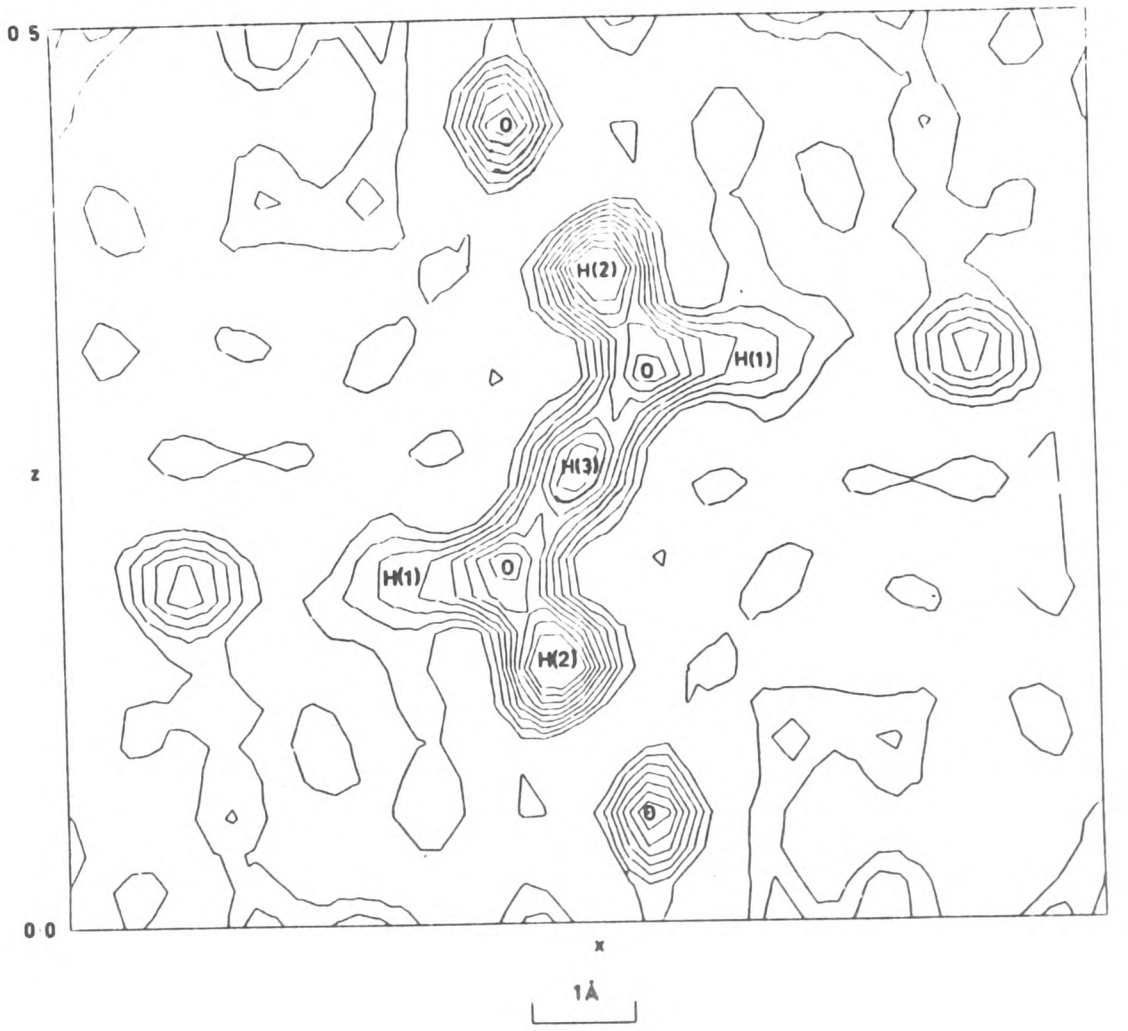


Fig. 4.3. Fourier section based on observed intensities and calculated phases for $DUO_2AsO_4.4D_2O$ at 305K. x is parallel to [110] in the tetragonal unit cell. The maximum in scattering density between the water layers is at z = 1/4.

parameter to correct for a small amount of allignment of the plate-like crystals normal to [001]. There are 265 reflections. The refinement indicated that the degree of deuteration of the sample was better than 98% and that the arrangement of UO_2^{2+} and AsO_4^{3-} ions is essentially identical to that found in HUP. The final R factors were $R_I = 3.88$, $R_{wp} = 6.22$, $R_p = 7.05$, $R_E = 3.58$. The final parameters are shown in Table 4.1. Important interatomic distances are in Table 4.2. The observed, calculated and difference profiles are in Fig. 4.4.

In a second refinement, involving an extra four atomic parameters, the linking hydrogens H(3) were allowed to occupy the general position 16g (x y z), ie with half-occupied equivalent sites on either side of the two-fold symmetry axis. The R factors were $R_I = 3.94$, $R_{wp} = 6.19$, $R_p = 7.03$, $R_E = 3.58$, but the esd's on the atomic co-ordinates and thermal parameters of H(3) increased by factors of 3 and 2 respectively. The other atoms in the structure did not change position by more than one esd, except for O(4) to which H(3) is directly linked. As we shall see, however, neither description of H(3) is essentially correct; both are approximations to what we believe is a rather more complex system of hydrogen bonding, unresolved by the limited quality of powder data, which gives considerable insight into the mechanism of hydrogen transport within this compound.

We can understand the above results for the average unit cell if we assume there to be a mixture of $[H_5O_2]^+$ and H_4O_2 dimers, implying a chemical formula of $[H_5O_2]^+(UO_2AsO_4)^-H_4O_2$. An equal proportion of $[H(1)H(2)O---H(3)---OH(2)H(1)]^+$ and H(1)H(2)O---H(3)-OH(2) formula units gives the required proton to water

Table 4.1.

Final parameters for $DUO_2AsO_4.4D_2O$ at 305K in space group P4/ncc (origin at $\bar{1}$). a = 7.1615(1), c = 17.6390(2) Å. ESD's of refined parameters in parenthesis.

Atom	Position	Point Symmetry	x	y	z	N	B_{11}	B_{22}	B_{33}	B_{12}	B_{13}	B_{23}
U	4c	4	1/4	1/4	0.0527(1)	4	0.62(6)	0.62(6)	1.0(1)	0	0	0
As	4b	$\bar{4}$	3/4	1/4	0	4	0.35(6)	0.35(6)	1.7(1)	0	0	0
O(1)	4c	4	1/4	1/4	0.1545(2)	4	1.86(8)	1.86(8)	1.42(2)	0	0	0
O(2)	4c	4	1/4	1/4	-0.0482(2)	4	2.04(9)	2.04(9)	1.2(2)	0	0	0
O(3)	16g	1	0.5681(2)	0.2048(2)	0.0573(1)	16	0.56(5)	1.48(5)	2.07(8)	-0.02(4)	0.41(7)	0.47(5)
O(4)	16g	1	0.1476(5)	0.9977(5)	0.3095(2)	16	5.4(2)	9.8(3)	2.6(2)	-2.9(1)	0.8(1)	2.3(2)
H(1)	16g	1	0.3037(9)	0.0404(6)	0.3112(2)	12	15.3(3)	7.6(2)	2.7(2)	5.3(2)	0.9(2)	0.9(2)
H(2)	16g	1	0.5757(3)	0.1283(2)	0.3556(2)	16	5.7(1)	3.4(1)	3.0(1)	1.2(1)	-0.2(1)	0.2(1)
H(3)	8f	2	0.4057(3)	-0.4057(3)	1/4	8	6.3(1)	6.3(1)	10.0(4)	1.8(2)	-3.8(2)	-3.8(2)

$R_p = 7.05$ $R_{wp} = 6.22$ $R_I = 3.88$ $R_E = 3.58$

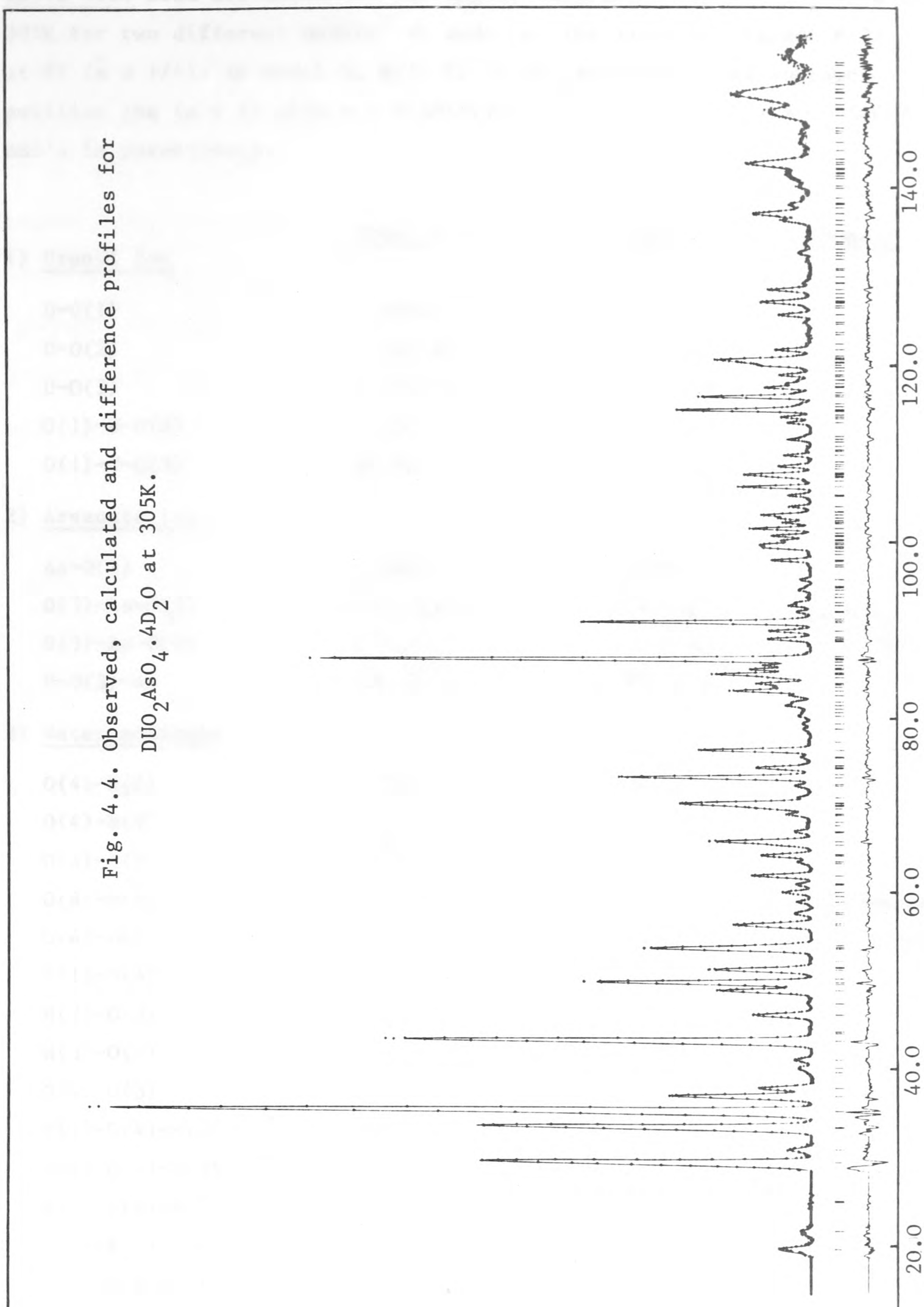


Fig. 4.4. Observed, calculated and difference profiles for $DUO_2AsO_4.4D_2O$ at 305K.

Table 4.2. Bond distances (Å) and angles (degrees) for $DUO_2AsO_4.4D_2O$ at 305K for two different models. In model a, the linking hydrogen H(3) is at 8f ($\bar{x}$ x 1/4). In model b, H(3) is in the general crystallographic position 16g (x y z) with x = 0.3847(11), y = 0.5710(11), z = 0.2640(7). ESD's in parenthesis.

	Model a	Model b	Comment
1) Uranyl ion			
U-O(1)	1.796(3)	1.794(3)	
U-O(2)	1.781(4)	1.782(4)	
U-O(3)	2.303(1)	2.304(1)	
O(1)-U-O(2)	180	180	
O(1)-U-O(3)	88.00(6)	88.00(6)	
2) Arsenate ion			
As-O(3)	1.680(1)	1.680(1)	
O(3)-As-O(3)	106.00(7)	105.93(7)	$z_1 = z_2$
O(3)-As-O(3)	111.23(6)	111.27(6)	$z_1 = -z_2$
U-O(3)-As	136.0(1)	136.0(1)	
3) Water molecule			
O(4)-H(1)	1.159(7)	1.145(8)	
O(4)-H(2)	0.979(4)	0.984(5)	
O(4)-H(3)	1.297(4)†	0.99(1)	
O(4)-O(4)	2.758(5)	2.751(5)	side of square
O(4)-O(4)	2.565(5)	2.576(5)	link distance
H(1)-O(4)	1.617(7)	1.624(8)	
H(2)-O(3)	1.845(3)	1.839(3)	
H(3)-O(4)	1.297(4)†	1.62(1)	
O(4)-O(3)	2.820(4)	2.821(4)	
H(1)-O(4)-H(2)	104.9(4)	105.5(4)	
H(1)-O(4)-H(3)	116.0(3)	112.1(6)	
H(2)-O(4)-H(3)	111.1(3)	113.4(7)	
O(4)-H(1)-O(4)	166.7(4)	166.6(4)	
O(3)-H(2)-O(4)	174.3(3)	174.7(3)	
O(4)-H(3)-O(4)	162.6(3)	162.0(8)	

† Related by symmetry in model a

ratio of 1 : 4 and an occupancy of H(1) of 3/4, as observed. The average oxygen oxygen separation within a dimer, 2.565(5) Å, is shorter than that between water molecules within a square, 2.758(5) Å, which justifies our description in terms of dimers. From powder data, however, we are unable to refine the atomic parameters of these two species separately. Thus the average oxygen oxygen separation of 2.565(5) Å probably hides a considerable difference between the actual distances in the $[H_5O_2]^+$ and H_4O_2, and this leads to abnormally large temperature factors for the water molecule oxygen. We are also unable to assess whether the hydrogen bond in $[H_5O_2]^+$ is centred and symmetric, or composed of two equally populated asymmetric hydrogen bonds. We would not expect the former case unless the actual oxygen oxygen separation in $[H_5O_2]^+$ were close to 2.4 Å (Thomas and Liminga, 1978). In the H_2O_4 dimer, however, there must be a displacement of the linking hydrogen H(3) towards the water oxygen which is lacking an H(1) hydrogen.

We therefore consider our single maximum in scattering density at $(\bar{x}$ x 1/4) to be best described as the statistical superposition of two pairs of dimeric units of the type $[H_2O\text{-}H\text{——}OH_2]^+$ and $[H_2O\text{——}H\text{-}OH_2]^+$, and $HO\text{-}H\text{——}OH_2$ and $H_2O\text{——}H\text{-}OH$, with the two units of each pair being symmetrically related to one another by the two-fold axis passing through their mid-point. A large anisotropy in H(3) along the O-O direction may be evidence for the displacement of H(3) from the central position on the symmetry axis in $[H_5O_2]^+$ as well as in H_4O_2. Both types of species are constrained to very similar orientations by a strong interaction between H(2) and the charged arsenate group.

The powder neutron diffraction evidence is sufficient to show that hydrogen migration between adjacent H(1) sites within a square of water molecules involves an overall jump distance of 2.191(8) Å. That such a process is occurring at room temperature is strongly suggested by the very high temperature factors on H(1), which is indicative of a marked interaction between H(1) and its next nearest water oxygen. The principal axis of the thermal elipsoid is almost colinear with the O-O separation, Fig. 4.5. Attempts to refine two statistically occupied hydrogen sites between each water molecule were however unsuccessful, in agreement with the observed Fourier map. The hopping of the H(1) hydrogen to an adjacent empty site allows the interchange between the $[H_5O_2]^+$ and H_4O_2 species. Transport of hydrogen atoms between neighbouring layers can then be easily effected by the coupled rotation through $\approx$ 120° of the two water molecules of a H_4O_2 unit about their respective O-H(2) axes, Fig. 4.6.

Bernard et al (1981) have taken this simple basic mechanism, and, by a detailed consideration of the ionic pathway required for charge migration (conduction) or charge circulation (diffusion), have suggested how this picture might account for the observed difference in activation energies for the two processes.

$DUO_2AsO_4.4D_2O$ (DUAs) at low temperature

The diffraction patterns of DUAs at 250K and 4K appeared to be almost identical, and were more complex than at room temperature with obvious splitting of certain peaks, as was previously reported by Shilton and Howe (1980). The latter's postulated model in the orthorhombic space group $P2_12_12$, however, cannot be correct due to the presence of the weak peak at 15.3 degrees which may be

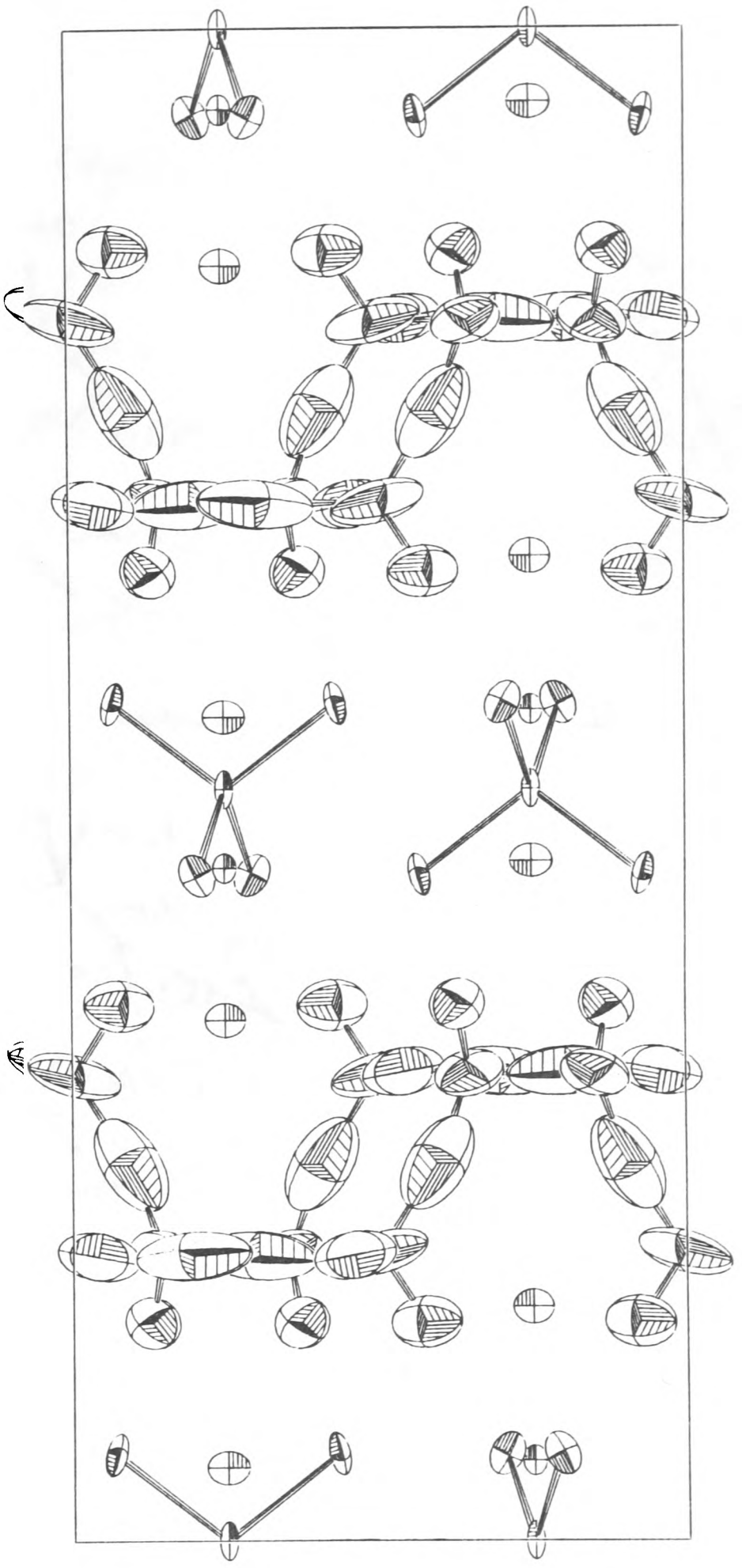


Fig. 4.5. ORTEP plot of $DUO_2AsO_4.4D_2O$ at 305K. Both hydrogen atoms H(1) and H(3) show a marked anisotropy along the direction of their respective hydrogen bonds.

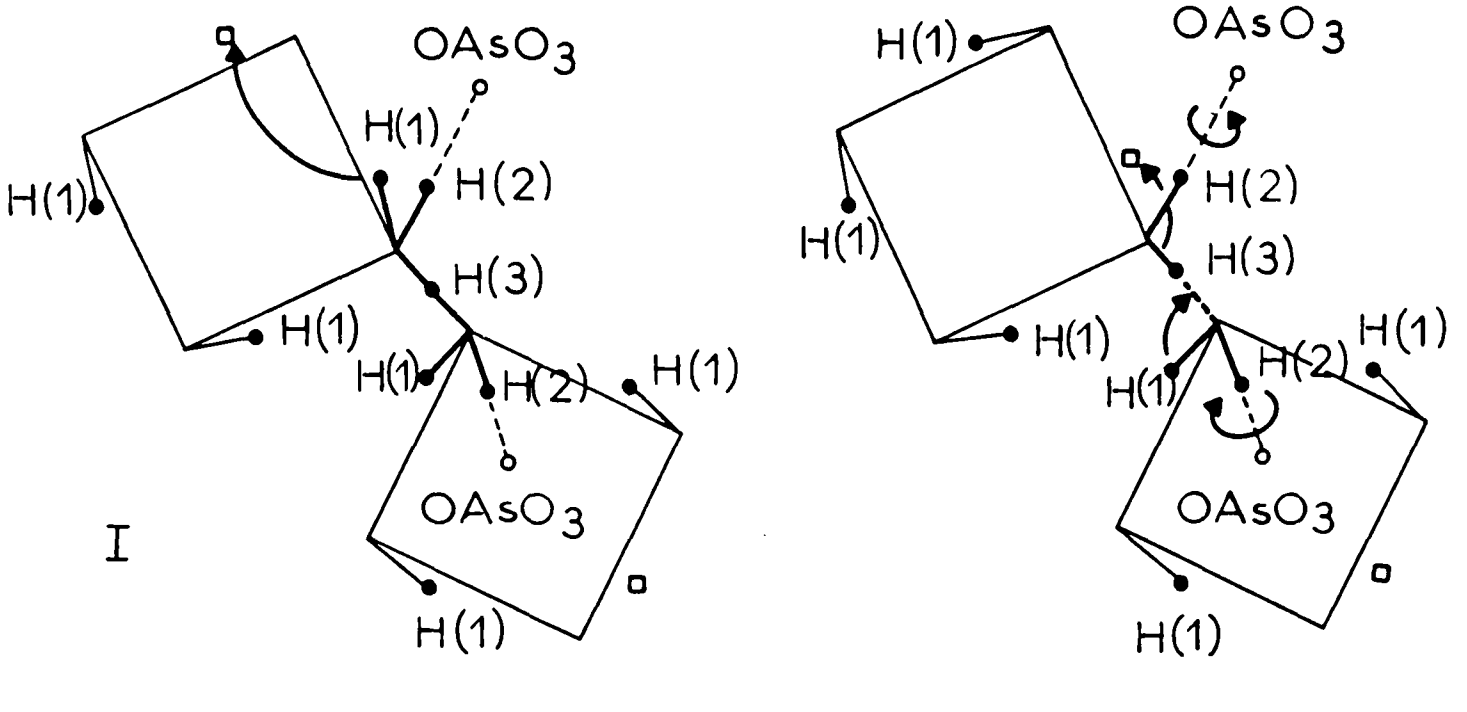


Fig 4.6. Each square contains on average one vacant H(1) hydrogen bond site. Proton hops between filled and unfilled sites convert $[H_5O_2]^+$ units into H_4O_2 dimers, sequence (I)→(II). The H_4O_2 dimer may reverse configuration by means of two coupled rotations of the water molecules about the O(4)-H(2)-O(3) axes, thus transferring a proton from one layer to the next, sequence (II)→(III).

indexed as 010.

To ensure that the room temperature structure determination was of the fully hydrated compound, the sample had been sealed in its vanadium can whilst still slightly wet. As a result, a number of peaks from deuterated ice were visible in the pattern. There are no visible superlattice reflections, which is compatible with a transition from a paraelectric phase whose unit cell contains an even number of equivalent molecules (Känzig, 1957).

The structure of ice at atmospheric pressure has been studied by Peterson and Levy (1957), Chamberlain et al (1973), and by Kuhs and Lehmann (1981) by single crystal neutron diffraction. The space group is $P6_3/mmc$, with lattice parameters determined as a = 4.4968, c = 7.1398 Å from X-ray powder studies at 13K (Brill and Tippe, 1967). There were therefore a total of 41 ice peaks distributed throughout and overlapping with the diffraction pattern of DUAs, which makes exclusion of these regions practically impossible since there would be very little data left to refine. Use was therefore made of the modified Rietveld procedure of Bendall and Thomas (1980) which allows the simultaneous refinement of both patterns. In the following discussion of the structural refinements attempted for DUAs, in each case the 41 ice peaks were accounted for by refining a contribution due to the ice in space group $P6_3/mmc$. This requires an effective scale factor, by means of the stoichiometrically constrained atomic occupation factors as discussed in Chapter 2, two lattice parameters, three halfwidth parameters, a single isotropic temperature factor for both crystallographically distinct hydrogen atoms, an isotropic

temperature factor for oxygen, and atomic positional parameters which are given by Peterson and Levy at 123K as

D(1)	4f	1/3	2/3	z		z = 0.1980(7); N = 2
D(2)	12k	x	2x	z	x = 0.4545(9);	z = 0.0172(4); N = 6
O	4f	1/3	2/3	z		z = 0.0620(4); N = 4

ie a total of 5 machine parameters and 7 structural parameters exclusive to ice. In addition, in each refinement there was a single scale factor, zero point and asymmetry parameter for the pattern. For DUAs there was the appropriate number of atomic, thermal and lattice parameters, three halfwidth parameters, a preferred orientation parameter applied with normal [001] as at room temperature, and finally the scattering length of deuterium. Since there are no visible superlattice peaks, models were only attempted based on the original sized unit cell. According to de Benyacar and de Dussel (1979), who also note the absence of any clear evidence for the formation of a supercell, the structure must exist in point group 222, 2, $\bar{1}$ or 1. There is no suitable orthorhombic space group which fits a sensible structure and the extinction rules. The structure must then be monoclinic or triclinic, which requires a model with more reflections and more parameters than the standard multi-pattern Rietveld program can handle. The program was therefore redimensioned to accommodate up to 3000 reflections, 300 independent variables, 100 cyrstallographically distinct atoms, with a maximum of 60 reflections contributing to any single data point. This probably exceeds any future demand.

Because the available evidence suggests a displacive transition from the room temperature structure with ordering of the hydrogen bond network, only space groups which were subgroups of P4/ncc were considered. A tentative refinement was attempted for the 4K data in $P2_1/c$, which provides the simplest structural model conforming to our criteria, though is incompatible with the arguments of de Benycar et al. The hydrogen atoms H(1) within the squares of water molecules were arbitrarily ordered over three of the four possible hydrogen bond sites so as to simulate the freezing out of $[H_5O_2]^+$ and H_4O_2 units at opposite corners of the square. All atoms were placed in general positions 4e (x y z), with isotropic temperature factors which were constrained to be equal for all atoms which were symmetrically equivalent at room temperature. With a total of 72 atomic parameters for DUAs (making a grand total of 96 variables) and 1073 reflections, the refinement terminated with R_{wp} = 16.13 and R_E = 3.04. There were negative temperature factors for U, As, O1 and O3, indicating a far from satisfactory result. The values of the positional parameters, however, were not unreasonable.

Reducing the symmetry to $P2_1$ or Pc (the latter again disallowed by de Benyacar et al) doubles the number of crystallographically distinct atoms. A similar regime of atomic positions and temperature factors was followed as for $P2_1/c$, to give in each case 135 atomic parameters, and a total of 159 variables. The program consistently failed with a singular least squares matrix, which may have been due to strong correlations between parameters as a result of an improperly chosen space group, or possible because the sheer size of the normal matrix makes it very difficult to invert

(Acton, 1970). If the refinements were split up into two steps, the first involving 85 variables and keeping the uranyl arsenate atomic parameters fixed, followed by the second of 87 variables keeping the water atomic parameters fixed, then a progressive reduction in the R factor could be obtained. For $P2_1$, with 1178 total reflections, the best fit produced R_{wp} = 12.81, R_E = 3.05, but with negative temperature factors in As and O2. The refinement in Pc with 1077 reflections resulted in R_{wp} = 12.85, R_E = 3.03 but with negative temperature factors on many atoms. Neither of these models was considered satisfactory.

The inclusion of two extra lattice parameters in space group $P\bar{1}$ led to a dramatic improvement in fit. With a total of 2098 reflections, the 161 variables could all be refined simultaneously and terminated with R_{wp} = 4.19, R_E = 3.00, R_p = 4.37, R_I = 2.57. The observed, calculated and difference profiles are shown in Fig. 4.7. The final parameters are in Table 4.3. All the temperature factors are sensible, and the occupancy of deuterium indicated that deuteration was 98 ± 1% complete. A Fourier map based on observed intensities and calculated phases was in very good agreement with the final atomic parameters, and a difference map showed no peaks of intensity greater than 1.3% of the maximum observed peak. This however is hardly surprising, for in profile refinement the partitioning of the scattered intensity between overlapping peaks is done on the basis of the calculated model. In this pattern there is extreme overlap of reflections with an average of about 2.4 profile points per reflection in the first 80°, and for the last 80° about 1.0 profile points per reflection, making an average for the pattern of 1.4 profile points per reflection.

Table 4.3. - Final parameters for $DUO_2AsO_4.4D_2O$ at 4K in space group $P\bar{1}$. a = 7.1644(1), b = 7.1124(1), c = 17.5537(3) Å, α = 90.187(3), β = 89.947(4), γ = 90.003(4). ESD's of refined parameters in parenthesis.

Atom	x	y	z	B_{iso}
U(1)	0.742(1)	0.750(2)	0.4466(6)	0.07(4)
U(2)	0.256(1)	0.250(2)	0.0549(6)	0.07(4)
As(1)	0.752(2)	0.250(2)	0.5004(9)	0.21(6)
As(2)	0.756(2)	0.255(2)	0.0029(9)	0.21(6)
O1(1)	0.746(2)	0.751(2)	0.3451(11)	0.35(7)
O1(2)	0.251(2)	0.249(2)	0.1562(11)	0.35(7)
O2(1)	0.259(2)	0.252(3)	0.4510(9)	0.13(7)
O2(2)	0.757(2)	0.743(3)	0.0463(9)	0.13(7)
O3A	0.072(2)	0.795(2)	0.4399(9)	0.17(4)
O3A2	0.557(2)	0.196(2)	0.0543(9)	0.17(4)
O3B	0.426(2)	0.691(2)	0.4387(9)	0.17(4)
O3B2	0.930(2)	0.300(2)	0.0604(9)	0.17(4)
O3C	0.791(2)	0.424(2)	0.4391(7)	0.17(4)
O3C2	0.298(2)	0.564(2)	0.0515(7)	0.17(4)
O3D	0.694(2)	0.063(2)	0.4429(9)	0.17(4)
O3D2	0.191(2)	0.930(2)	0.0528(9)	0.17(4)
O4A	0.142(2)	0.994(3)	0.3116(10)	0.72(4)
O4A2	0.629(2)	0.995(3)	0.1881(10)	0.72(4)
O4B	0.354(2)	0.496(3)	0.3096(10)	0.72(4)
O4B2	0.843(2)	0.492(3)	0.1894(9)	0.72(4)
O4C	0.893(1)	0.296(2)	0.2970(8)	0.72(4)
O4C2	0.423(2)	0.697(2)	0.1989(9)	0.72(4)
O4D	0.484(2)	0.166(3)	0.3106(10)	0.72(4)
O4D2	0.994(2)	0.834(3)	0.1872(10)	0.72(4)
H1A	0.272(2)	0.051(3)	0.3116(12)	1.45(5)
H1A2	0.761(2)	0.955(3)	0.1874(12)	1.45(5)
H1B	0.415(2)	0.373(3)	0.3118(11)	1.45(5)
H1B2	0.906(2)	0.623(3)	0.1901(11)	1.45(5)
H1C	0.996(2)	0.202(2)	0.3044(10)	1.45(5)
H1C2	0.505(2)	0.807(2)	0.1951(10)	1.45(5)
H2A	0.122(2)	0.922(2)	0.3558(10)	1.32(5)
H2A2	0.617(2)	0.051(2)	0.1399(10)	1.32(5)
H2B	0.380(2)	0.565(2)	0.3576(11)	1.32(5)
H2B2	0.879(2)	0.428(2)	0.1395(12)	1.32(5)
H2C	0.885(2)	0.342(2)	0.3517(9)	1.32(5)
H2C2	0.379(2)	0.643(2)	0.1504(9)	1.32(5)
H2D	0.565(2)	0.135(2)	0.3568(11)	1.32(5)
H2D2	0.060(2)	0.855(2)	0.1395(11)	1.32(5)
H3B	0.389(2)	0.578(2)	0.2650(8)	1.40(8)
H3B2	0.881(2)	0.395(2)	0.2418(9)	1.40(8)
H3D	0.565(3)	0.111(2)	0.2665(10)	1.40(8)
H3D2	0.056(3)	0.876(2)	0.2294(10)	1.40(8)

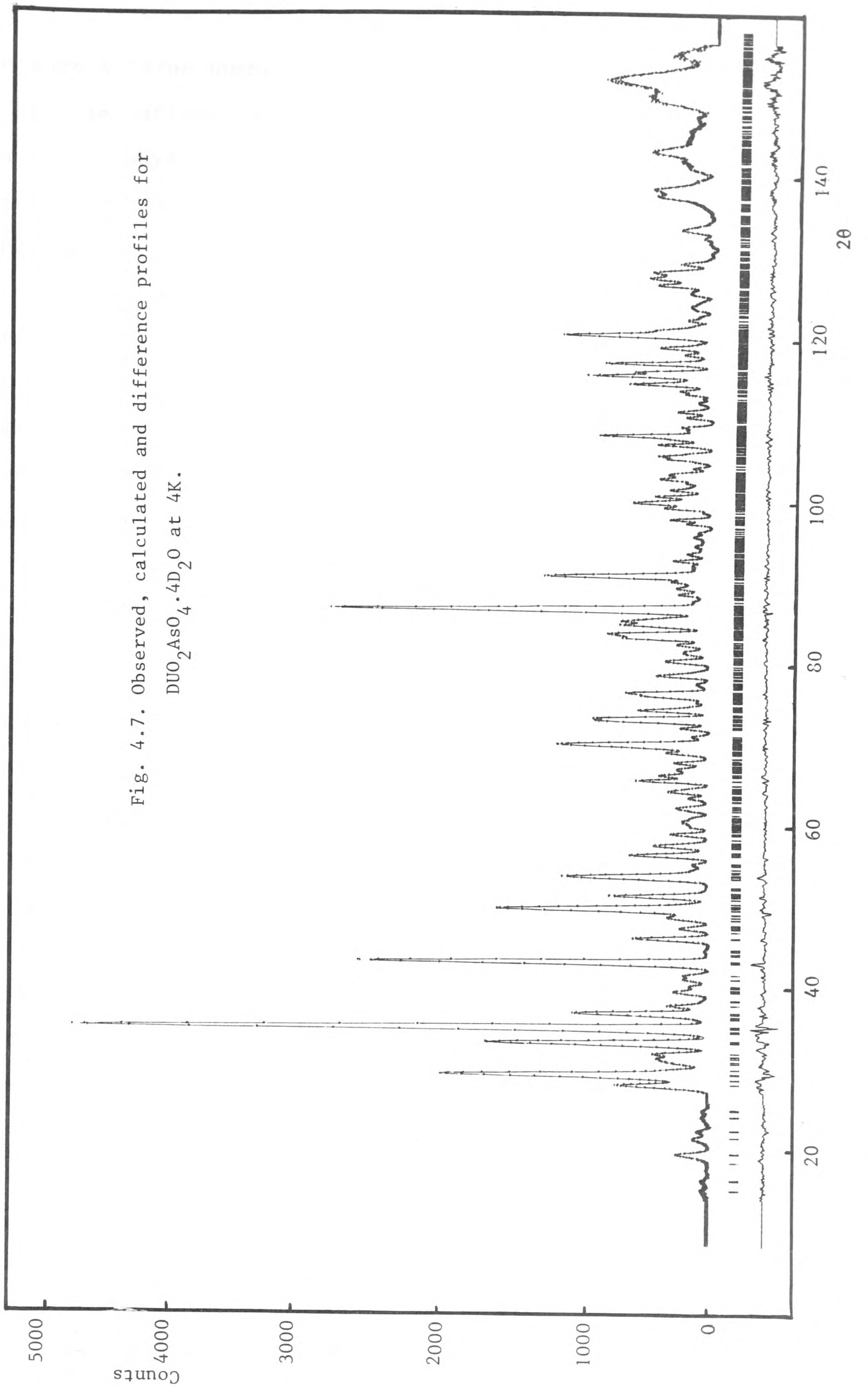


Fig. 4.7. Observed, calculated and difference profiles for $DUO_2AsO_4.4D_2O$ at 4K.

With such a large number of parameters, one might imagine that any profile pattern could be fitted to this degree of accuracy, with little physical significance for the result. However, we have argued that the structure is of low symmetry, and the models in $P2_1$ and Pc each have only two less parameters than $P\bar{1}$. All three models describe the same qualitative arrangement of atoms and differ essentially in the symmetry relationship between the various groups of atoms. The large difference in R factors between the triclinic and monoclinic models is clear evidence that the former is a far superior description, and that the parameters themselves are of structural significance. Indeed, if the space group really is $P\bar{1}$ then it would be impossible to properly describe the structure without them.

Sakata and Cooper (1979) have recognised the difficulty in assessing the accuracy of structural parameters obtained by profile refinement, as discussed in Chapter 2. They considered that correlations between profile points in a single Bragg peak, which were treated as independent observations, gave rise to statistical errors which may become more acute with peak overlap. In DUAs at 4K, there is extreme peak overlap and the pattern approaches the limit where on average each profile point represents a piece of structural information, ie the structure factor, although this information is severely scrambled in a powder pattern and can only be retrieved by the method of profile analysis with an essentially correct structural model. In this example we are perhaps fortunate due to the presence of the contaminating ice which has a well defined structure. As far as the profile analysis method or least squares fit is concerned, there is no particular signifi-

cance attached to one phase or the other, so we may use the result for ice to assess the quality of the information that may be extracted from the pattern.

The final parameters, bond lengths and bond angles for ice, compared to some other values found in the literature, are given in Table 4.4. The agreement is quite good although quantitatively there are considerable differences of several standard deviations. This may reflect an essentially statistically well defined structure, with badly underestimated esd's, or a rather poorer fit of the atomic parameters with good esd's, due to the simplicity of the structural model employed and the unfavourable nature of the data to which it must be fitted. The ice atomic parameters are determined wholly from weak peaks in the diffraction pattern, which contribute only 5.4% of the total scattered Bragg intensity. Considering this, it is perhaps remarkable that such close agreement could be achieved. We must recognise however that the errors in this result may be underestimated for the major phase DUAs, and so concentrate more fully on the qualitative nature of the structure. The lattice parameters of ice, $a = 4.5050(7)$, $c = 7.3347(5)$ Å, are well determined with $c/a = 1.6281$, which compares well with Brill and Tippe (1967) who at 13K have $c/a = 1.6278$ for H_2O.

Some actual and average values of the lengths and angles for the various bond types found in DUAs are given in Tables 4.5 and 4.6. Although the uranyl arsenate framework is somewhat distorted from room temperature in this low temperature phase, the arrangement of atoms is very similar and the average interatomic distances

Table 4.4(a). Final atomic parameters for deuterated ice at 4K compared to some others taken from the literature. ESD's in parenthesis.

	4K[a]	123K[b]	223K[b]
z D(1)	0.205(1)	0.1980(7)	0.1989(9)
x D(2)	0.454(1)	0.4545(9)	0.4551(13)
z D(2)	0.017(1)	0.0172(4)	0.0182(6)
z O	0.066(1)	0.0620(4)	0.0629(6)
B D	2.2(2)	-	-
B O	1.2(1)	-	-
B_{11} D(1)	-	2.41(13)	3.23(22)
B_{33} D(1)	-	1.81(12)	2.97(28)
B_{11} D(2)	-	2.29(21)	3.30(27)
B_{22} D(2)	-	1.85(12)	2.80(26)
B_{33} D(2)	-	2.43(10)	3.05(15)
B_{13} D(2)	-	0.24(18)	0.24(18)
B_{11} O	-	1.53(11)	2.39(22)
B_{33} O	-	1.48(10)	2.29(17)

Table 4.4(b). Bond distances and angles for ice.

	4K[a]	60K[c]	60K[d]	77K[e]	123K[b]	223K[b]
O-O'	2.695(7)	2.7490(10)	2.7490	2.744(2)	2.755(6)	2.752(8)
O-O''	2.777(2)	2.7517(6)	2.7517	2.741(1)	2.746(2)	2.765(2)
$O-D_1$	1.019(10)	1.0036(13)	1.0127	0.999(9)	0.997(7)	1.000(9)
$O-D_1$ †	-	-	-	1.018(9)	1.008	1.011
$O-D_2$	1.009(7)	1.0040(6)	1.0121	1.006(5)	0.997(4)	1.007(5)
$O-D_2$ †	-	-	-	1.023(5)	1.009	1.015
O'-O-O''	110.49(13)	109.34(1)	109.35	109.33(10)	109.30(2)	109.55(15)
O''-O-O'''	108.43(12)	109.60(2)	109.60	109.55(18)	109.63(2)	109.40(2)
D_2-O-D_2'	108.0(7)	109.68(9)	110.10	109.83(33)	109.90(25)	109.87(27)
D_1-O-D_2	110.9(4)	109.26(9)	108.84	109.15(47)	109.18(22)	109.10(30)

† Corrected for thermal motion.

a, This work, D_2O; b, Peterson and Levy (1957), single crystal, D_2O; c, Kuhs and Lehmann (1981), single crystal, H_2O; d, Kuhs and Lehmann (1981), with an anharmonic probability density function for hydrogen; e, Chamberlain et al (1973), single crystal, D_2O.

and angles are only moderately altered. For the water layers, there are most significant changes with ordering of the three H(1) hydrogens over the four possible sites per water square. Fig. 4.8 shows the new arrangement of oxygen and hydrogen atoms at z = 0.19 and z = 0.31. Each "square" posseses a hydrogen vacancy and a single water molecule whose plane runs roughly parallel with the z-axis and has no H1 hydrogen of its own (ie O4D and O4D2). The "squares" are rather distorted and buckled from room temperature. Each water oxygen is connected to the oxygen of an arsenate group via a hydrogen (H2) bond and to another water molecule in the next level via a linking (H3) hydrogen.

From Fig. 4.9 it can be seen that the water molecules have formed hydrogen bonded chains which alternate between z $\tilde{\sim}$ 0.19 and z $\tilde{\sim}$ 0.31 via the H3 linking hydrogens. Two such chains, B and B', run in the direction of the b-axis, and are cross linked by only one chain, A, along the a-axis. The intersection of two chains always involves a water molecule which has no directly bound H1 (O4D or O4D2), and the A chain may be considered as being composed of sets of two H_4O_2 dimers which are ordered such that they occupy two adjacent corners of a water square, but with reversed configurations so they are linked by a single in-square hydrogen bond. Thus water oxygens O4A and O4D each comprise part of two different adjacent H_4O_2 dimers, which are bonded in the square by hydrogen H1A and linked to the second oxygen of each dimer, O4D2 and O4A2, by H3D2 and H3D respectively. The oxygen oxygen distances within dimers, 2.67(2) and 2.68(2) Å, are less than the distances between them, 2.86(2) and 2.74(2) Å, and the sequence along the A chain is, (ignoring all hydrogens directed towards the arsenate oxygens),

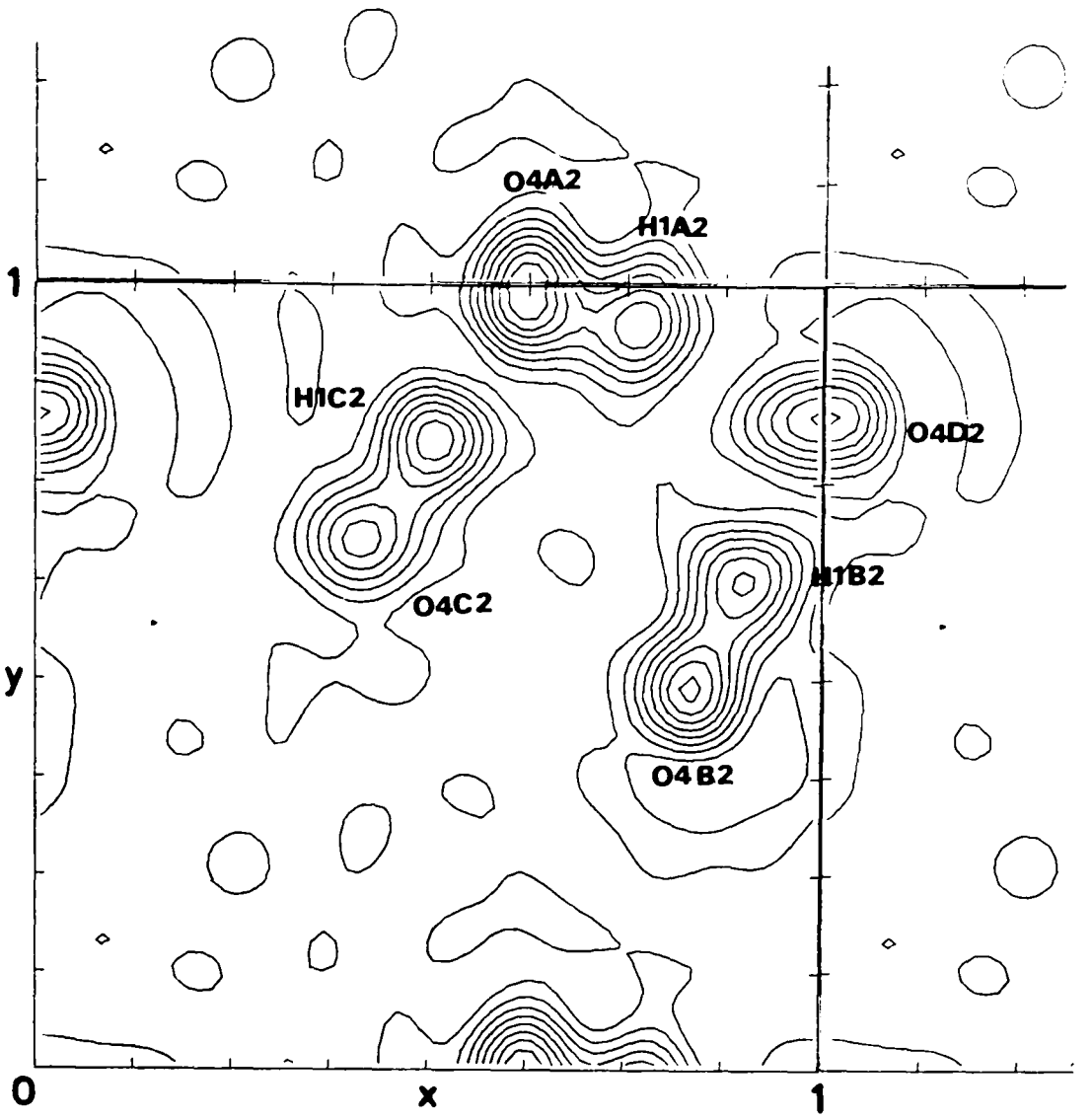


Fig. 4.8. Fourier sections based on observed intensities and calculated phases, for $DUO_2AsO_4.4D_2O$ at 4K, through z = 0.19, (top), and z = 0.31, (bottom), showing the arrangement of the water layers.

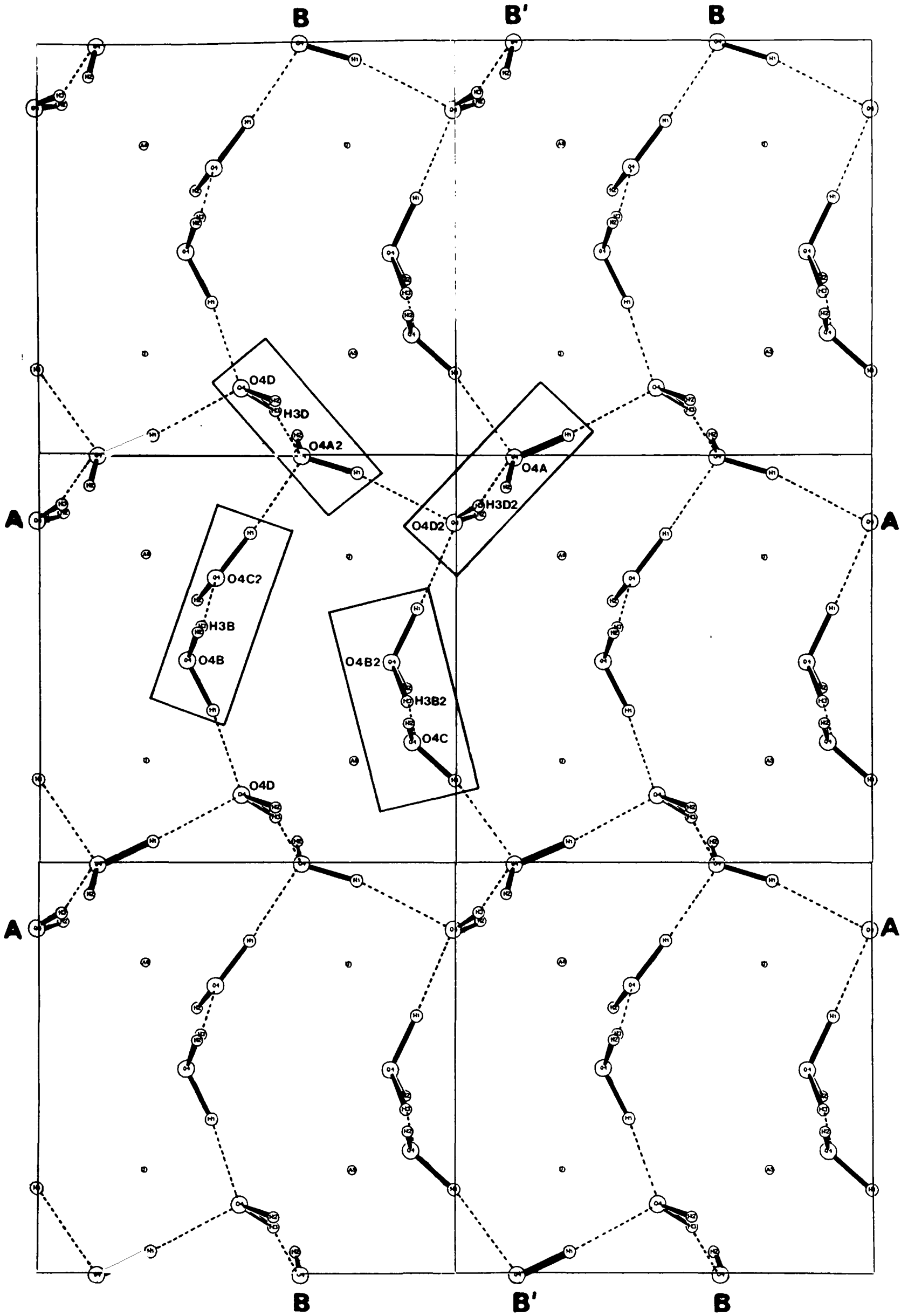


Fig. 4.9. Six unit cells of $DUO_2AsO_4.4D_2O$ at 4K showing the formation of the hydrogen bonded water chains. Hydrogen bonds are shown dotted.

-{O4D-H3D---O4A2-H1A}-{O4D2-H3D2---O4A-H1A}-. The alternating short then long hydrogen oxygen distances along the chain, as adjacent dimers reverse configuration, ensure that the chain is essentially neutral and non-polarised.

Each of the two types of water dimer in the A chain also comprises part of either the B or the B' chains for which they effect the intersection with the A chain. The rest of the B and B' chains is formed by an $[H_5O_2]^+$ ion. The extra proton is accommodated on the water molecule (B or B2) which is hydrogen bonded in the square to the oxygen of a water dimer which has no H1 hydrogen, and must stabilise this configuration. The oxygen oxygen distance within the $[H_5O_2]^+$ units is very short, 2.38(2) and 2.47(2) Å, with the effect of the extra proton being such that the distance to the water dimer of the A chain is generally shorter than within the dimer itself, (the O4C-O4A separation of 2.80(2) Å being an exception). The sequence along the B chain is -{O4B-H3D---O4A2}-{H1C2-O4C2---H3B-O4B-H3B2}$^{+}_{-}$ and along B', -{O4A---H3D2-O4D2}-{H1B2-O4B2-H3B2---O4C-H1C}$^{+}_{-}$.

For the latter chain, the linking hydrogen H3B2 which joins the two water oxygens of the $[H_5O_2]^+$ unit (separated by 2.38(2) Å) is situated almost midway, with O-H distances of 1.18(2) and 1.21(2) Å and a hydrogen bond angle of 175.3(18) degrees. The geometry of the water molecule O4C is very distorted, with H-O-H angles of 97.5(18), 123.3(17) and 124.5(16) degrees, whilst its neighbouring water molecule, O4B2, is not. A similar situation is observed for the very short (O-O = 2.41 Å), almost centred, though non-symmetric $[H_5O_2]^+$ unit found in $HCl.2H_2O$, which has one almost planar water molecule with H-O-H angles of 108, 122 and 123 degrees, but H-O-H angles of 107, 109 and 111 degrees for its

Table 4.5. Bond distances (Å) and angles (degrees) for the uranyl arsenate framework in $DUO_2AsO_4.4D_2O$ at 4K, compared to the values at room temperature. ESD's in parenthesis. For certain bond types, only the extreme and average values are given. In these cases, "X" stands for either A, B, C or D.

1) Uranyl ion	Value(s)	Average	Room temperature
U(1)-O1(1)	1.78(2)		
U(2)-O1(2)	1.78(2)	1.78(2)	1.796(3)
U(1)-O2(1)	1.80(2)		
U(2)-O2(2)	1.78(2)	1.79(2)	1.781(4)
O1(1)-U(1)-O2(1)	179.5(10)		
O1(2)-U(2)-O2(2)	175.6(10)	177.5(10)	180
U(1)-O3A	2.39(2)		
U(1)-O3B	2.31(2)		
U(1)-O3C	2.35(2)		
U(1)-O3D	2.26(2)	2.33(2)	2.303(1)
U(2)-O3A2	2.19(2)		
U(2)-O3B2	2.36(2)		
U(2)-O3C2	2.26(2)		
U(2)-O3D2	2.32(2)	2.28(2)	2.303(1)
O1(1)-U(1)-O3X	86.3(7) - 88.1(7)	87.2(7)	88.00(6)
O2(1)-U(1)-O3X	92.3(8) - 93.3(7)	92.8(8)	92.00(6)
O1(2)-U(2)-O3X2	86.6(7) - 92.0(8)	90.1(8)	88.00(6)
O2(2)-U(2)-O3X2	87.0(8) - 93.0(8)	89.9(8)	92.00(6)
2) Arsenate ion			
As(1)-O3X	See Table 4.6.	1.70(2)	1.680(1)
As(2)-O3X2	See Table 4.6.	1.68(2)	1.680(1)
O3A-As(1)-O3B	102.5(11)		
O3C-As(1)-O3D	103.6(11)	103.1(11)	106.00(7)
O3A-As(1)-O3C	115.1(10)		
O3A-As(1)-O3D	113.8(11)		
O3B-As(1)-O3C	110.2(10)		
O3B-As(1)-O3D	111.8(10)	112.7(10)	111.23(6)
O3A2-As(2)-O3B2	110.6(12)		
O3C2-As(2)-O3D2	109.0(11)	109.8(12)	106.00(7)
O3A2-As(2)-O3C2	107.4(9)		
O3A2-As(2)-O3D2	107.5(10)		
O3B2-As(2)-O3C2	112.4(11)		
O3B2-As(2)-O3D2	109.8(10)	109.3(10)	111.23(6)
U(1)-O3X-As(1)	130.4(10) - 134.9(10)	132.8(10)	136.0(1)
U(2)-O3X2-As(2)	134.4(10) - 140.1(10)	137.7(10)	136.0(1)

Table 4.6. Bond distances (Å) and angles (degrees) for the water networks in $DUO_2AsO_4.4D_2O$ at 4K. ESD's in parenthesis.

a) The water molecules themselves and the hydrogen bond to the arsenate group.Mean values are compared with models a,b at 305K.

Type	O4-H1	O4-H2	O4-H3	H2-O3	O4-O3	O3-As	H1-O4-H2	H1-O4-H3	H2-O4-H3	O4-H2-O3
A	1.02(2)	0.94(2)	-	1.77(2)	2.71(2)	1.67(2)	110.8(22)	-	-	176.1(18)
A2	0.99(2)	0.94(2)	-	1.88(2)	2.80(2)	1.74(2)†	101.5(21)	-	-	167.7(17)
B	0.98(3)	0.99(3)	1.01(2)	1.71(2)	2.70(2)	1.72(2)	108.7(22)	116.2(21)	108.9(22)	178.0(20)
B2	1.03(3)	1.02(3)	1.18(2)	1.70(2)	2.71(2)	1.64(2)†	107.5(20)	114.8(18)	110.8(19)	173.9(19)
C	1.00(2)	1.01(2)	-	1.77(2)	2.75(2)	1.67(2)	97.5(18)	-	-	160.9(16)
C2	0.98(2)	0.98(2)	-	1.92(2)	2.90(2)	1.65(2)†	116.2(20)	-	-	173.9(17)
D	-	1.02(2)	1.05(2)	1.84(2)	2.86(2)	1.72(2)	-	-	100.9(19)	174.5(18)
D2	-	0.97(3)	0.91(2)	1.87(2)	2.83(2)	1.68(2)†	-	-	114.9(22)	171.8(18)
Mean	1.00(2)	0.98(2)	1.04(2)	1.81(2)	2.78(2)	1.69(2)	107.0(20)	115.5(19)	108.9(21)	172.1(18)
a	1.159(7)	0.979(4)	1.297(4)	1.845(3)	2.820(4)	1.680(1)	104.9(4)	116.0(3)	111.1(3)	174.3(3)
b	1.145(8)	0.984(5)	0.99(1)	1.839(3)	2.821(4)	1.680(1)	105.5(4)	112.1(6)	113.4(7)	174.7(3)

† O3-As(2) distance

b) The bonds between water oxygens to form the chains.

A chain	H3D-O4A2	1.66(2)	O4D-O4A2	2.67(2)	O4D-H3D-O4A2	161.5(19)			
	H1A2-O4D2	1.88(2)	O4A2-O4D2	2.86(2)	O4A2-H1A2-O4D2	169.9(21)			
	H3D2-O4A	1.78(2)	O4D2-O4A	2.68(2)	O4D2-H3D2-O4A	168.3(19)			
	H1A-O4D	1.72(2)	O4A-O4D	2.74(2)	O4A-H1A-O4D	175.2(22)			
B chain	O4A2-H1C2	1.61(2)	O4A2-O4C2	2.59(2)	O4A2-H1C2-O4C2	176.1(17)			
	O4C2-H3B	1.46(2)	O4C2-O4B	2.47(2)	O4C2-H3B-O4B	175.3(16)			
	H1B-O4D	1.56(3)	O4B-O4D	2.53(3)	O4B-H1B-O4D	171.1(19)			
	H3D-O4A2	1.66(2)	O4D-O4A2	2.67(2)	O4D-H3D-O4A2	161.5(19)			
B' chain	O4D2-H1B2	1.64(3)	O4D2-O4B2	2.67(2)	O4D2-H1B2-O4B2	176.4(19)	H1C-O4C-H2C	97.5(18)	
	H3B2-O4C	1.21(2)	O4B2-O4C	2.38(2)	O4B2-H3B2-O4C	171.1(15)	H1C-O4C-H3B2	123.3(17)	
	H1C-O4A	1.82(2)	O4C-O4A	2.80(2)	O4C-H1C-O4A	166.6(17)	H2C-O4C-H3B2	124.5(16)	
	O4A-H3D2	1.78(2)	O4A-O4D2	2.68(2)	O4A-H3D2-O4D2	168.3(19)			

other water molecule (Lundgren and Olovsson, 1967).

The former chain B, with an O-O separation of 2.47(2) Å in the $[H_5O_2]^+$ unit, has the linking hydrogen H3B well displaced towards one of the water oxygens with distances of 1.01(2) and 1.46(2) Å. This supports the earlier remark when discussing the nature of the H_4O_2 and $[H_5O_2]^+$ units in the room temperature structure of DUAs, that the linking hydrogen H3 of the latter species is unlikely to be situated centrally and symmetric unless the O-O separation is very close to 2.4 Å (Thomas and Liminga, 1978). We still cannot assess whether this is the case in the room temperature structure, although the observation that sufficiently short O-O distances may be attained, at least at low temperature, is evidence that it could be.

The structure deduced for DUAs at low temperature is compatable with the other physical observations characterising the transition. This is a displacive transition without a gross rearrangement of the atomic positions and results in a unit cell which is only very slightly distorted from the "orthorhombic" cell observed by Shilton and Howe (1980). The ordering scheme of the hydrogen atoms leads to a very large reduction in hydrogen mobility as seen from conductivity and NMR measurements, and is compatable with IR data which indicates the presence of H_3O^+ species and that the arsenate hydrogens stay firmly attached to water oxygens. de Benyacar and de Dussel (1979) observed the domain structure of the low temperature phase, which has equal volumes of domains oriented at about 90° to one another with domain walls parallel to the tetragonal (110). The lattice parameters indicate

that a has expanded and b contracted relative to the tetragonal phase. The a and b axes are crystallographically equivalent in the tetragonal system and such a distortion can occur with equal probability with the cell axes reversed, resulting in equal volumes of domains which are oriented at about 90° to one another. The (110) tetragonal planes remain almost undistorted by this model and can appear as domain walls. Each domain consists of a series of subdomains with walls parallel to (010) tetragonal. The shearing of the tetragonal cell, which is almost parallel to (010), may also occur with equal probability in either direction, and leaves the (010) planes virtually unchanged. These can now appear as subdomain walls.

In the high temperature phase of DUAs, the averaging effect of the dynamic interchange of H_4O_2 and $[H_5O_2]^+$ results in layers of water molecules which have no net polarisation. Below the transition temperature, as shown in Fig. 4.9 for $0 < z < 0.5$, the extra protons are ordered and accommodated in two $[H_5O_2]^+$ units which occur alternately at $z \tilde{\sim} 0.31$ and $z \tilde{\sim} 0.19$ in the B and B' chains. Both these $[H_5O_2]^+$ units have similarities in their configuration,with a resulting polarisation which has a significant component along the crystallographic a-direction. The unit cell however is centrosymmetric, so that for the volume $0.5 < z < 1.0$ there will be an equal and opposite polarisation, and for the unit cell as a whole there is no net polarisation. A crystal is antiferroelectric if the superstructure formed by the transition from the paraelectric state may be described in terms of sublattices which have equal and opposite polarisation. Hence our structure for DUAs at low temperature is compatible

with the observed antiferroelectricity of this phase.

No refinements have yet been attempted for the data at 250K, but this should prove a more demanding problem because the effects of anisotropic vibration of the various atoms, particularly in the water layers as the crystals approach the phase transition, will lead to the need for many more parameters. It is unlikely that these could be reliably defined by the data.

$Li_2UO_2AsO_4.4D_2O$ at 294K

For the analysis of the diffraction pattern of $LiUO_2AsO_4.4D_2O$, the normal Rietveld procedure was followed. A trial structure was refined in space group P4/ncc using starting parameters closely related to those found for DUAs at room temperature, but excluding the Li atom which contributes only 1.7% of the coherent scattering. The refinement was unsuccessful, with a poor fit and very high or physically unreal temperature parameters. It was sufficient to show however, that the linking hydrogens H(3) between water squares in DUAs were almost certainly absent in $LiUO_2AsO_4.4D_2O$, which is compatible with the larger c lattice parameter in this compound. In this case, the specific orientation between water sqaures found in DUAs, necessary for effective three dimensional bonding between water squares and between layers via the arsenate groups , would no longer be needed. What is required, therefore, is a space group which allows a simpler relationship between water squares whilst maintaining the basic uranyl-arsenate framework.

The only suitable tetragonal space group appears to be P4/n, which is a sub-group of P4/ncc to which it can be related

by halving the unit cell along the c-axis. Refinement in this space group proceeded satisfactorily to an $R_{wp} \approx 11$. Inclusion of the lithium atom in the centre of the water square, (ie at 1/4 1/4 z), as suggested by Johnson et al (1981), resulted in no improvement to the fit, and the anihilation of the atom by very high temperature factors (≈ 30 $\mathring{A}^2$). Careful examination of the atomic co-ordinates, however, revealed that the water squares had changed their orientation, and that a possible tetrahedral lithium site now existed at position 2b (1/4 3/4 1/2).

The refinement then converged with 51 atomic parameters, 8 machine parameters and 258 reflections. The occupancy of the water molecules was refined because Weigel and Hoffman (1976) state that this may be variable. The occupancy of water was found to be 3.804(2). The final R factors were $R_I = 3.80$, $R_{wp} = 7.92$, $R_p = 8.16$, $R_E = 4.04$. The final parameters are given in Table 4.7, bond distances in Table 4.8, and the observed, calculated and difference profiles in Fig. 4.10. The basic structure of $LiUO_2AsO_4.4D_2O$ is closely related to that of HUAs at room temperature. Layers of linear UO_2^{2+} ions, co-ordinated by the oxygen atoms of the surrounding arsenate tetrahedra, alternate with arrays of water molecules. The bond distances and bond angles are very similar for the uranyl arsenate skeleton of both these compounds. The water molecules are grouped in squares, with the oxygen atom of a water molecule bound to the oxygen of an arsenate tetrahedron by a hydrogen bond, H(2). The in-square hydrogen bonding H(1) has a definite sense associated with it, with only one of the two chemically similar hydrogen bond sites between two water oxygens occupied, Fig. 4.11.

Table 4.7.

Final parameters for $LiUO_2AsO_4.4D_2O$ at 294K in space group P4/n (origin at $\bar{1}$). a = 7.0969(1), c = 9.1903(2) Å. ESD's of refined parameters in parenthesis.

Atom	Position	Point Symmetry	x	y	z	B_{11}	B_{22}	B_{33}	B_{12}	B_{13}	B_{23}
U	2c	4	1/4	1/4	0.1041(5)	0.3(1)	0.3(1)	3.1(2)	0	0	0
As	2a	$\bar{4}$	1/4	3/4	0	1.2(1)	1.2(1)	2.0(2)	0	0	0
O(1)	2c	4	1/4	1/4	0.3013(5)	2.2(2)	2.2(2)	2.2(3)	0	0	0
O(2)	2c	4	1/4	1/4	-0.0873(6)	1.3(2)	1.3(2)	2.8(3)	0	0	0
O(3)	8g	1	0.5709(3)	0.3032(3)	0.1103(3)	1.1(1)	1.9(1)	2.5(1)	0.2(1)	0.0(1)	-0.3(1)
O(4)	8g	1	0.1937(6)	-0.0387(5)	0.6293(5)	3.8(3)	4.0(2)	1.4(2)	2.2(1)	-1.1(2)	-0.0(2)
H(1)	8g	1	0.1053(6)	0.0691(7)	0.6087(4)	5.3(2)	11.9(3)	6.2(2)	-5.8(1)	-1.6(2)	3.3(3)
H(2)	8g	1	0.5762(5)	0.1592(4)	0.7235(4)	3.8(2)	3.9(2)	2.5(2)	-0.8(2)	-0.9(2)	-0.2(2)
Li	2b	$\bar{4}$	1/4	3/4	1/2	5.2(5)	5.2(5)	0.6(6)	0	0	0

R_p = 8.16 R_{wp} = 7.92 R_I = 3.80 R_E = 4.04

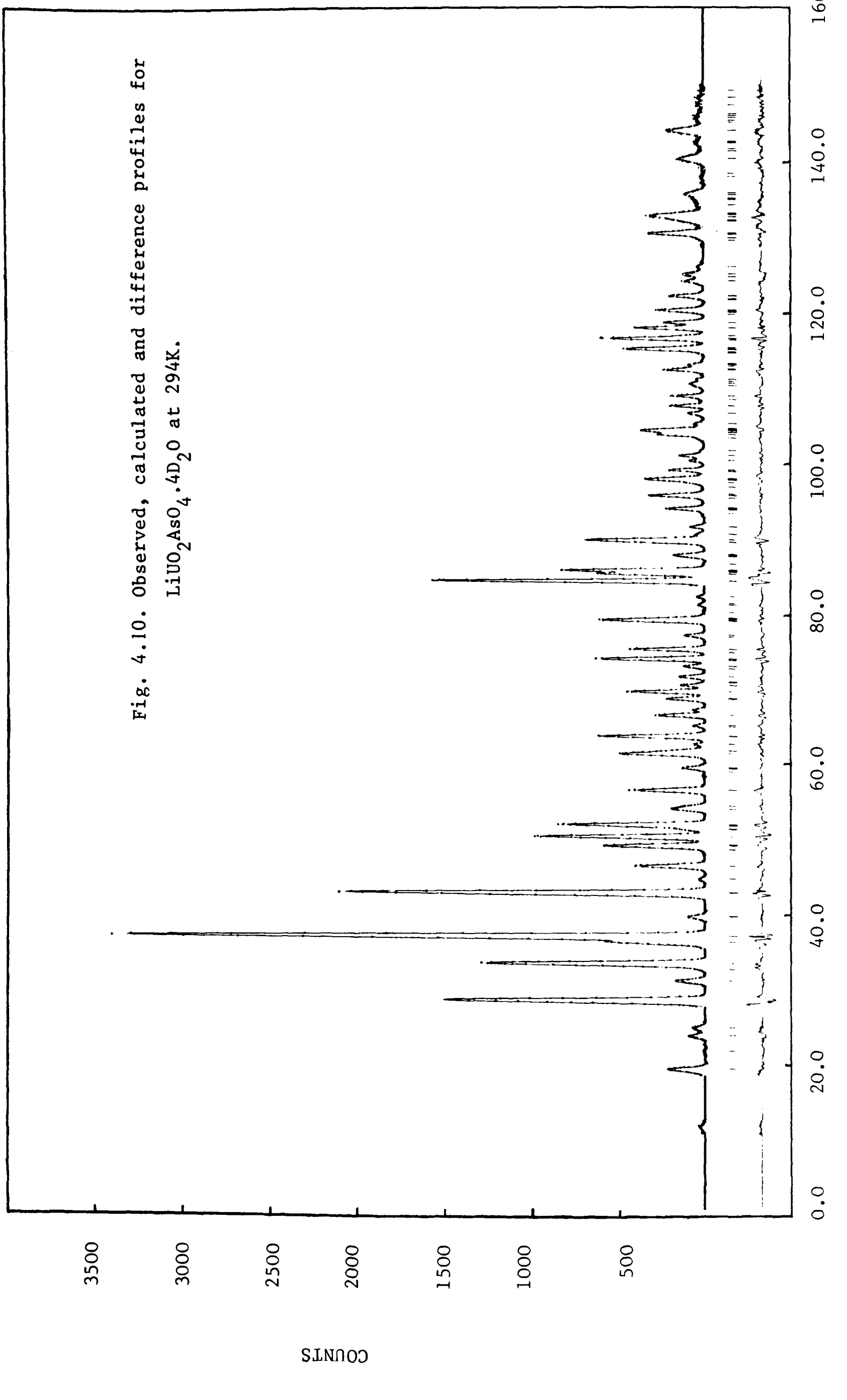


Fig. 4.10. Observed, calculated and difference profiles for $LiUO_2AsO_4 \cdot 4D_2O$ at 294K.

Table 4.8. Bond distances (Å) and angles (degrees) for $LiUO_2AsO_4.4D_2O$ at 294K. ESD's in parenthesis.

		Comment
1) Uranyl ion		
U-O(1)	1.812(7)	
U-O(2)	1.759(7)	
U-O(3)	2.309(2)	
O(1)-U-O(2)	180	
O(1)-U-O(3)	88.6(1)	
2) Arsenate ion		
As-O(3)	1.669(3)	
O(3)-As-O(3)	105.2(1)	$z_1 = z_2$
O(3)-As-O(3)	111.6(1)	$z_1 = -z_2$
U-O(3)-As	134.4(2)	
3) Water molecule		
O(4)-H(1)	1.007(6)	
O(4)-H(2)	0.938(5)	
O(4)-O(4)	2.953(6)	
H(1)-O(4)	1.979(6)	
O(4)-O(3)	2.783(5)	
H(2)-O(3)	1.860(4)	
H(1)-O(4)-H(2)	103.1(5)	
O(4)-H(1)-O(4)	161.8(5)	
O(4)-H(2)-O(3)	167.5(4)	
4) Lithium		
Li-O(4)	1.955(4)	
O(4)-Li-O(4)	105.1(2)	$z_1 = z_2$
O(4)-Li-O(4)	111.7(2)	$z_1 = -z_2$
Li-O(4)-H(1)	99.4(2)	
Li-O(4)-H(2)	113.4(4)	

There are however some important differences caused by the replacement of 1/9 of the hydrogens with lithium ions. The three dimensional linking between two squares of adjacent water molecules by H(3) hydrogens is no longer possible, and linking between squares is now effected by the lithium ion. This causes a rotation of the water squares about their four-fold axes, such that the oxygen atoms of the water molecules of four adjacent squares surround the lithium ion at the verticies of a tetrahedron, which is elongated slightly along [001]. This rotation of the water squares is accompanied by reorientation of the arsenate tetrahedra which are connected to the next level of water layers (ie in the next unit cell in $LiUO_2AsO_4.4H_2O$, or the top half of the unit cell in HUAs). The water squares or arsenate tetrahedra in two different levels are now alligned with the same orientation, whereas in HUAs the orientations of these species are staggered about the directions parallel with the unit cell axes (eg see the orientations of the arsenate tetrahedra in Fig. 4.1 for HUAs). The in-square O(4)-O(4) distance increases considerably from 2.758(5) Å in DUAs to 2.953(6) Å.
This must reflect a decrease in the polarity of the water molecules as a result of the replacement of the linking proton H(3) with the larger less polarising lithium ion, which must also bind together four water oxygens rather than just two. The effect of this is to some extent balanced by the increase in the occupancy of the H(1) hydrogen bonding sites from three quarters to fully occupied. With all the hydrogen bonding sites H(1) and H(2) completely filled, and the water molecules unable to rotate due to the combination of the strong O(4)-H(2)-O(3), and O(4)-Li^+

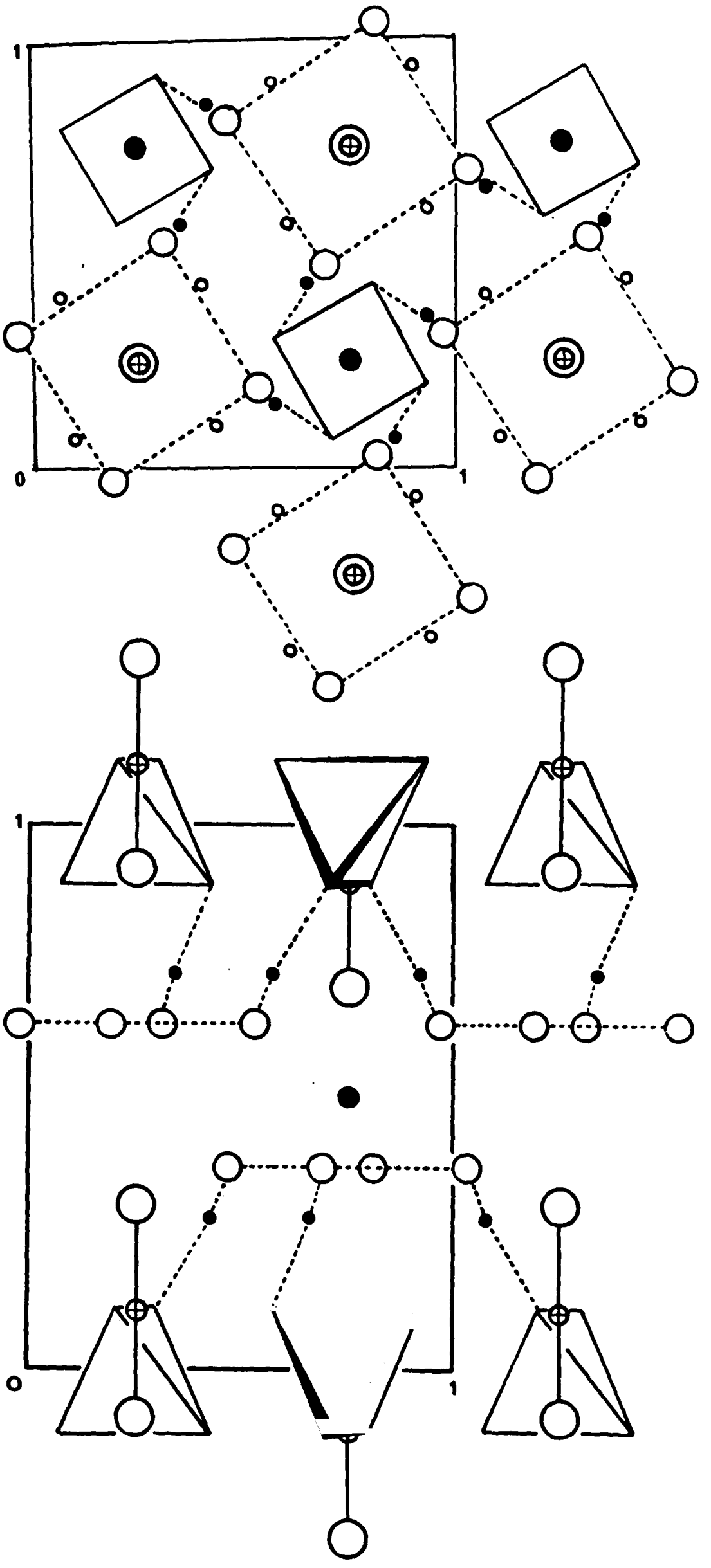


Fig. 4.11. Projection of $LiUO_2AsO_4.4D_2O$ structure along [001],(top), and [001], (bottom). Large open circles, uranyl oxygens; medium open circles, water oxygens; smaller crossed circles, U; small open and solid circles, H(1) and H(2), respectively; larger solid circles, Li.

interactions, there is no easy mechanism for proton conduction in this compound.

In the two other closely related compounds, $KUO_2AsO_4.3H_2O$ and $NH_4UO_2AsO_4.3H_2O$, both the potassium and the ammonium ions are too big to participate effectively in three dimensional square linking via a site tetrahedrally co-ordinated by oxygen atoms. Neither are they sufficiently polarising to reside like copper in the centre of a water square and cause drastic reorganisation of the in-square hydrogen bonding. They have no option therefore but to replace (randomly at room temperature) an H_3O^+ ion from the hydrogen bonded water network.

The structure of $NaUO_2PO_4.3H_2O$ is unknown. A plausible structure is one based on that of $LiUO_2AsO_4.4H_2O$, ie with four water molecules of four different water squares forming a tetrahedral site, but with the water squares only 3/4 occupied. If the sodium ion was then statistically disordered over two possible sites, i) at the centre of the water oxygen tetrahedron as in $LiUO_2AsO_4.4H_2O$, or ii) in the water squares as in $KUO_2AsO_4.3H_2O$, then sodium conductivity, between water squares via the tetrahedral site, and within squares by sodium hops and exchange with a water molecule, could be envisaged.

CHAPTER 5

STRUCTURAL STUDIES ON A_2UCl_6 COMPOUNDS

5.1. Introduction

A considerable number of systems which display ionic conductivity are based on lattices containing a high proportion of halide ions. Thus the copper(I) and silver(I) halides, various fluorites, solid solutions of simple salts, eg the LiCl-Li_3N system, and other more complex compounds, eg $H_xK_2OsCl_6$ or Na_2UBr_6, are all good conductors at the appropriate temperature, and demonstrate a variety of different mechanisms.

At temperatures within about 100°C of their melting points, AgCl and AgBr show anomalously high conductivities and have very high silver Frenkel defect concentrations of about 0.2% and 2% respectively (Aboagye and Friauf, 1975). Conductivity is due to the motion of these cation Frenkel defects via vacancy and interstitial jumps (Friauf, 1977). Batra and Slifkin (1975) have confirmed that this high conductivity increase is connected with the temperature dependence of the Frenkel defect formation energy rather than an increase in ionic mobility or the onset of a new transport mechanism. Theoretical attempts to model this temperature dependence also emphasize the importance of the quadrupolar deformation of the mobile d^{10} Ag^+ ion in the saddle point region between adjacent cation positions, thus reducing the activation energy for mobility (Jacobs, Corish, Devlin and Catlow, 1979).

A number of divalent metal fluorides or chlorides with the

fluorite structure, eg CaF_2, BaF_2, SrF_2, PbF_2, and $SrCl_2$, exhibit a diffuse transition at elevated temperatures in which the conductivity rises rapidly and can approach those of ionic melts (Lindner and O'Keefe, 1975; Barsis and Taylor, 1966; O'Keefe, 1976). In the fluorite lattice the cations occupy a fcc lattice of side a_o with anions at $\pm$ (1/4 1/4 1/4). The anions therefore from a simple cubic lattice of side $a_o/2$, in which the body centre of every other cube is occupied by a cation. Powder and single crystal neutron diffraction studies (Dickens et al, 1979 a,b) show that in $SrCl_2$ and PbF_2, 3.5% and 4% of anions form Frenkel defects by relaxation away from their ideal positions in the fluorite lattice towards the unoccupied cube centres, whilst the cation sublattice remains almost perfect. A similar effect is seen by Cheetham et al (1970) for CaF_2 doped with YF_3. Other experiments involving doping with aliovalent impurities demonstrate that these Frenkel defects are dominant in the conduction mechanism and moreover that the anion vacancies are more mobile than the anion interstitials (Barsis and Taylor, 1968a,b).

An antifluorite lattice in which the cation is the principle charge carrier is formed by the solid solution of Li_3N with LiCl with the composition $(Li_3N)_2\ (LiCl)_3$, or more revealingly $Li_{1.8}N_{0.4}Cl_{0.6}$. This compound is characterised by a large number of structural defects in which the anions form a close packed fcc lattice with a statictical distribution of Cl^- and N^{3-} ions and 10% of all cation sites are vacant (Hartwig, Weppner and Wickelhaus, 1979).

At room temperature βAgI is poorly conducting and has the würtzite structure ($P6_3mc$) in which half the tetrahedral sites in a hcp iodide lattice are occupied in an ordered manner (Burley, 1963). At 147°C βAgI transforms into body centred αAgI (Im3m) which has high conductivity of 10^{-2} $ohm^{-1}m^{-1}$. NMR measurements show a large increase in the mobility of the silver ions at the transition (Brinkmann and Freudenreich, 1978). A single crystal neutron diffraction study of the α phase indicates that large scale disorder of the cations occurs where two silvers per unit cell are distributed over 12 tetrahedral sites. Third and fourth order thermal tensors are required to adequately describe the observed build-up of scattering density away from the centre of the site in the direction [110], ie towards the neighbouring tetrahedral site at a jump distance 1.8 Å. This demonstrates that the silver ion disorder is dynamic and responsible for the high conductivity (Cava, Reidenger and Wuensch, 1977). CuI behaves in a similar manner, undergoing a transition from a poorly conducting ordered zinc blende structure at room temperature, to a fcc lattice with Cu^+ occupying half of 8 tetrahedral sites in the unit cell in a dynamically disordered manner (Wagner and Wagner, 1957; Boyce and Hayes, 1979; Boyce and Huberman, 1977).

An unusual compound is that derived from K_2OsCl_6 which has the K_2PtCl_6 structure (Novotney et al, 1977). When this substance is produced by precipitation from slightly acidic solution, protons are accommodated in the lattice with a reduction in the formal charge on Osmium from 4+ to 3+. Concentrations of protons as high as 0.25 have been reported from NMR measurements (Willemsen, Armstrong and Meincke, 1979). These also indicate

that the protons are in a rapid state of motion which is thermally activated above 180K and temperature independent at lower temperatures. No structural studies to locate the protons have been done, but it is suggested they might occupy the site in the fluorite lattice near (1/2 0 0), octahedrally surrounded by chloride ions.

Other schemes exist whereby unoccupied sites in a crystal lattice may be partially injected with smaller ions without causing gross distortions to the original structure. Under suitable conditions these smaller ions then move from filled to unfilled sites. Such a system is illustrated by Na_2UBr_6, which is structurally derived from UCl_6.

UCl_6 has a hexagonally close packed array of chloride ions in which one sixth of the available octahedral sites are filled with U^{6+} ions, Fig. 5.1 (Zachariasen, 1948; Taylor and Wilson, 1974b). The lattice is trigonal, space group $P\bar{3}m1$, a = 10.97(1), c = 6.025(8) Å, with atoms in the special positions

U(1)	1a	0	0	0	
U(2)	2d	1/3	2/3	u	u = 0.518(5)
Cl(1)	6i	u	$\bar{u}$	v	u = 0.109(2), v = 0.222(8)
Cl(2)	6i	u	$\bar{u}$	v	u = 0.431(2), v = 0.237(8)
Cl(3)	6i	u	$\bar{u}$	v	u = 0.777(2), v = 0.286(8)

The Cl^- lattice contracts slightly around the uranium atoms with a corresponding expansion around the remaining octahedral holes which exist at

6g	u	0	0	$u \approx 1/3$
1b	0	0	1/2	
2d	1/3	2/3	u	$u \approx 0$
6h	u	0	1/2	$u \approx 1/3$

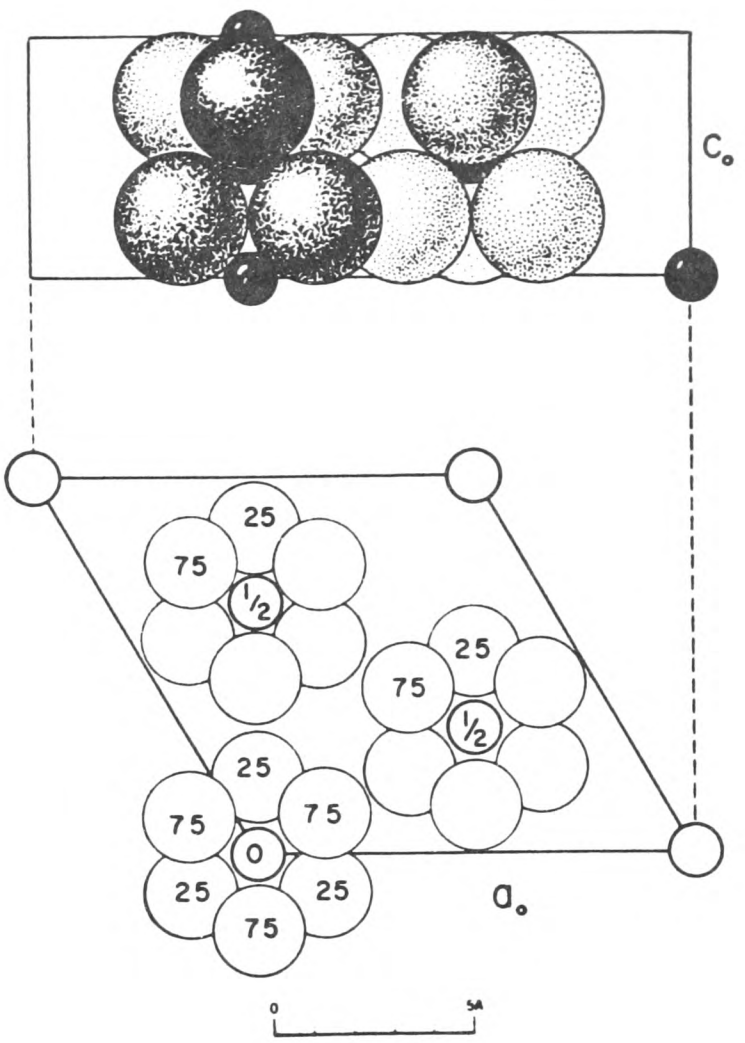


Fig. 5.1. Two projections of the structure of UCl_6 in which the chloride ions form a close packed hexagonal array. U^{6+} ions occupy one sixth of the available octahedral sites (Wyckoff, 1965).

The structure of Na_2UBr_6 is closely related to that of UCl_6 only with the first set of octahedral holes at (u 0 0) filled with sodium ions, and with a reduction in the formal charge on uranium from 6+ to 4+ (Bogacz et al, 1980). These sodium ions, it is thought, become available for fast ion transport due to the large number of remaining unoccupied sites, particularly since the $[UBr_6]$ octahedra tend to rotate as rather rigid "molecular" units, dynamically unblocking the channels between holes at higher temperatures. Thus, at room temperature, Na_2UBr_6 is poorly conducting, but this rises steadily to 2.7 ohm^{-1} m^{-1} at 650K with an activation energy of 98 kJ $mole^{-1}$ (Fouque et al, 1978).

At 652K the conductivity rises abruptly to 33 $ohm^{-1}m^{-1}$ (activation energy = 49 kJ $mole^{-1}$) and again at 663K where the conductivity jumps from 49 $ohm^{-1}m^{-1}$ to 93 $ohm^{-1}m^{-1}$ with an activation energy of only 9.34 $\pm$ 0.065 kJ $mole^{-1}$. Large entropy changes of 21 and 27 J $mole^{-1}K^{-1}$ respectively accompany the conductivity transitions which are associated with a change of crystal structure (Hewat et al, 1980). On melting, at 784K, the conductivity drops by 13 $ohm^{-1}m^{-1}$, so that in this compound the conductivity in the solid state is higher than that found for the liquid.

Of the compounds which are chemically and structurally related to Na_2UBr_6, it is the fluorides which have received the bulk of the attention. Thus it has been shown that the ternary fluorides of alkali metals and tetravalent transition metal ions fall broadly into four different structure types, the first three of which are based on a close packed array of fluoride ions with cations occupying the octahedral sites (Babel, 1967). Fig. 5.2

shows some of these structures.

1) Li_2ZrF_6 - Type (Hoppe and Dähne, 1960).

Trigonal, $P\bar{3}1m$, Z = 1, a = 4.98, c = 4.66 Å.

Positions : Zr (1a) (0 0 0); Li (2d) (1/3 2/3 1/2);

F (6k) (x 0 z) with x = 0.33, z = 0.24.

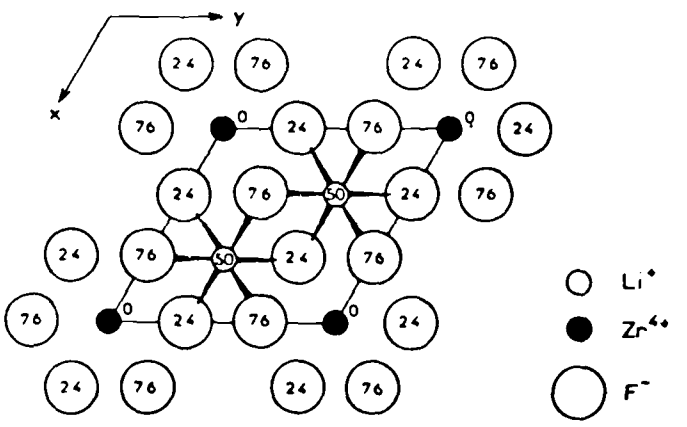
The Zr and Li ions exist in almost regular octahedral holes with Li-F and Li-Li distances almost identical to those found in LiF. The $[ZrF_6]$ groups are isolated, yet with the $[LiF_6]$ octahedra they form a framework of corner sharing octahedra. αLi_2SnF_6 and Li_2PbF_6 are reported to be isostructural (Hebecker and Hoppe, 1966).

2) Na_2SiF_6 - Type (Zalkin, Forrester and Templeton, 1964).

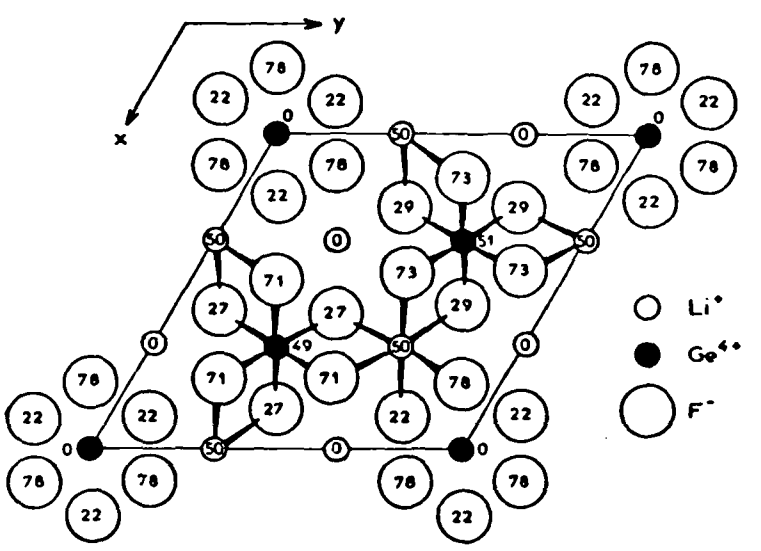
Trigonal, P321, Z = 3, a = 8.859, c = 5.038 Å.

Positions : Si(1) (1a) (0 0 0); Si(2) (2d) (1/3 2/3 z) with z = 0.506; Na(1) (3e) (x 0 0) with x = 0.379; Na(2) (3f) (x 0 1/2) with x = 0.714; F(1), F(2) and F(3) each in (6g) (x y z) with x = 0.087, 0.444, 0.230; y =-0.092, - 0.401, - 0.260; z = 0.810, 0.701, 0.310, respectively.

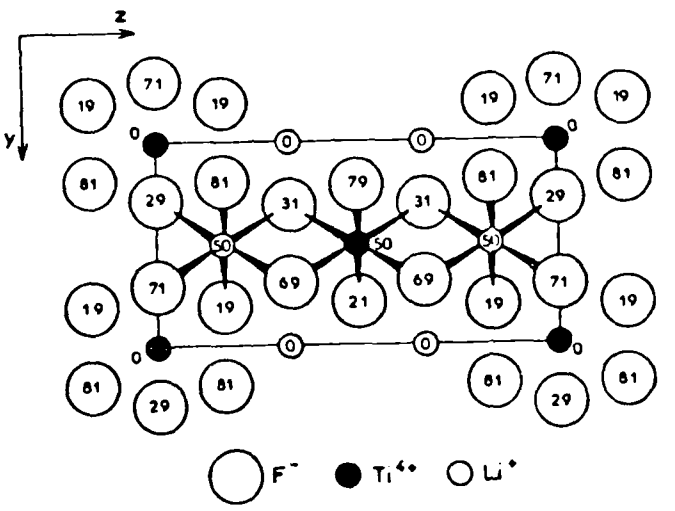
This structure is very similar to that of Na_2UBr_6, except that alternate sodium ions exist in octahedral sites at z = 1/2. As compared to Li_2ZrF_6, there is an enlargement of the a-axis by a factor of $\sqrt{3}$ with M^{4+} ions now existing at different heights (z = 0, 1/2) where formally they were all at z = 0. The $[MF_6]$ octahedra remain almost regular, but the increased size of the sodium ion causes strong distortions of the $[NaF_6]$ octahedra. The isolated $[MF_6]$ groups now share corners and edges with the $[NaF_6]$ octahedra which causes a closer approach of the two types of cations. This structure therefore is restricted to those compounds which contain the smallest transition



(a) Li_2ZrF_6-(Type 1). Projection along [001].

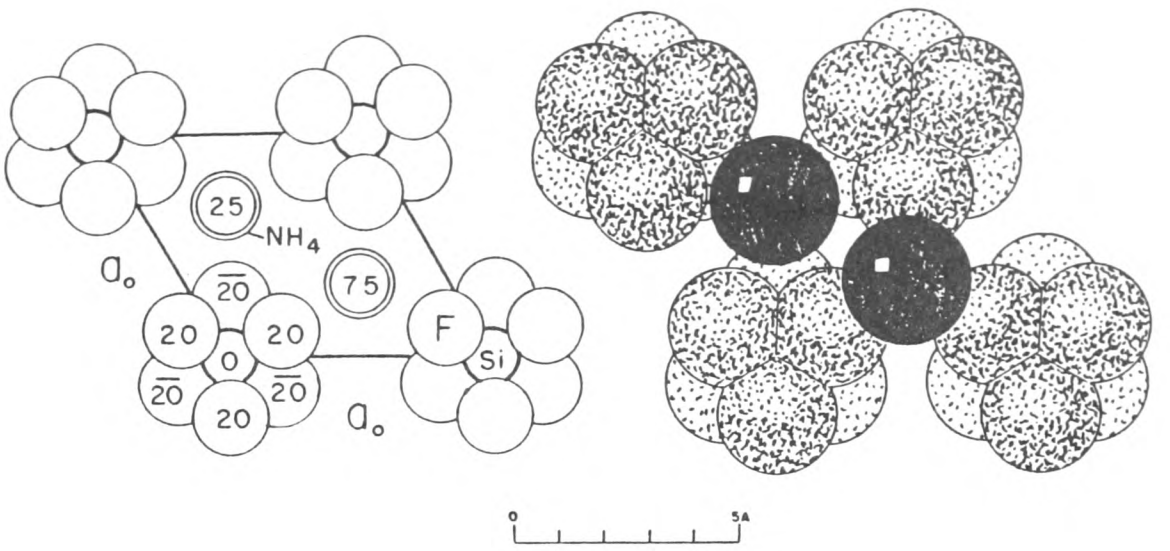


(b) β-Li_2GeF_6-(Type 2, Na_2SiF_6). Projection along [001]

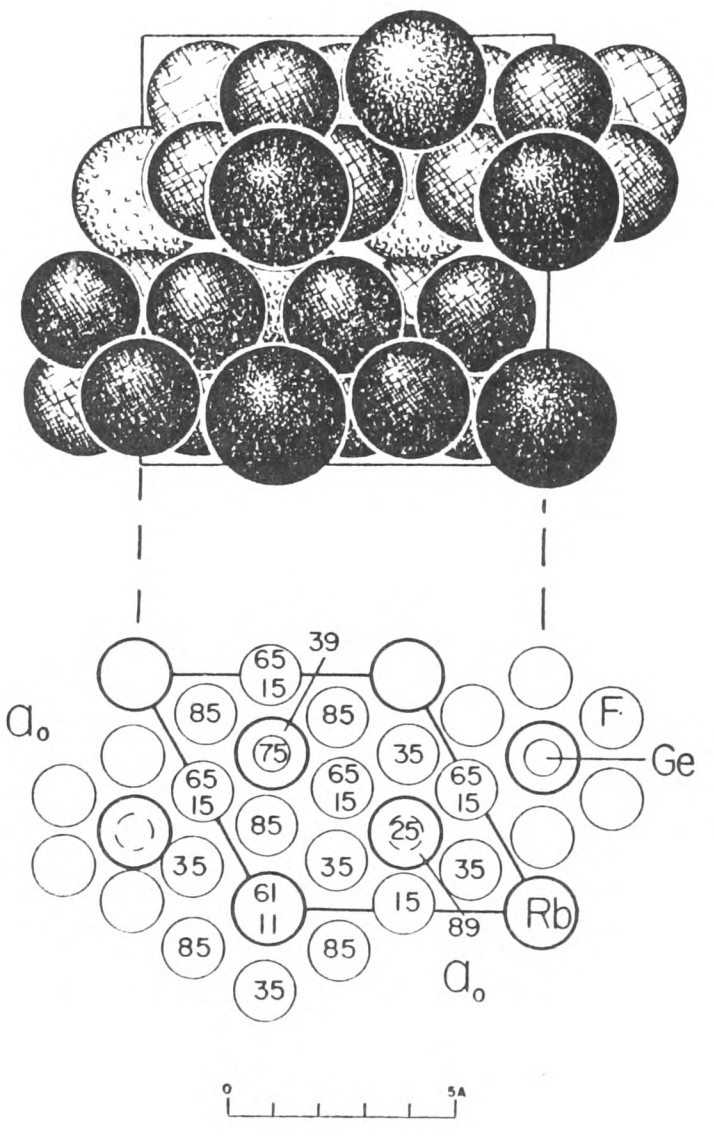


(c) Li_2TiF_6-(Type 3, non-distorted Na_2SnF_6). Projection along [100].

Fig. 5.2a,b,c. Some examples of the structures adopted by A_2MeF_6 compounds (Portier, Menil and Hagenmuller, 1970).



(d) β-$(NH_4)_2SiF_6$-(Type 4a, K_2GeF_6). Projection along [001].



(e) β-Rb_2GeF_6-(Type 4b, K_2MnF_6).

Fig. 5.2d,e. Some examples of the structures adopted by A_2MeF_6 compounds (Wyckoff, 1965).

metal ions, eg Li_2SiF_6, Li_2MnF_6, or βLi_2GeF_6 (Cox, 1954; Hoppe, Liebe and Dähne, 1961; Portier, Menil and Grannec, 1969).

3) Na_2SnF_6 - Type (Hebecker, von Schnering and Hoppe, 1966).

Monoclinic, $P2_1/c$, Z = 2, a = 11.3, b = 5.06, c = 5.06 Å, β = 116.6°.

Positions : Sn (2a) (0 0 0); Na (4e) (x y z) with x = 0.366, y = 0.0, z = 0.340; F(1), F(2) and F(3) in (4e) with x = 0.008, 0.143, 0.145; y = 0.252, 0.167, 0.817; z = 0.252, -0.043, 0.326, respectively.

This structure is a monoclinically distorted Li_2ZrF_6 type with the unit cell enlarged by a factor of two to account for the alternation of the M^{4+} ion between sites at z = 0 and z = 1/2. Each type of cation exists in a highly distorted octahedral environment with $[NaF_6]$ octahedra sharing corners and edges with the $[SnF_6]$ groups. In the absence of a monoclinic distortion to the fluoride lattice the space group is $P4_2/mnm$ as found for Li_2TiF_6 (Portier et al, 1969) or αLi_2GeF_6 (Portier, Menil and Grannec, 1969).

4) K_2GeF_6, K_2MnF_6 and K_2SiF_6 - Types

Many transition metal compounds A_2MF_6 appear in three modifications which are closely related to each other.

a) K_2GeF_6 - Type (Hoard and Vincent, 1939).

Trigonal, $P\bar{3}m1$, Z = 1, a = 5.62, c = 4.65 Å, c/a = 0.827.

Positions : Ge (1a) (0 0 0); K (2d) (1/3 2/3 z) with z = 0.7; F (6i) (x $\bar{x}$ z) with x = 0.148, z = 0.220.

b) K_2MnF_6 - Type (Bode and Wendt, 1952).

Hexagonal, $P6_3mc$, Z = 2, a = 5.67, c = 9.35 Å, c/a = 1.649.

Positions : Mn (2b) (2/3 1/3 z) with z = 0.75; K(1) (2b) with z = 0.40;

K(2) (2a) (0 0 z) with z = 0.10; F(1) and F(2) each in (6c) (x $\bar{x}$ z), with x = 0.19, 0.48; z = 0.36, 0.14 respectively.

c) K_2PtCl_6 - Type (antifluorite) (Williams, Dillin and Milligan, 1973).

Cubic, Z = 4, a = 8.430 Å for Rb_2MnF_6.

Positions : Mn (4a) (0 0 0); Rb (8c) (1/4 1/4 1/4);

F (24e) (x 0 0) with x = 0.20.

In hexagonal-rhombohedral orientation ($R\bar{3}m$), Z = 3, a = 5.96, c = 14.61 Å, c/a = 2.45, ($\sqrt{3}$ x $\sqrt{2}$).

From an examination of the lattice parameters and the c/a values, it is clear that these three structure types differ in the identity periods in the c-direction of essentially similar close packed layers, where the close packed species is AF_3 tetrahedra. In type a) there are two such layers with M^{4+} occupying the octahedral holes between every second layer leading to hexagonal packing of the type AcBAcB. In the cubic K_2PtCl_6 type the corresponding sequence of M^{4+} in the octahedral holes between every second layer leads to a three-fold c-period, AcBCbABaC. For K_2MnF_6 there is double hexagonal packing AcBAbC. An alternative description for K_2PtCl_6 is, of course, antifluorite, with a fcc array of $[MF_6]^{2-}$ ions with A^+ occupying the tetrahedral sites.

In all three structure types we find approximately regular $[MF_6]$ octahedra. The alkali ions exhibit co-ordination numbers of 12, but only in the highly symmetric cubic case are all M - F distances equal. For the other two structures these split into groups of 6 + 3 + 3. Hence for trigonal K_2TiF_6,

Siegel (1952) found 6K-F = 2.87 Å, 3K-F = 2.75 Å, 3K-F = 3.08 Å and Ti-F = 1.91 Å.

In general, the differences and relationships between the structures adopted by different A_2MF_6 compounds may be rationalised in terms of relative ionic size and charge of the constituent ions. Thus for compounds containing lithium it has been shown by Portier, Menil and Hagenmuller (1970) that increasing the size of the M^{4+} cation causes a change in the adopted structure from Type 2 (eg Li_2SiF_6) to Type 3 (eg Li_2PdF_6) to Type 1 (eg Li_2PbF_6). For transition metal ions with radii very close to the two change over points at 0.54 Å (eg Ge^{4+}) and 0.71 Å (eg Sn^{4+}) either structure may be adopted.

Increasing the size of the alkali metal ion leads to structures with a greater distortion of the $[AF_6]$ octahedra. Thus Li_2PbF_6 exists in structure Type 1 with almost regular $[LiF_6]$ octahedra whereas Na_2PbF_6 exists as Type 3 where the close packed array of fluoride ions suffers a monoclinic distortion (Hebecker and Hoppe, 1966). For the larger alkali metal ions, eg K^+, NH_4^+ or Tl^+, structures of Type 4 are found where the cation exists in 12-fold co-ordination.

For the actinide alkali fluorides, eg K_2UF_6 or Na_2ThF_6, the larger tetravalent actinide cations often demand a co-ordination number higher than 6. Thus in αK_2UF_6 there is 8-fold co-ordination of U^{4+} and in β_2-Na_2ThF_6 9-fold co-ordination of Th^{4+}. The latter structure is trigonal and consists of tricapped trigonal prisms sharing triangular faces perpendicular to the three fold axis of the ideal polyhedron to form infinite chains.

These compounds have been reviewed by Penneman, Ryan and Rosenzweig (1973).

Compounds containing the other halide ions have been less extensively studied, although we might expect similarities between the structures of alkali actinide chlorides and bromides with the transition metal fluorides because the ratios of the M^{4+} to halide radii are broadly similar. Thus both Ce_2UCl_6 and Ce_2ThCl_6 are isostructural with K_2GeF_6 (Type 4a) (Siegel, 1956), and Cs_2BkCl_6 is isostructural with K_2MnF_6 (Type 4b) (Morss and Fuger, 1969). We would, however, expect modifications to the basic close packed halide lattices found for the fluorides due to the increased polarisability of the larger halide ions, under the influence of the small highly charged cations. This leads to structures containing $[MX_6]^{2-}$ octahedra which are considerably more "molecular" in character. Hence at 280K K_2SnCl_6 is cubic, Fm3m, with the K_2PtCl_6 type structure. On cooling to 261K and 255K, phase transitions occur, leading to a reduction in the symmetry to tetragonal P4/mnc and monoclinic $P2_1/n$ respectively. These transitions have been shown to result from two successive rotations of the essentially rigid $[SnCl_6]^{2-}$ octahedra, 1) in an alternating manner around [001] in layers perpendicular to the c-axis, and 2) as in-phase rotations about $[1\bar{1}0]$ (Boysen and Hewat, 1978).

It is this increase in the molecular nature of the $[MeX_6]^{2-}$ octahedra which is of interest in the study of fast ion conduc-

tors. With the larger halides, the alkali ions have more freedom to move because a greater proportion of the negative charge becomes associated with the M^{4+} ion, thus reducing the strength of the $A^+ - Cl^-$ interaction, which is also diminished by the greater atomic separation required by the larger anion. Librations and rotations of the "molecular" species open up the channels between occupied and unoccupied sites, thus reducing the activation energy required for the transport of charge through the lattice.

We are interested in how a particular close packed basis lattice is influenced by the inclusion of different alkali metal cations, ie the potential charge carrier in an ionic conductor. Such studies are necessary to understand the relative importance of the M^{4+} and A^+ ions in determining the structure or dynamics exhibited by a particular system. We have chosen the system A_2UCl_6, A = Li, Na and K because : 1) the structure of UCl_6, the basis lattice is well known; 2) thermodynamic studies have been performed on this system which indicate that each compound, A = Li to Cs, undergoes two phase transitions before melting, as does Na_2UBr_6, a proven good conductor (Bogacz and Trzebiatowski, 1964; and 3) comparison with Na_2UBr_6 may reveal the effect of the halide ion. The phase diagrams of these three compounds are shown in Fig. 5.3.

5.2. Experimental

Li_2UCl_6, Na_2UCl_6 and K_2UCl_6 were made according to the method used by Fouque et al (1978) for Na_2UBr_6. Stoichiometric quantities of alkali halide (Ventron, Ultrapure), which had been dried

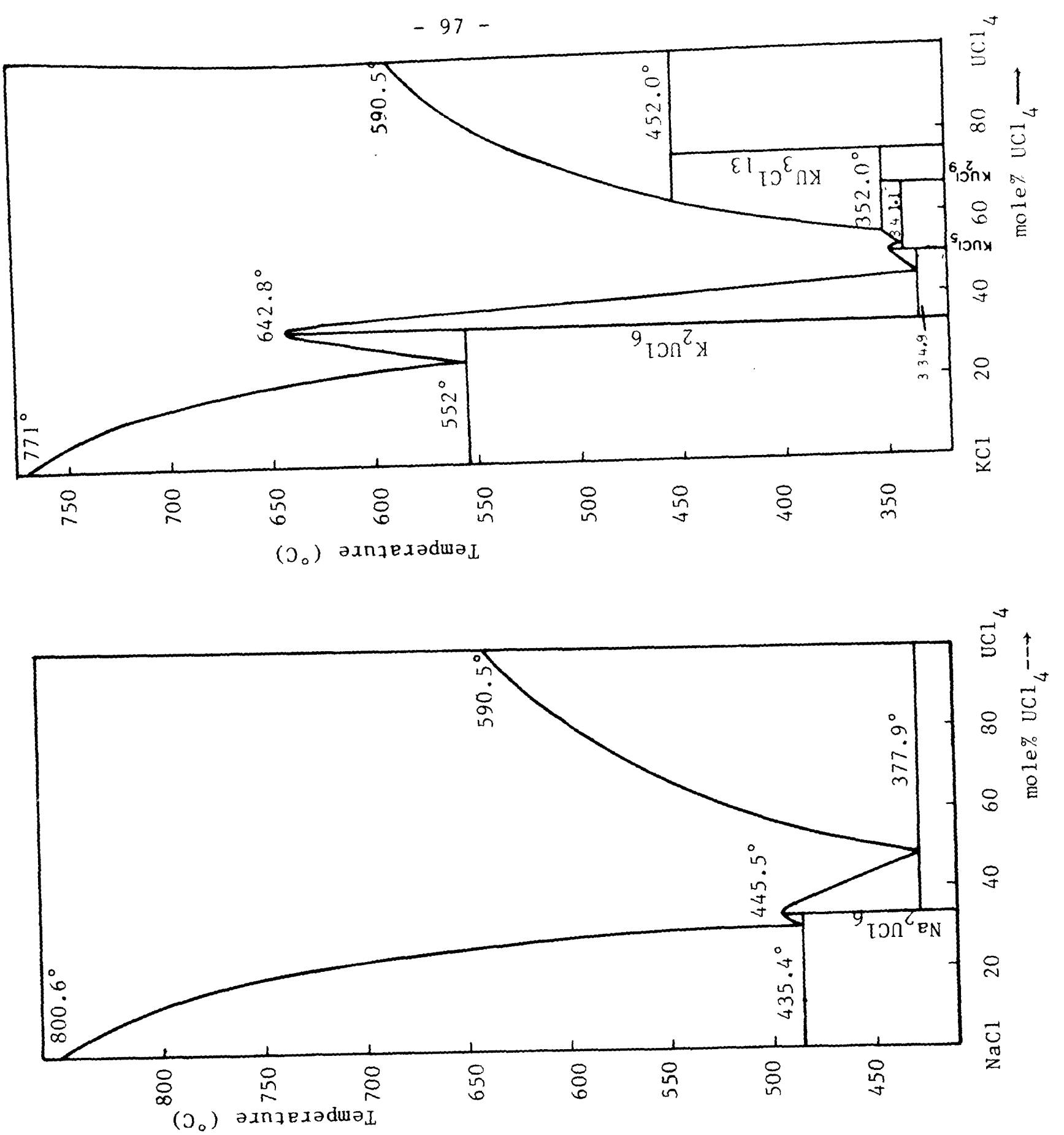


Fig. 5.3. Phase diagrams for Li_2UCl_6, Na_2UCl_6 and K_2UCl_6, from Bogacz and Trzebiatowski, 1964.

by heating overnight to 150°C under vacuum, were mixed with UCl_4 (Metals Research Corporation, 99%) and sealed in evacuated quartz ampoules. Prior to filling, these ampoules had been baked out at 1000°C for 24 hours. The mixtures of starting materials were heated in a furnace to about 100°C above the melting point of the desired product for several hours, ie 650°C for Li_2UCl_6 and Na_2UCl_6 , and 800°C for K_2UCl_6, before being allowed to cool slowly to room temperature. The initial dark-green-looking solids were ground to form light green powders. Both Na_2UCl_6 and K_2UCl_6 were very hard to grind. Li_2UCl_6 was somewhat easier. A sample of each compound was sealed in a 0.3mm capilliary tube and a Debye-Scherrer photograph taken. The X-ray powder diffraction patterns for Li_2UCl_6 and Na_2UCl_6 were very weak, due to the high absorption of uranium, but could both be indexed on a hexagonal cell. For Li_2UCl_6 a = 11.158(7), c = 6.042(2) Å and for Na_2UCl_6 a = 11.739(2), c = 6.278(6)Å. No correction was made for film shrinkage. There appeared to be no impurity peaks. For K_2UCl_6 the Debye-Scherrer photograph showed no peaks above the background. Even after long exposures using a Guinear camera ie 20 hours, only two very faint broad lines were visible. The samples, about 10g each, were sealed with gold washers in 12mm diameter thin walled vanadium cans. Due to the hygroscopic nature of UCl_4 and the various products, all weighings and manipulations were performed in a glove box under dry nitrogen or argon.

The three samples of Li_2UCl_6, Na_2UCl_6 and K_2UCl_6 were run on D1A at room temperature from 6-160° 2θ at a wavelength of 1.909 Å, each run lasting about 12 hours. In the time remaining we were

able to run K_2UCl_6 at 349°C,ie above the first phase transition reported by Bogacz and Trzebiatowski (1964) at 334.9°C.

5.3. Data Analysis and Discussion

The scattering lengths used were Li =-0.214×10^{-12}cm, Na = 0.36×10^{-12}cm, U = 0.853×10^{-12}cm, K = 0.37×10^{-12}cm and Cl = 0.958×10^{-12}cm. (Bacon, 1975).

Na_2UCl_6

The neutron diffraction pattern obtained for Na_2UCl_6 confirmed the X-ray powder photograph and could be indexed as hexagonal with very similar lattice parameters. It was noticed, however, that 11 medium to weak peaks were incompatible with this assignment. These were the result of 12 reflections from a small amount of unreacted NaCl contaminating the sample. This NaCl remained undetected on the Debye-Scherrer photograph due to the high absorption and dominant scattering of the uranium in Na_2UCl_6. Since the structure of NaCl is well defined, with known temperature factors from a previous neutron powder experiment (Butt, Cheetham and Willis, 1973), the refinement was attempted using the program of Bendall and Thomas (1980). This program can refine the profile obtained from up to three overlapping diffraction patterns, rather than chopping out these regions containing the NaCl peaks (which produces rather unsightly gaps in the data, as well as excluding a considerable amount of structural information for Na_2UCl_6).

The structure was refined in space group $P\bar{3}m1$ using chlorine and uranium positions as for UCl_6 with sodium ions occupying the octahedral sites at 6g (x 0 0) with $x \approx 1/3$. Anisotropic

thermal parameters were refined for sodium and chlorine since it appears that the sodium atom is coupled with strong librational motion of the $[UCl_6]$ octahedra. The uranium atoms were refined isotropically, making a total of 27 structural parameters, including the scale factor, for 346 reflections from Na_2UCl_6. The contribution to the observed profile arising from the NaCl was accounted for in space group Fm3m with Na at 4a (0 0 0) and Cl at 4b (1/2 1/2 1/2) with $B_{iso}(Na) = 1.70$ and $B_{iso}(Cl) = 1.43$ $\AA^2$. A single zeropoint, asymmetry parameter and scale factor were refined for both patterns, the relative amount of NaCl being taken account of by refining the occupancy of the Na and Cl ions constrained to be equal. For each pattern we refined the lattice parameters, and three halfwidth parameters to give a total of 28 structural parameters and 11 instrumental parameters for 358 reflections.

The refinement converged satisfactorily to $R_I = 6.51$, $R_{wp} = 10.96$, $R_p = 15.00$, $R_E = 10.69$. The final parameters are in Table 5.1, with the observed, calculated and difference profiles shown in Fig. 5.4. Following the method of Hewat (1979), a small estimated correction of $\Delta B = 0.4$ has been applied to the measured temperature factors to account for absorption by the sample, due mainly to the chlorine. The lattice parameter of NaCl refined to $a = 5.6454(1)$ $\AA$ against a published value of $a = 5.6402$ $\AA$ (Wyckoff, 1963), indicating that the true wavelength of the neutrons was 1.907 $\AA$. The refined lattice parameters of Na_2UCl_6 are $a = 11.8062(9)$, $c = 6.3243(2)$ $\AA$.

Na_2UCl_6 is isostructural with Na_2UBr_6 at room temperature with sodium ions occupying 2/5 of the remaining octahedral sites

Table 5.1.

Final parameters for Na_2UCl_6 at room temperature in space group $P\bar{3}m1$. a = 11.8062(9), c = 6.3243(2) Å.
ESD's of refined parameters in parenthesis.

Atom	Position	Point Symmetry	x	y	z	B_{iso}	B_{11}	B_{22}	B_{33}	B_{12}	B_{13}	B_{23}
Na	6g	2	0.340(1)	0	0		5.3(4)	14.5(12)	3.2(6)	7.3(6)	-0.9(6)	-1.8(12)
U(1)	1a	$\bar{3}$m	0	0	0	0.8(3)						
U(2)	2d	3m	1/3	2/3	0.479(3)	3.7(3)						
Cl(1)	6i	m	0.1102(3)	-0.1102(3)	0.239(1)		3.8(2)	3.8(2)	4.7(4)	3.8(3)	-0.9(1)	0.9(i)
Cl(2)	6i	m	0.2301(4)	-0.2301(4)	0.738(2)		10.2(5)	10.2(5)	12.0(6)	8.1(5)	2.7(2)	-2.7(2)
Cl(3)	6i	m	0.4341(4)	-0.4341(4)	0.244(1)		5.7(3)	5.7(3)	3.2(3)	3.7(3)	0.5(1)	-0.5(1)

R_p = 15.00 R_{wp} = 10.96 R_I = 6.51 R_E = 10.69

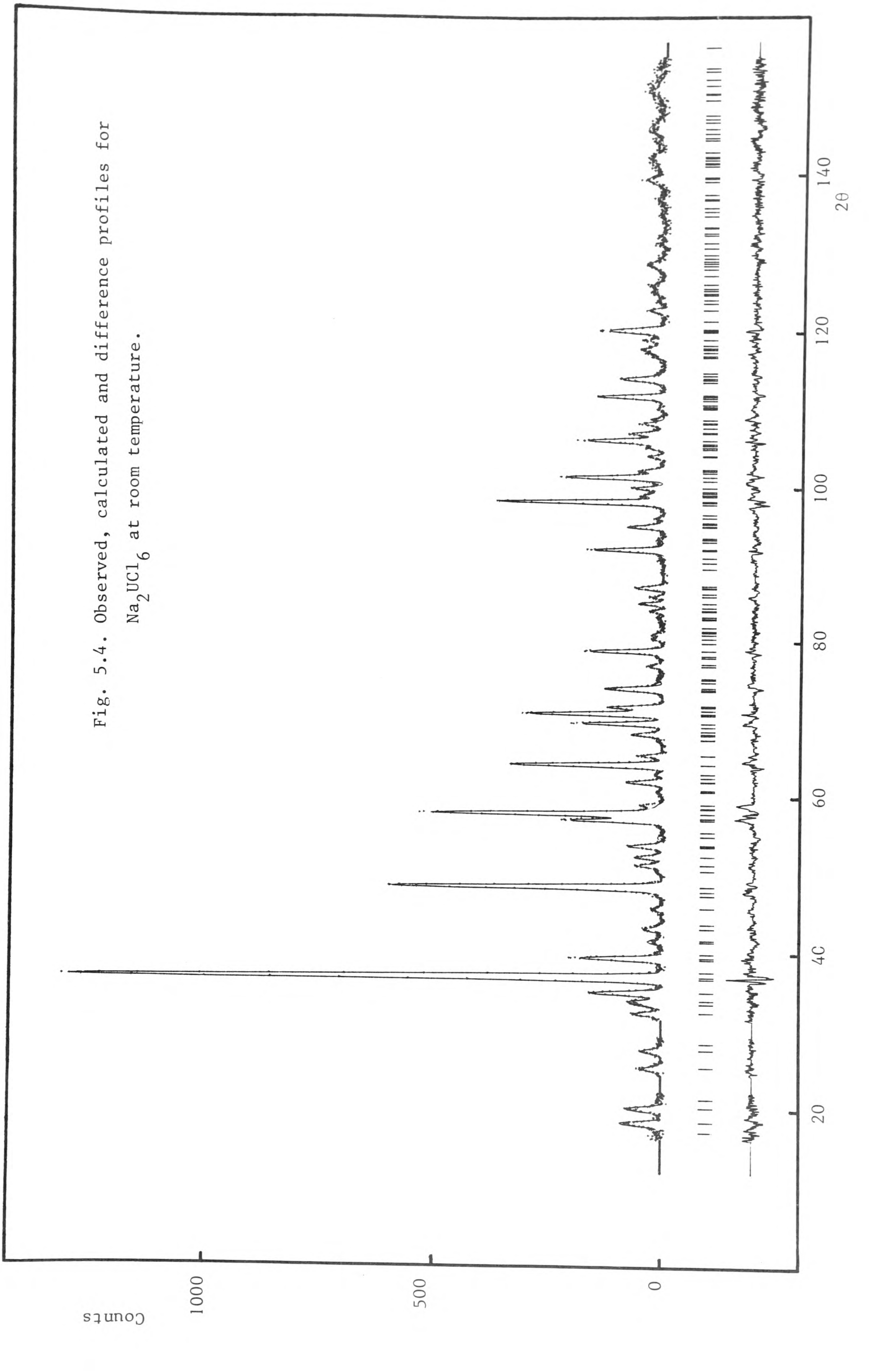


Fig. 5.4. Observed, calculated and difference profiles for Na_2UCl_6 at room temperature.

in the basic UCl_6 lattice. The cation distribution at z = 0 is shown in Fig. 5.5. The ORTEP plot, Fig. 5.6 indicates that the $[UCl_6]$ octahedra are performing marked molecular librations, with the principal axes of the thermal ellipsoids being almost normal to U-Cl bond direction.

The description of the thermal distribution function of an atom whose motion is mainly due to molecular libration, rather than atomic oscillations about a mean position, is only poorly approximated by the use of a thermal ellipsoid. The true tdf has a more banana-like appearance. We therefore might expect the B factors obtained to be rather anomalous. Indeed they are rather high, but nevertheless can be interpreted to show that the $[UCl_6]$ octahedron is librating with an average angular displacement of about 8° either side of its mean position. A better treatment of molecular motion in crystals has been proposed by Schomaker and Trueblood (1968), which makes use of three 3 x 3 symmetric tensors, T, L and S, for translation, libration, and correlations between translation and libration, respectively. A generalised version of this procedure has unfortunately not yet been incorporated into the profile refinement program. Busing and Levy (1964) have shown that diffraction experiments tend to underestimate bond lengths calculated for librating molecules and describe an appropriate correction in terms of the rigid body motion of the molecule. The bond distances for Na_2UCl_6 presented in Table 5.2 have not been so corrected, although some preliminary calculations using the CRYSTALS crystallographic package (available at Oxford) indicated the magnitude of this correction for the U-Cl bond

Table 5.2. Bond distances (Å) and angles (degrees) for Na_2UCl_6 at room temperature, uncorrected for thermal motion. ESD's in parenthesis.

1) U-Cl		2) Na-Cl	
U(1)-Cl(1)	2.714(5)	Na-Cl(1)	2.80(1)
U(2)-Cl(2)	2.67(1)	Na-Cl(2)	2.87(1)
U(2)-Cl(3)	2.54(1)	Na-Cl(3)	2.79(1)
Cl(1)-U(1)-Cl(1)	92.0(2)∞	Cl(1)-Na-Cl(2)	91.9(3)∞
Cl(1)-U(1)-Cl(1)	88.0(2)	Cl(1)-Na-Cl(3)	90.3(2)∞
Cl(1)-U(1)-Cl(1)	180	Cl(2)-Na-Cl(3)	93.6(3)∞
Cl(2)-U(2)-Cl(2)	86.3(5)∞	Cl(1)-Na-Cl(1)	84.8(3)
Cl(3)-U(2)-Cl(3)	89.3(5)∞	Cl(1)-Na-Cl(2)	89.8(3)
Cl(2)-U(2)-Cl(3)	92.2(2)	Cl(2)-Na-Cl(3)	84.8(3)
Cl(2)-U(2)-Cl(3)	177.9(7)	Cl(3)-Na-Cl(3)	94.7(5)
		Cl(2)-Na-Cl(2)	177.7(7)
		Cl(1)-Na-Cl(3)	174.2(4)
3) Intralayer Cl-Cl		4) Interlayer Cl-Cl	
Cl(1)-Cl(1)	3.90(1)†	Cl(1)-Cl(1)	3.77(1)†
Cl(2)-Cl(2)	3.66(1)†	Cl(3)-Cl(3)	4.10(1)
Cl(3)-Cl(3)	3.57(1)†	Cl(1)-Cl(2)	4.00(1)
Cl(1)-Cl(2)	4.04(1)	Cl(2)-Cl(3)	3.76(1)†
Cl(1)-Cl(3)	3.96(1)		
Cl(2)-Cl(3)	4.13(1)		

∞ Both Cl atoms are in the same layer, ie $z_1 \sim z_2$.

† Both Cl atoms are within the same $[UCl_6]$ octahedron.

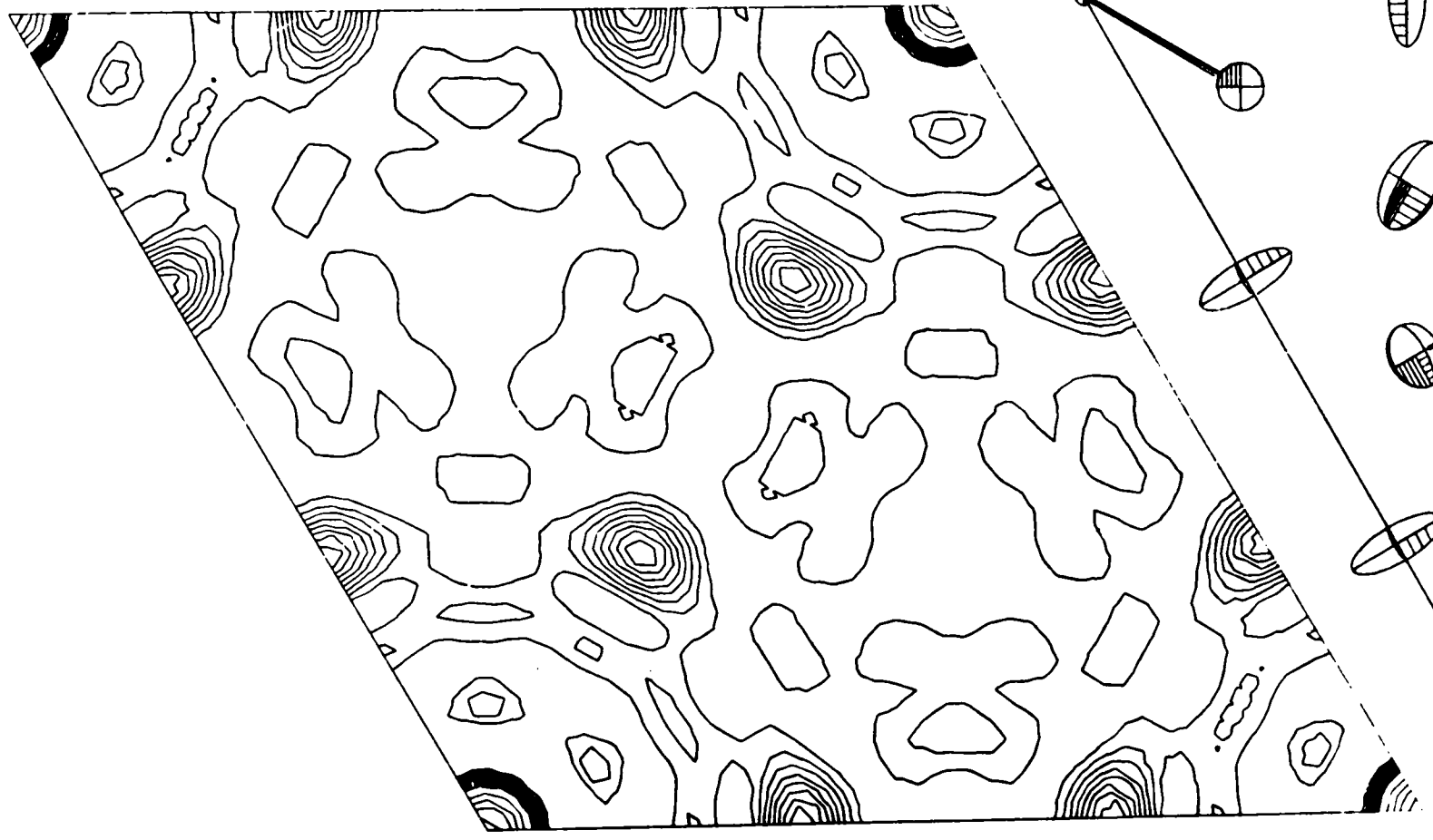


Fig. 5.5. Fourier section based on observed intensities and calculated phases showing the cation distribution at z = 0 for Na_2UCl_6 at room temperature. The motion of the sodium ions is only poorly described by the use of a thermal ellipsoid.

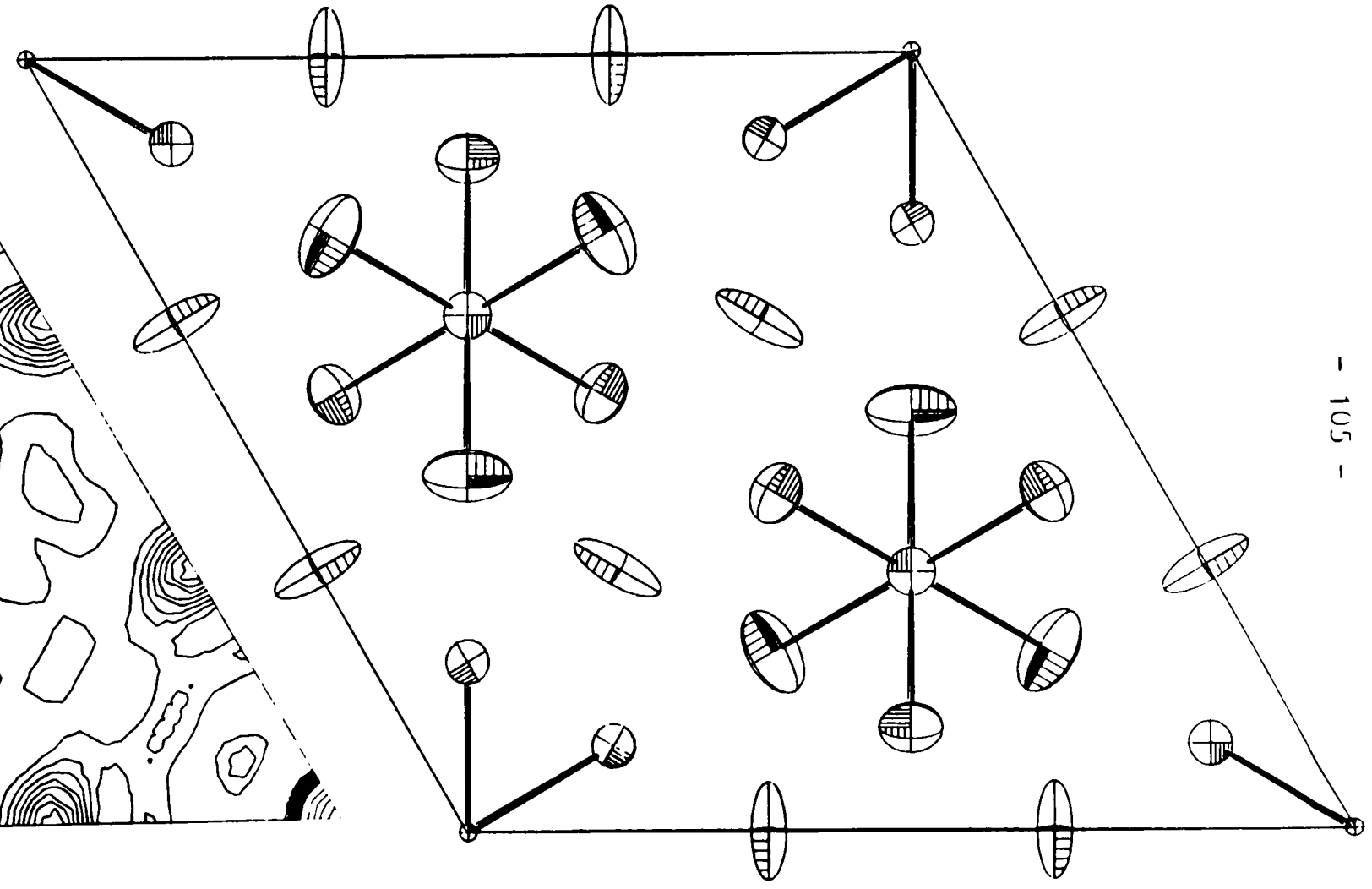


Fig. 5.6. ORTEP plot of Na_2UCl_6 at room temperature showing the librational motion of the $[UCl_6]$ octahedra.

distance to be about 0.02 Å.

Comparison of the measured bond lengths with those calculated from standard ionic radii (Cl^- = 1.81, U^{4+} = 0.97, Na^+ = 0.97 Å; Shannon and Prewitt, 1969) shows that the chloride ion lattice contracts considerably around the polarising U^{4+} ion to produce almost regular $[UCl_6]$ octahedra. The average U-Cl distance is 2.64 Å as compared to 2.78 Å from the ionic model. Chlorine chlorine distances within octahedra range from 3.57 Å to 3.90 Å, whereas distances between octahedra lie between 3.96 and 4.13 Å. Each $[U(1)Cl(1)_6]$ unit shares edges with six $[NaCl_6]$ octahedra whilst the $[U(2)Cl_6]$ units share edges with six octahedra at the centre of which there is a vacant site. The latter therefore show an average U-Cl distance of 2.61(1)Å, somewhat smaller than the value of 2.714(5)Å found for U(1)-Cl(1). The holes left for the sodium ions are close to the idealised size of 2.78 Å with an average Na-Cl distance of 2.82 Å. The $[NaCl_6]$ octahedra are more distorted than the $[UCl_6]$ and share edges with three other $[NaCl_6]$ octahedra, one $[U(1)Cl(1)_6]$ unit and two vacant octahedra. The sodium ions vibrate with largest amplitude in the direction of the most distant Cl(2) atoms which are at 2.87 Å, although comparison of the Fourier map and the ORTEP plot (page 104) indicates that an ellipsoidal description of the thermal distribution function of sodium is only moderately good. Similar dynamic behaviour is seen in Na_2UBr_6 (Hewat et al, 1980), where it is believed that there is an interaction between bromine and sodium, opening up the channels between the holes available to the Na^+, as a precursor to the observed ionic conductivity.

$\underline{Li_2UCl_6}$

The powder diffraction pattern of Li_2UCl_6 showed strong similarities with that of Na_2UCl_6 and could likewise be indexed as hexagonal with $c/a \approx 0.54$. There were however 10 peaks (equivalent to 11 reflections) from unreacted LiCl starting material, so that use was again made of the multi-pattern profile refinement program of Bendall and Thomas (1980). The structure was refined in spacegroup $P\bar{3}m1$ using the procedure and starting parameters as for Na_2UCl_6. The refinement terminated with $R_{wp} = 13.92$, $R_I = 11.50$ and $R_E=7.34$, ie satisfying the nominal condition that for a good structural model $R_{wp} < 2R_E$. This condition however becomes increasingly less reliable at higher values of R_E and we did not consider the refinement to be adequate because (i) there were regions where the differences between the observed and calculated profiles were obviously more than merely statistical and (ii) the temperature factors on the lithium and uranium atoms were very high,(eg 22 and 28 $\mathring{A}^2$ for B_{33} for Li and U(1) respectively, when attempts were subsequently made to refine the lithium and uranium atoms anisotropically). A refinement in which Li was allowed to reside in the previously vacant octahedral sites in the basic UCl_6 structure, at 6h(x 0 1/2), failed to eradicate the high temperature factors and led to a small deterioration in the fit with $R_{wp} = 14.03$, $R_E = 7.34$.

In considering the possible differences that could occur between Li_2UCl_6 and Na_2UCl_6, the smaller more polarising lithium ion should take a higher proportion of the chloride ion charge than the larger sodium ion. This would result in a decrease in the molecularity of the $[UCl_6]$ units and thus a structure which was

considerably more ionic in character and possibly closely related to one of the previously mentioned fluorides, ie Na_2SiF_6, since none of the other lattices have dimensions or reflections compatible with those observed for Li_2UCl_6, although the differences are sometimes quite small. A refinement in space group P321 with the Na_2SiF_6 structure led to a marginal improvement in fit with R_{wp} = 13.27, R_E = 7.35, but a ridiculous x parameter of 0.43(1) for Li(2) in 3f (x 0 1/2), which corresponds to a position 1.1 Å from the centre of the octahedral site. Constraining both lithium atoms to be equally displaced in opposite directions along the a-axis resulted in sensible positional parameters, somewhat improved temperature factors, but an increase in R_{wp} to 14.01. Hence despite the increase in the number of structural parameters on lowering the symmetry to P321, we have a worse fit than before in $P\bar{3}m1$.

If Li_2UCl_6 is considerably more ionic than Na_2UCl_6, then the radius ratio rules suggest that lithium might prefer to occupy a tetrahedral site in the close packed chloride array, particularly since the chloride ions contract around the U^{4+} ions, (Li^+ = 0.68, Cl^- = 1.81 Å, Li^+/Cl^- = 0.38, which is less than the tetrahedral boundary of 0.414; Wells, 1975). In $P\bar{3}m1$ six sets of tetrahedral sites exist at 6i(x $\bar{x}$ z), above and below each chloride ion. A series of refinements was performed, in $P\bar{3}m1$, where the lithium ions were allowed to occupy each of these sets of tetrahedral sites in turn. Five of the refinements diverged rapidly or failed with a singular least squares matrix. The sixth converged to R_{wp} = 14.06, R_E = 7.34, but again had huge and physically nonsensical temperature factors. Further attempts with tetrahedral

lithium were consequently abandoned.

The lithium atom in Li_2UCl_6 is therefore in an octahedral site, which is somewhat too large for it, whereas for the sodium ion in Na_2UCl_6 there is rather a good fit. We might then expect the small polarising lithium ion to relax away from its idealised position close to the centre of the octahedral site, which would cause distortions to the close packed chloride lattice and a reduction in symmetry from $P\bar{3}m1$. Various relaxation models were tried in spacegroups P3m1, $P\bar{3}$ and P3 without success. Attempts were next made at positioning the lithium ions in the various vacant sites in the rhombohedral lattice based on the α-WCl_6 structure (spacegroup $R\bar{3}$) in which there is an alternative ordering scheme for the heavy metal cation (Ketelaar and van Oosterhout, 1943). The unit cells are related by $a' = (1/\sqrt{3})a$, $c' = 3c$. The two ordering schemes for the heavy ions are closely related energetically because at 228°C α-WCl_6 transforms into β-WCl_6, which is isostructural with UCl_6 (Taylor and Wilson, 1974a). Lithium ions were introduced into the vacant octahedral sites in the close packed chloride lattice at 6c (0 0 z). Unfortunately no R_{wp} less than 17.0 could be achieved with this approach, with an R_E of 7.24.

This, we believe, concludes those possible structures which contain ordered arrangements of cations within the close packed chloride lattice. If, as suggested earlier, the more polarising Li^+ ion takes a higher proportion of the anion charge with a decrease in the molecularity of the$[UCl_6]$groups, (as compared Na_2UCl_6), then the differences between the various octahedral sites should become

less marked. The possibility of cation disorder then becomes more attractive. Some exploratory disordering schemes were therefore investigated.

Returning to spacegroup $P\bar{3}m1$, the lithium ions were first allowed to disorder equally over the octahedral sites as 6g (x 0 0) and 6h (x 0 1/2). This led to a very small reduction in R_{wp} to 13.80 for the inclusion of one extra lithium positional parameter, the temperature factors of the two types of lithium having been constrained to be equal.

Allowing U(1) to disorder equally over the two octahedral sites at 1a (0 0 0) and 1b (0 0 1/2) produced a dramatic drop in R_{wp} to 11.30, R_E = 7.78, with a reduction in the temperature factor to a sensible value. Refinement of the occupancy of the two sites indicated that this was a real effect. If U(1) is disordered over two possible sites there should be a random oscillation of potentials throughout the lattice which might induce the remaining cations to disorder likewise. Distributing Li over 6g (x 0 0) and 6h(x 0 1/2), U(1) over 1a (0 0 0) and 1b (0 0 1/2) and U(2) over 2d (1/3 2/3 z) twice, with $z \approx 0, 1/2$, produced a further fall in R_{wp} to 10.51, R_E = 7.77. Temperature factors on all atoms were sensible, and refinement of occupancies again indicated that the effect was real. Examination of the positional parameters indicated that all chlorine positions were within two standard deviations of z = 0.25, and that the structure could be equally well described in spacegroup $P\bar{3}1c$ with a great reduction in the number of variables if we allowed Li^+ to relax from the centre of its octahedral site. Refinement of the structure in $P\bar{3}1c$, with 248 Li_2UCl_6 reflections, 11 LiCl reflections and 24 structural

parameters (the cation temperature factors having been set isotropic) converged with the best value of R_{wp} = 10.09, R_E = 7.61.

If cation disorder is present in Li_2UCl_6, the structure may exist in a hexagonal spacegroup which contains a 6_3 screw axis. Disordering schemes were also attempted in a variety of spacegroups, ie $P6_3/mmc$, $P6_3mc$, $P6_322$, $P6_3/m$, $P6_3$, and also $P\bar{6}2c$. These again indicated that there was complete cation disorder over the available octahedral sites, with all the chloride ions very close to z = 0.25. There are therefore two most probable hexagonal spacegroups: 1) $P6_3/mmc$ which gives a structure equivalent to Na_2UCl_6 but with all the octahedral sites in the z = 0 and z = 1/2 layers half occupied with cations, and the chloride ion position averaged to z = 1/4; or 2) $P6_3/m$ which further allows the lithium ions to relax from the centre of their octahedral sites accompanied by a small distortion of the chloride lattice. The refinement in $P6_3/mmc$ with 19 structural parameters and 164 reflections (excluding 11 for LiCl) converged to R_{wp} = 10.31, R_E = 7.59. For $P6_3/m$, with 27 structural parameters and 273 reflections (excluding LiCl), the refinement converged to R_{wp} = 10.15, R_E = 7.66. The final atomic and thermal parameters and R factors for the three best refinements in $P6_3/mmc$, $P6_3/m$ and $P\bar{3}1c$ are shown in Tables 5.3-5.5. The thermal parameters have been corrected for absorption with ΔB = 0.5 (Hewat, 1979). The lattice parameter of LiCl refined to 5.1432(3) Å (published 5.1395 Å), thus confirming the true wavelength to be 1.907 Å. The observed, calculated and difference profiles for the refinement with the highest R_{wp} in $P6_3/mmc$ are shown in Fig. 5.7.

Table 5.3.

Final parameters for Li_2UCl_6 at room temperature in space group $P6_3/mmc$. a = 11.1915(5), c = 6.0356(1) Å. ESD's of refined parameters in parenthesis. There are 19 structural parameters (including an effective scale factor for LiCl) and 175 reflections (including 11 for LiCl).

Atom	Position	Point Symmetry	x	y	z	N	B_{iso}	B_{11}	B_{22}	B_{33}	B_{12}	B_{13}	B_{23}
Li	12i	2	0.338(5)	0	0	6	5.9(4)						
U(1)	2a	$\bar{3}$m	0	0	0	1	2.5(5)						
U(2)	4f	3m	1/3	2/3	0.504(4)	2	2.9(3)						
Cl(1)	6h	mm	0.1076(3)	0.2152(6)	1/4	6		4.0(3)	2.8(3)	3.5(5)	1.4(2)	0	0
Cl(2)	6h	mm	-0.2185(3)	-0.4370(6)	1/4	6		4.0(3)	5.0(4)	5.0(5)	2.5(2)	0	0
Cl(3)	6h	mm	0.4455(4)	0.8910(8)	1/4	6		3.0(2)	2.3(3)	2.7(3)	1.2(2)	0	0

R_p = 14.77 R_{wp} = 10.31 R_I = 7.69 R_E = 7.59

Table 5.4.

Final parameters for Li_2UCl_6 at room temperature in space group $P\bar{3}1c$. a = 11.1907(5), c = 6.0354(1) Å. ESD's of refined parameters in parenthesis. There are 24 structural parameters (including an effective scale factor for LiCl) and 259 reflections (including 11 for LiCl).

Atom	Position	Point Symmetry	x	y	z	N	B_{iso}	B_{11}	B_{22}	B_{33}	B_{12}	B_{13}	B_{23}
Li	12i	1	0.321(7)	0.012(8)	-0.046(4)	6	4.1(9)						
U(1)	2b	$\bar{3}$	0	0	0	1	2.8(6)						
U(2)	4f	3	1/3	2/3	0.499(6)	2	3.5(3)						
Cl(1)	6h	2	0.1153(4)	-0.1153(4)	1/4	6		2.8(2)	2.8(2)	3.6(5)	1.0(3)	-0.4(3)	-0.4(3)
Cl(2)	6h	2	-0.2247(3)	0.2247(3)	1/4	6		4.1(3)	4.1(3)	3.8(8)	3.2(3)	1.9(5)	1.9(5)
Cl(3)	6h	2	0.4450(5)	-0.4450(5)	1/4	6		4.3(3)	4.3(3)	4.1(8)	1.8(4)	2.1(4)	2.1(4)

R_p = 14.43 R_{wp} = 10.09 R_I = 7.52 R_E = 7.61

Table 5.5.

Final parameters for Li_2UCl_6 at room temperature in space group $P6_3/m$. a = 11.1911(5), c = 6.0356(1) Å. ESD's of refined parameters in parenthesis. There are 27 structural parameters (including an effective scale factor for LiCl) and 284 reflections (including 11 for LiCl).

Atom	Position	Point Symmetry	x	y	z	N	B_{iso}	B_{11}	B_{22}	B_{33}	B_{12}	B_{13}	B_{23}
Li	12i	1	0.314(6)	-0.014(9)	-0.048(4)	6	4.2(9)						
U(1)	2b	$\bar{3}$	0	0	0	1	3.5(6)						
U(2)	4f	3	1/3	2/3	0.511(4)	2	2.8(3)						
Cl(1)	6h	m	0.107(1)	-0.113(1)	1/4	6		5.0(5)	3.3(5)	4.1(6)	1.8(3)	0	0
Cl(2)	6h	m	-0.227(1)	0.219(1)	1/4	6		4.6(4)	4.0(5)	3.0(5)	3.7(3)	0	0
Cl(3)	6h	m	0.445(1)	-0.451(1)	1/4	6		0.9(3)	4.8(4)	4.0(5)	0.1(3)	0	0

$R_p = 14.69$ $R_{wp} = 10.15$ $R_I = 7.40$ $R_E = 7.66$

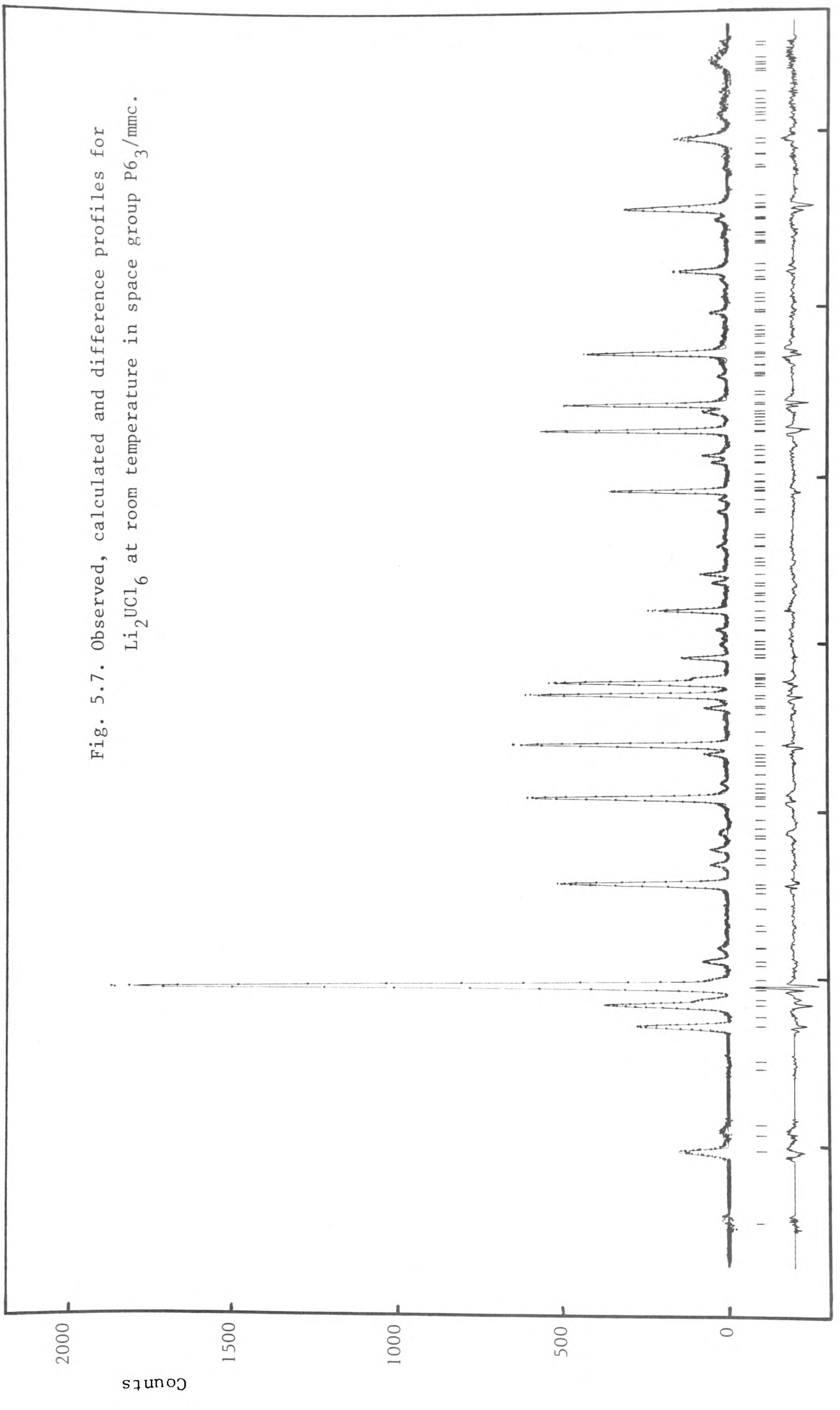


Fig. 5.7. Observed, calculated and difference profiles for Li_2UCl_6 at room temperature in space group $P6_3/mmc$.

It is very difficult to decide which of the three refinements provides the best description of the structure. There is no agreed procedure on how statistical tests (eg Hamilton, 1965) can be validly applied to profile refinement problems to assess whether the decrease in R factor for $P6_3/m$ and $P\bar{3}1c$, as compared to the simplest model in $P6_3/mmc$, is of statistical significance (and hence probably structural) or merely the result of a more flexible description with the greater number of parameters.

The least satisfactory model is $P6_3/m$ which has a worse R_{wp} than $P\bar{3}1c$ despite the presence of an extra three parameters. The esd's on the positional parameters of the principle scatterers, the chlorine atoms, are generally three times higher than in the other two models. As compared to $P6_3/mmc$, there is only a very small drop in R_{wp} by 0.16 on the addition of an extra eight parameters. This is most unlikely to be of statistical significance.

Hence we are left with two models, both very similar with respect to the placing of the chlorine and uranium atoms, and differing only as to whether the lithium atom, a very weak scatterer already disordered over twice as many positions, may relax from the centre of its octahedral site. The bond distances and bond angles for $P6_3/mmc$ and $P\bar{3}1c$ are presented in Tables 5.6 and 5.7 respectively. Both models show comparable average U-Cl bond distances of 2.62(1) and 2.66(1) Å with almost regular $[UCl_6]$ and $[LiCl_6]$ octahedra. In $P\bar{3}1c$ the lithium atom is displaced 0.385 Å from the centre of its six chloride nearest neighbours towards Cl(1), to produce a very short Li-Cl(1) bond length of 2.25(9) Å, although the average Li-Cl distance of 2.64(7) Å agrees rather well with 2.63(3) Å, as found for $P6_3/mmc$. From purely ionic considerations we would

Table 5.6. Bond distances (Å) and angles (degrees) for LI_2UCl_6 at room temperature in space group $P6_3/mmc$. ESD's in parenthesis.

1) U-Cl		2) Li-Cl	
U(1)-Cl(1)	2.575(5)	Li-Cl(1)	2.70(5)
U(2)-Cl(2)	2.67(1)	LiCl(2)	2.60(1)
U(2)-Cl(3)	2.66(1)	LiCl(3)	2.58(5)
Cl(1)-U(1)-Cl(1)	89.1(2)∞	Cl(1)-Li-Cl(2)	87.6(10)∞
Cl(1)-U(1)-Cl(1)	90.9(2)	Cl(1)-Li-Cl(3)	91.7(2)∞
Cl(1)-U(1)-Cl(1)	180	Cl(2)-Li-Cl(3)	91.4(10)∞
Cl(2)-U(2)-Cl(2)	92.2(6)∞	Cl(1)-Li-Cl(1)	85.7(19)
Cl(3)-U(2)-Cl(3)	90.1(6)∞	Cl(1)-Li-Cl(2)	88.7(11)
Cl(2)-U(2)-Cl(3)	88.8(1)	Cl(2)-Li-Cl(3)	92.1(10)
Cl(2)-U(2)-Cl(3)	178.5(8)	Cl(3)-Li-Cl(3)	91.0(20)
		Cl(2)-Li-Cl(2)	174.9(28)
3) Intralayer Cl-Cl		Cl(1)-Li-Cl(3)	177.3(20)
Cl(1)-Cl(1)	3.614(7)†		
Cl(2)-Cl(2)	3.855(8)†	4) Interlayer Cl-Cl	
Cl(3)-Cl(3)	3.767(9)†	Cl(1)-Cl(1)	3.669(7)†
Cl(1)-Cl(2)	3.669(11)	Cl(3)-Cl(3)	3.683(6)
Cl(1)-Cl(3)	3.789(14)	Cl(1)-Cl(2)	3.705(5)
Cl(2)-Cl(3)	3.713(12)	Cl(2)-Cl(3)	3.735(9)†

∞ Both Cl atoms are in the same layer, ie $z_1 \sim z_2$.

† Both Cl atoms are associated with the same two half U atoms.

Table 5.7. Bond distances (Å) and angles (degrees) for Li_2UCl_6 at room temperature in space group $P\bar{3}1c$. ESD's in parenthesis.

1) U-Cl	
U(1)-Cl(1)	2.696(4)
U(2)-Cl(2)	2.59(2)
U(2)-Cl(3)	2.63(2)
Cl(1)-U(1)-Cl(1)	91.7(1)∞
Cl(1)-U(1)-Cl(1)	88.3(1)
Cl(1)-U(1)-Cl(1)	180
Cl(2)-U(2)-Cl(2)	89.3(9)∞
Cl(3)-U(2)-Cl(3)	90.7(9)∞
Cl(2)-U(2)-Cl(3)	90.0(1)
Cl(2)-U(2)-Cl(3)	179.0(13)

3) Intralayer Cl-Cl	
Cl(1)-Cl(1)	3.870(9)†
Cl(2)-Cl(2)	3.648(7)†
Cl(3)-Cl(3)	3.748(13)†
Cl(1)-Cl(2)	3.772(4)
Cl(1)-Cl(3)	3.661(9)
Cl(2)-Cl(3)	3.722(8)

4) Interlayer Cl-Cl	
Cl(1)-Cl(1)	3.755(3)†
Cl(3)-Cl(3)	3.696(6)
Cl(1)-Cl(2)	3.688(4)
Cl(2)-Cl(3)	3.697(3)†

2) Li-Cl	
Li-Cl(1)	2.69(5)
Li-Cl(1)	2.25(9)
Li-Cl(2)	2.61(7)
Li-Cl(2)	2.74(6)
Li-Cl(3)	2.59(6)
Li-Cl(3)	2.98(8)
Cl(1)-Li-Cl(2)	101.5(15)∞
Cl(1)-Li-Cl(2)	88.1(14)∞
Cl(1)-Li-Cl(3)	80.3(14)∞
Cl(1)-Li-Cl(3)	98.0(17)∞
Cl(2)-Li-Cl(3)	91.3(24)∞
Cl(2)-Li-Cl(3)	81.1(12)∞
Cl(1)-Li-Cl(2)	94.8(32)
Cl(2)-Li-Cl(3)	87.7(17)
Cl(3)-Li-Cl(3)	82.8(24)
Cl(3)-Li-Cl(2)	82.5(27)
Cl(2)-Li-Cl(1)	88.2(19)
Cl(1)-Li-Cl(1)	98.7(30)
Cl(1)-Li-Cl(3)	175.8(29)
Cl(2)-Li-Cl(2)	163.6(34)
Cl(3)-Li-Cl(1)	163.1(33)

∞ Both Cl atoms are in the same layer, ie $z_1 \sim z_2$.

† Both Cl atoms are associated with the same two half U atoms.

expect the Li-Cl distance to be about 2.49 Å.
The presence of the highly polarising U^{4+} ion adjacent to the chloride should, if anything, lead to an increase in the Li-Cl distance, due to the relative decrease in the external anionic charge. Such a small atomic separation therefore is implausible, and must result from compensation in the refinement for an inadequate description of the real scattering density due to improper symmetry constraints, eg on the chlorine anisotropic temperature factors. We therefore consider that the model in spacegroup $P6_3/mmc$ provides the most probable description of the structure.

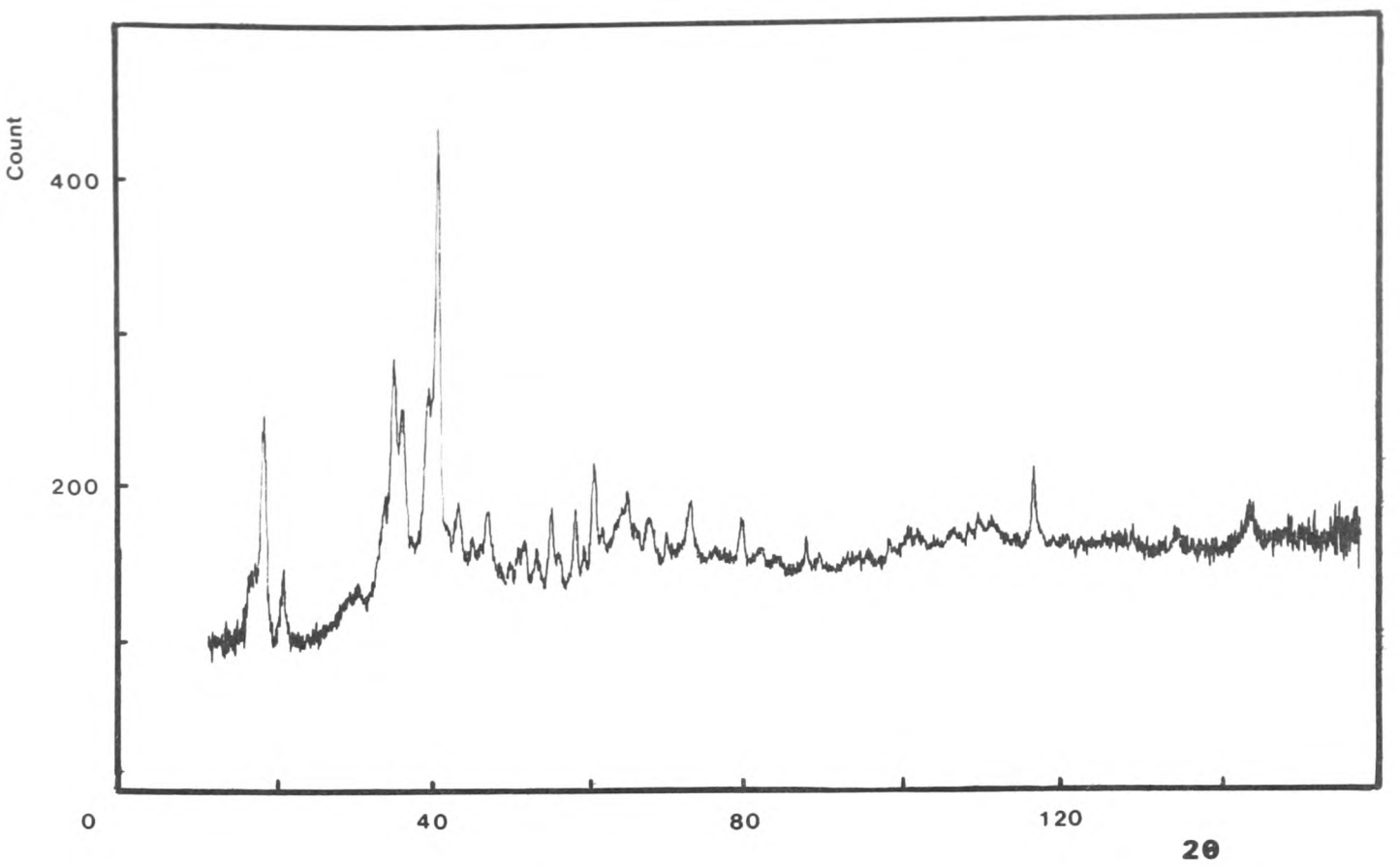
Comparison with Na_2UCl_6 shows clearly the effects of the lithium ion in abstracting a higher proportion of the anion charge. The chloride ion lattice contracts less markedly around the U^{4+} so that there no longer exists rather discrete $[UCl_6]$ units (as in UCl_6 itself). The chloride chloride distances within the $[UCl_6]$ octahedra are now comparable with those in between, ie within $[LiCl_6]$. The octahedra are themselves more regular with a spread in chlorine chlorine distances within a range of 0.12 Å for $[LiCl_6]$ and 0.24 Å for $[UCl_6]$ as compared to 0.17 and 0.33 Å respectively in Na_2UCl_6. The chlorine temperature factors are much less anisotropic and indicate that librational and molecular motion are much reduced. The high temperature factor on the lithium ion is characteristic of an atom averaged to the centre of a site which is somewhat too large for it, or may indicate that the lithiums are dynamically disordered. We believe the above observations are strong evidence in support of the structure of Li_2UCl_6 as a nearly regular close packed array of chloride ions in which 1/3 of the octahedral sites are half-filled by U^{4+}, and 2/3 are half-filled with Li^+, in a statistically disordered manner.

K_2UCl_6

The diffraction patterns for K_2UCl_6 at room temperature and at 349°C were both very weak and disappointing with high backgrounds exhibiting marked modulation. They are shown in Fig. 5.8. The strong peaks in each pattern can be indexed on a pseudo face-centred cubic lattice with a $\approx$ 10.97(2) Å. It is clear however from the presence of the often ill-defined small peaks between the major reflections, that the true symmetries are lower than this. The greater complexity of the room temperature pattern indicates that the phase change reported by Bogacz and Trzebiatowski (1964) at 334.9°C is a displacive transition to a more symmetric high temperature structure.

These observations indicate that the structure of K_2UCl_6 is based on that of K_2PtCl_6, Fig. 5.9, which is adopted by a very large number of A_2MX_6 compounds (see Pies and Weiss, 1973, or Wyckoff, 1965, for a comprehensive list). This structure, which was described briefly earlier, is of the antifluorite type and may be thought of as being composed of isolated $[MX_6]^{2-}$ octahedra which are centred at the origin of a fcc lattice. The A^+ ions then occupy the holes at (1/4 1/4 1/4) which are surrounded by the $[MX_6]^{2-}$ octahedra in a tetrahedral co-ordination. This gives the A^+ ion 12 equidistant X-atom nearest neighbours.

Brown (1964), from simple ionic packing arguments, has shown that if the A^+ ion is more than 2% smaller than the cavity available to it, then a distortion from the ideal cubic structure can be expected, at least at lower temperatures. In K_2TeI_6



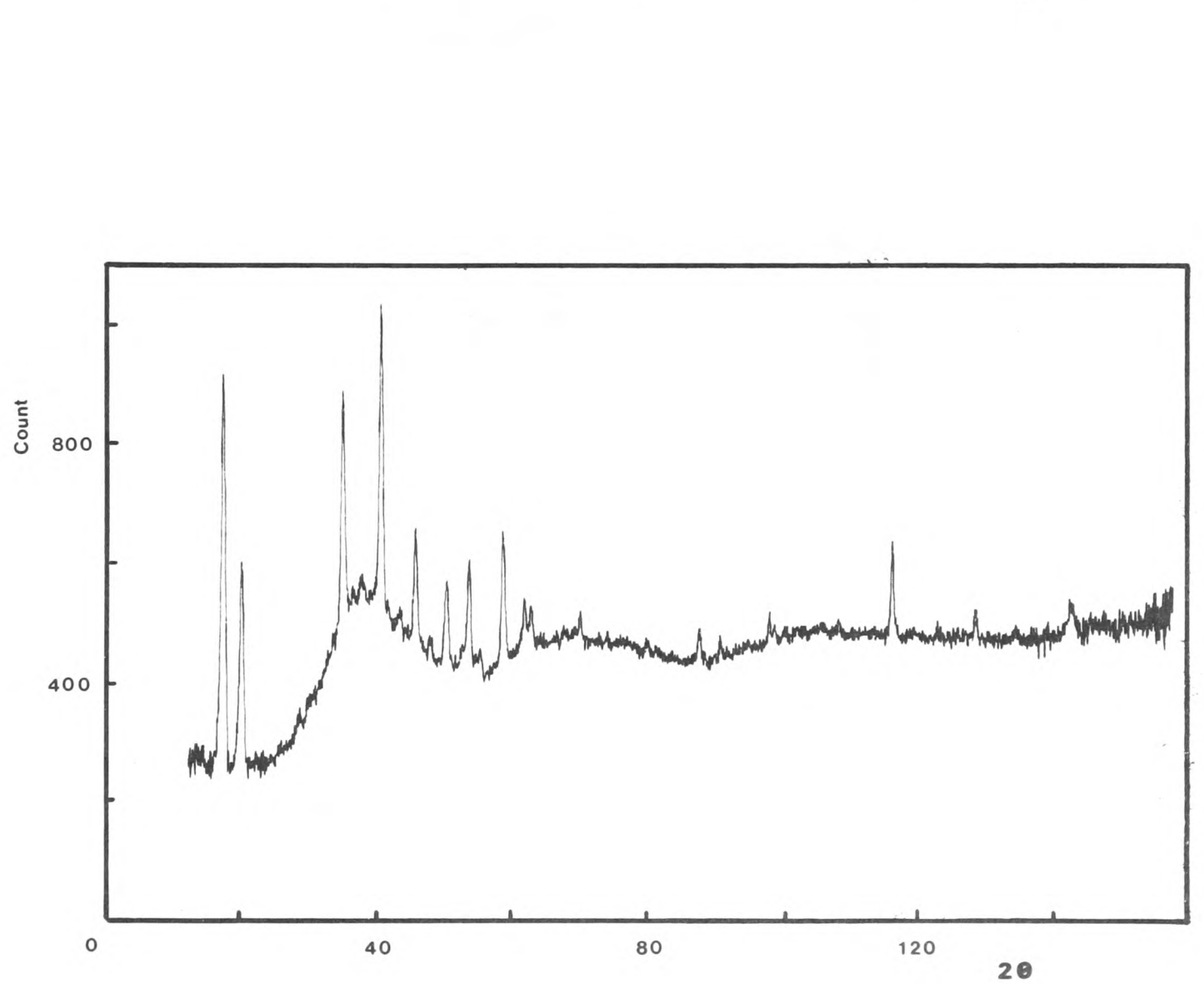
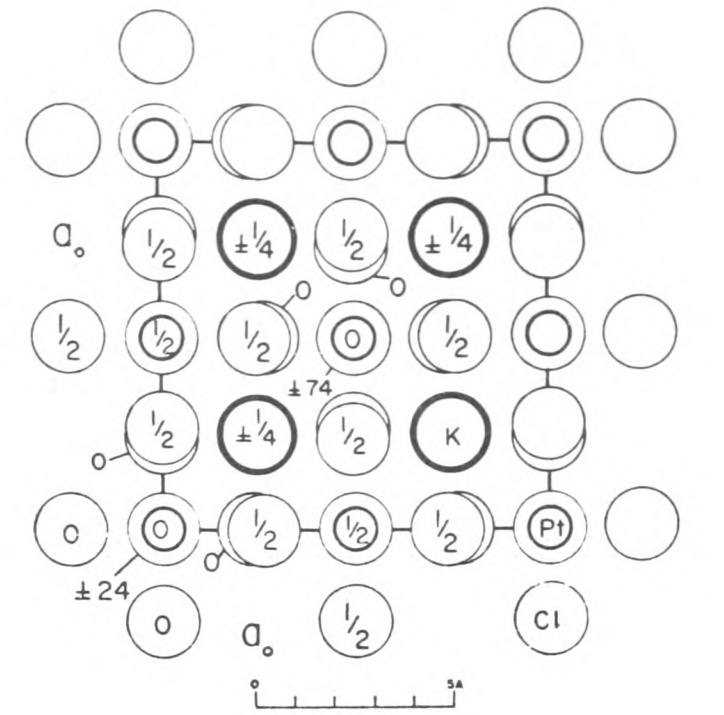
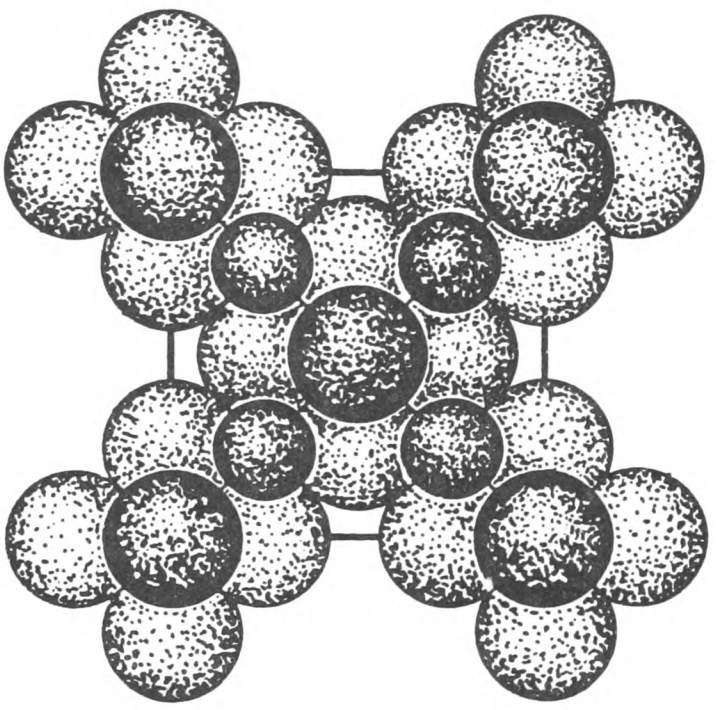


Fig. 5.8. The powder neutron diffraction patterns obtained for K_2UCl_6 at room temperature (top), and at 349°C (bottom).





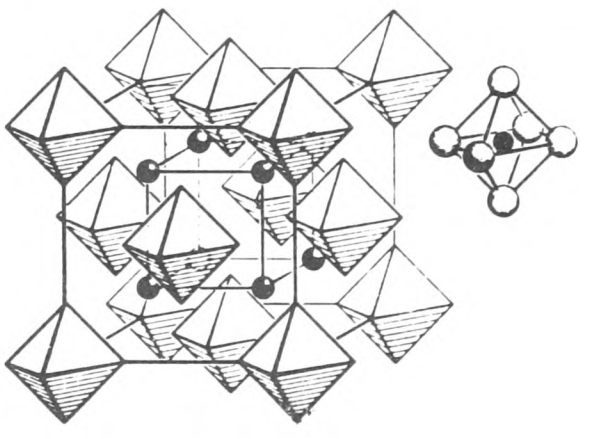


Fig. 5.9. Three views of the K_2UCl_6 structure; top, projection along a cube axis; middle, packing diagram of the lower half of the structure seen along a cube axis; bottom, showing the antiflourite arrangement with $[PtCl_6]^{2-}$ octahedra.

for example, where the cavity available to K^+ is particularly large, a triclinic structure is observed at room temperature. Similarly, K_2PbCl_6 shows a reversible transition at 60 ± 5°C from a monoclinic phase (spacegroup P21/m, a ≈ b = 7.13(1), c = 10.16(1) Å, β = 89.83(5)) to the cubic K_2PtCl_6 type structure (Brown and Lim, 1967), and whereas both Cs_2WBr_6 and Rb_2WBr_6 are cubic at room temperature (a = 10.70 and 10.50 Å respectively), K_2WBr_6 is tetragonal (a = 7.22, c = 10.64 Å). The analogous chlorotungstates are all cubic (Kennedy and Peacock, 1963). Indeed, there are rather few A_2MX_6 compounds, apart from K_2PtCl_6 itself, where the A^+ cation fits its cavity to within 2%, so that we might perhaps expect most of the cubic structures reported to distort at sufficiently low temperature.

Rössler and Winter (1977) have shown in an alternative approach that for A_2MX_6 compounds of tetravalent 4d and 5d transition metal ions, the temperature at which this distortion occurs falls systematically in crossing the series, or in passing from a larger to a smaller halogen ion. They correlate this observation with estimates and measured values of the ligand field stabilisation energy (LFSE) of the transition metal ion. On this basis, K_2PtCl_6 and K_2PdCl_6, which have large amounts of LFSE, should remain cubic down to temperatures very close to absolute zero, and indeed no transitions have yet been reported for these compounds.

Detailed and systematic structural studies have been performed on only two compounds, ie K_2SnCl_6 and K_2ReCl_6. At room temperature K_2SnCl_6 is cubic, Fm3m, a = 9.990(2) Å, (Lerbscher and Trotter, 1976). A variety of workers using different techniques, eg specific heat, NQR, Mössbauer and Raman spectroscopy etc,

have reported two phase transitions at 261K and 255K. From X-ray Guinier diffractometer studies (Ihringer, 1977), neutron and X-ray powder work (Boysen, Ihringer, Prandl and Yelon, 1976), single crystal X-ray diffraction (Ihringer, 1980), and high resolution powder neutron diffraction on D1A (Boysen and Hewat, 1978), it has been shown that these transitions involve a reduction in symmetry from Fm3m to P4/mnc then to $P2_1/n$, isostructural with K_2TeBr_6 (Brown, 1964). The structural changes involve small rotations of the essentially rigid $[SnCl_6]$ octahedra away from the cubic crystal axes. The first transition appears to be driven by a mode consisting of in-phase rotations of $[SnCl_6]$ octahedra within a layer about [001], the presence of which was deduced from the examination of the inelastic diffuse background seen in both X-ray and neutron diffraction studies. The diffuse background observed by us in K_2UCl_6 shows strong similarity with that for K_2SnCl_6.

For K_2ReCl_6 the series of transitions reported by Busey, Dearman and Bevan (1962) from specific heat studies at 111, 103 and 76K, in addition to the antiferromagnetic ordering at 11.9K, was suggested to follow the scheme Fm3m → I4/m → $P4_2/n$ → Pn3. This was deduced from an approach which combined lattice dynamics and Landau's theory (1937), in an attempt to provide a single consistent theoretical picture of the crystallographic phase transitions of all antifluorite A_2MX_6 compounds. The various transitions were described in terms of the temperature dependence of a single branch of the phonon spectrum, again involving the librational motion of the $[MX_6]$ octahedra as a rigid unit (O'Leary and Wheeler, 1970). NQR (Van Driel, Armstrong and McEnnan, 1975) and inelastic neutron scattering (Lynn, Patterson, Shirane and Wheeler, 1978) supported

this approach. From high resolution powder neutron diffraction studies, Brown, Forsyth and Hewat (1981) assigned the phases of K_2ReCl_6 as Fm3m → C4/mcn → C2/c → $P2_1/n$ → antiferromagnetic $P2_1/n$. These results are in agreement with group theoretical models and some "recent inelastic neutron scattering results". Furthermore the sequence is identical to that found in K_2SnCl_6 with an extra intermediate phase in C2/c which is the result of the separate condensation of two equal rotational modes which condense simultaneously in K_2SnCl_6. (C4/mcn is obtained from the standard setting P4/mcn by a doubling of the unit cell and rotating the (x,y) axes by 45°). By extrapolating the model further, Brown et al believe another phase change could theoretically be possible to a triclinic structure in $P\bar{1}$, as found for K_2TeI_6. This they believe probably describes all known phases of K_2PtCl_6 type compounds.

We attempted to refine our powder patterns of K_2UCl_6 at room temperature and 349°C in a number of spacegroups, including all those found by Brown et al for K_2ReCl_6 and all those suggested by O'Leary and Wheeler, plus a number of others which has been suggested in the literature,eg Pnnn (Ihringer, 1980). None were successful; although some of the atomic positional parameters were quite reasonable, the temperature factors were invarably ridiculous. Some of the models produced R_{wp} of about 30 with $R_E \approx 17$. With a powder pattern so weak, and R factors of this magnitude, sensible comparison between the various structures is impossible. Perhaps the weakness of the patterns, and the high temperature factors indicate a structure in which there is static

or dynamic disorder of the octahedra between several equivalent orientations. However, unambiguous assignment of a structure using this sort of model will require better data. This is unlikely to be obtained from X-ray diffraction studies due to the very high absorption of the sample. In addition, such a weak scatterer of neutrons would require a large crystal to enable the collection of enough reflections of sufficient intensity in a single crystal experiment. This is not available. Perhaps the best approach would be further powder studies on D1A at a longer wavelength, eg 2.98 Å (reflection from (113) of the Ge monochromator), where there is a threefold increase in neutron flux as compared to 1.909 Å. This would lead to better statistics and definition of the background and the weak reflections. The longer wavelength would improve the resolution of the broad composite peaks around 19, 36 and 42 degrees two theta at room temperature. There would be a reduction in the extent of the data collected to sin θ/λ = 0.33, ie up to 78° in 2θ at λ = 1.909 Å, but this would be a very small loss as there appears to be very few significant Bragg peaks above 80°. With improved statistics and peak resolution, we might then be better able to solve the structure of K_2UCl_6, which so far has proved resistant to all other reasonable models tried.

5.4. Conclusions

We have investigated the structures of Li_2UCl_6, Na_2UCl_6 and K_2UCl_6 at room temperature, and also a high temperature modification of K_2UCl_6, by powder neutron diffraction.

Na_2UCl_6 has a trigonal structure based on that of UCl_6, in which 1/6 and 1/3 of the octahedral sites of a hexagonally close packed

array of chlorine atoms are occupied selectively by uranium and sodium ions. There are essentially distinct almost regular $[UCl_6]$ octahedra which are performing marked molecular librations, probably coupled to the motion of the sodium ions. In Na_2UBr_6, with which Na_2UCl_6 is isostructural, similar dynamic behaviour is observed, leading to two structural transitions at higher temperatures accompanied by a marked increase in the ionic conductivity. We might expect Na_2UCl_6 to behave similarly.

On replacing the sodium ions in Na_2UCl_6 with lithium ions to produce Li_2UCl_6, there is a marked contraction of the chloride lattice with a reduction in the volume of the unit cell by 14.2%. There is a decrease in the molecular nature of the $[UCl_6]$ groups due to the higher proportion of the anion charge abstracted by the more polarising lithium ion. Signs of librational motion diminish, and the chlorine chlorine distances within $[UCl_6]$ octahedra are comparable with those in between. The distinction between the various octahedral sites is therefore reduced and the uranium and lithium cations disorder over 1/3 and 2/3 of these sites respectively. We are unable to state with certitude whether the lithium ion resides at the centre of its octahedral site, or whether there is a relaxation towards one of the surrounding chlorine atoms. The available evidence favours a lithium ion performing quite marked oscillations, but averaged about the central position. The high lithium temperature factor might be evidence for the lithium ions being dynamically disordered over the available sites. This is more likely to occur at higher temperatures so that like AgI and CuI, we could expect Li_2UCl_6 to be a good fast ion conductor, even before its first

phase transition at 415.9°C.

We were unable to solve the structure of K_2UCl_6 at room temperature or at 349°C due to the inadequacy of the data obtained. It is clear however that the increase in the size of the cation to potassium causes a rearrangement of the crystal lattice to one based on K_2PtCl_6, in which there are essentially rigid $[UCl_6]^{2-}$ octahedra arranged in an antifluorite lattice with K^+ occupying the tetrahedral sites. In the ideal cubic lattice, each K^+ would then have twelve equidistant chlorine nearest neighbours. Since in K_2UCl_6 K^+ is slightly too small for the cavity available to it, distortion to a lower symmetry occurs via the rotation of the $[UCl_6]$ octahedra away from the cubic axes. It has been shown in K_2SnCl_6 that such distortions may be driven by the softening of a mode involving the rigid body libration of the $[SnCl_6]$ unit. The similarity of the diffuse background observed for K_2UCl_6 with that of K_2SnCl_6 suggests that a similar process may be active here. No high solid state conductivities have been reported for this type of compound, except for K_2OsCl_6 in which a number of extra protons have been incorporated into the lattice.

Increasing the size of the cation further in Cs_2UCl_6 leads to the trigonal structure (Siegel, 1956) which we described in section 5.1 as Type 4a, K_2GeF_6, ie a hexagonal close packed array of KF_3 tetrahedra with Ge^{4+} occupying the octahedral sites between every second layer. However, comparing the quite similar ionic radii of Cs^+ (1.67 Å) and Cl^- (1.81 Å) and examining the atomic positions shows that a far better description is as an ordered hexagonally close packed array of Cl^- and Cs^+ ions, with U^{4+} occupying

1/8 of the octahedral holes. The potassium ion in K_2UCl_6 is too small to be close packed with chloride ions and therefore prefers the antifluorite type structure.

Hence we have shown that the room temperature structures of the series of compounds A_2UCl_6, as with the fluorides, may be rationalised in terms of the simple ideas of ionic size and charge distribution. By comparison of our structures with those of compounds with proven good ionic conductivity, we have suggested those which we think could be worthy of further investigation.

CHAPTER 6

AN NMR STUDY OF TITANIUM RICH $TiS_2(NH_3)$

6.1. Introduction

Many crystals with anisotropic layer structures can be chemically modified by insertion of foreign species which take up positions between the lamellar units of the host. Such reactions are often characterised by a marked swelling of the crystals perpendicular to the layers (the crystallographic c-direction) whereas lattice dimensions within the layers show only very slight changes (Gamble and Geballe, 1976; Whittingham, 1978a; or see Mat. Sci. Eng. 31, (1977), which is devoted entirely to these intercalation compounds). Examples of crystals which exhibit this property are graphite, the isoelectronic boron nitride, transition metal dichalcogenides, and PbI_2 or BiI_3 (Koshkin et al, 1976). The intercalated species may be a simple electropositive metal (eg H, Li, Na, etc), as in the graphite intercalates KC_{24}, LiC_6, CsC_8; a transition metal, eg M_xNbSe_2 (M = Fe, Co, Ni) or $Cu_{0.65}NbS_2$ (Koertz, 1963; Hauser, Robbins and DiSalvo, 1973); or a more complex Lewis base such as ammonia or substituted pyridines, as in $TiS_2(NH_3)$ or $TaS_2(pyridine)_{1/2}$ (Whittingham, 1978a). Even organometallic molecules such as chromocene and cobaltocene have been incorporated into several compounds, eg $TaS_2(cobaltocene)_{1/4}$ or $HfS_2(chromocene)_{1/4}$ (Gamble and Thompson, 1978; Dines, 1975a).

In the process of intercalation there is a transfer of electronic charge to the conduction band of the host layers from the intercalated species. This has been demonstrated from the transmission spectra of some of these complexes (Beale and Liang, 1973), photoelectron spectroscopy (Gamble, Osiecki and DiSalvo, 1971), incoherent inelastic neutron scattering (Tofield and Wright, 1977), and also from observations of the changes in electronic and transport properties of the host. Thus measurements of the resistivity, Hall constant and magnetic susceptability of some intercalation complexes of various substituted pyridines in TaS_2 were compatible with the donation of charge to the TaS_2. For a similar set of guest molecules, Bray and Sauer (1972) correlated the increase in the superconductin transition temperature of TaS_2, on intercalation, with the electron density on the nitrogen atom as determined by ^{14}N NQR.

Intercalation compounds have been the subject of a great many investigations, both experimental and theoretical, for they represent a most unusual state of matter. In studying the transport properties of the host layers separated by an organic Lewis base,we are effectively observing the properties of electrons confined to a two dimensional volume only 6 Å thick. Prober, Beasley and Schwall (1977) have therefore investigated fluctuation induced diamagnetism of $TaS_2(pyridine)_{1/2}$ above the superconducting transition temperature to assess the dimensionalit of the superconductivity, and compare this "quasi reduced" dimensionality with a number of theoretical models. Lattice distortions and charge density waves observed in alkali metal intercalation compounds of 1T-TaS_2 are related by Clark and Williams (1977) to the geometry of the Fermi surface of this

material. A great deal of experimental work has been directed towards elucidation of the structure and dynamics of these compounds to gain a better understanding of the interaction between the two components. To a large extent these retain rather separate identities, and the intercalation process is readily reversible.

Layered transition metal dichalcogenides of Groups IVA, VA and VIA show a variety of structures and polymorphs based on two basic structural units with either octahedral or triginal prismatic co-ordination of the metal atom by chalcogenide (Lieth and Terhell, 1977), Fig. 6.1. TiS_2 (which has the cadmium iodide structure, Wyckoff, 1963) has an almost perfect close packed array of sulphur atoms with titanium ions occupying all the octahedral sites between alternate planes of sulphur to form a series of S-Ti-S layers. The space group is $P\bar{3}m1$, a = 3.4073(2), c = 5.6953(2) Å, Z = 1, with Ti at 1a (0 0 0) and S at 2d (1/3 2/3 z) with z = 0.2501(4) (Chianelli, Scanlon and Thompson, 1975). The layers are stacked identically in passing along the c-axis. In 2H-TaS_2 the layers are formed by tantalum atoms surrounded by sulphurs at the verticies of a trigonal prism. Alternate layers are stacked with the sulphur planes rotated by 60° in the sequence AcABcB , so there are two layers per unit cell. The space group is hexagonal, $P6_3/mmc$, a = 3.315, c = 12.10 Å, Z = 2, with Ta at 2b (0 0 1/4) and S at 4f (1/3 2/3 z) with $z \approx 1/8$ (Jellinek, 1962). Other polymorphs of TaS_2 exist which have different stacking sequences of the hexagonal layers. 1T-TaS_2 is isostructural with TiS_2 (Balchin, 1976). Fig. 6.2.

In TaS_2 and TiS_2, and indeed the other related layered transition

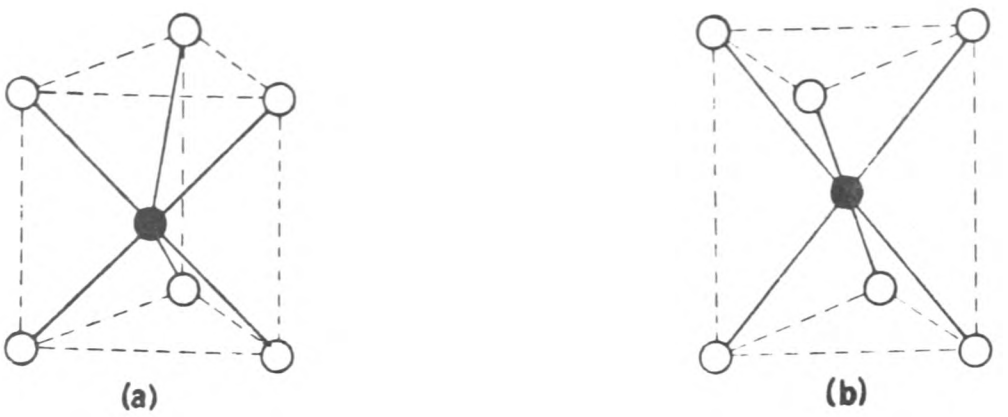


Fig. 6.1. The basic structural units found in layered transition metal dichalcogenides, (a) trigonal prismatic, and (b) octahedral, coordination of the metal atom.

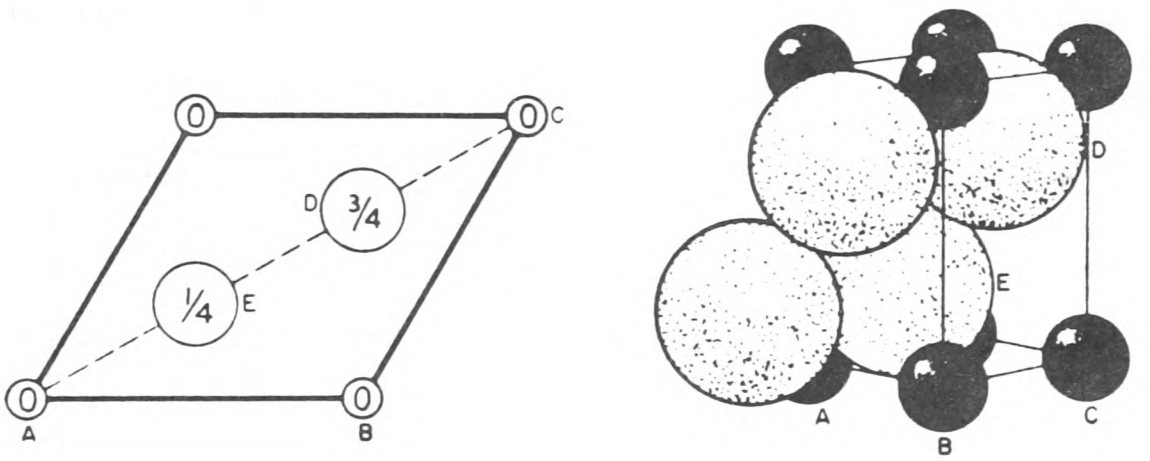


Fig. 6.2. A basal projection and the stacking arrangement in the hexagonal unit cell of the cadmium iodide structure, which is adopted by TiS_2 and 1T-TaS_2 (Wyckoff, 1963).

metal dichalcogenides, the anion lattice contracts around the cations forming electrically neutral layers, but with a greater bulk of the negative charge associated with the sulphide ion exterior. Not surprisingly, therefore, the forces within layers, strong covalent bonds, are about 100 times more powerful than the weak van der Waals attractions between layers (Verble and Wietling, 1972), and the crystals are readily cleaved.

On intercalation with pyridine, the lattice parameter of TaS_2 increases strikingly in the c-direction, with a = 3.32, c = 23.7 Å, and there is a change in stacking sequence as the pyridine is incorporated into the interlayer region. Consideration of the stereochemistry (Whittingham, 1978b), and single crystal X-ray and electron diffraction studies show that the pyridine molecule is oriented with its plane perpendicular to the layers (Parry, Scruby and Williams, 1974). Single crystal neutron diffraction on $NbS_2(pyridine)_{1/2}$ by Riekel and Hohlwein (1976) confirmed this, and indicated that the nitrogen atom was situated midway between the layers, whereas earlier work had assumed it to be "plugged in", so as to maximise the interaction between the nitrogen lone pair and the metal atom (Ruthardt, Schöllhorn and Weiss, 1972). The nitrogen atom of the ammonia molecule in $TaS_2(NH_3)$ or $TiS_2(NH_3)$ is likewise situated midway between the layers with the lone pair parallel to the layers, as demonstrated by a combination of powder X-ray diffraction, wide-line and pulsed NMR (Chianelli et al 1975; Gamble and Silbernage 1975; Silbernagel et al 1976). The ammonia molecules occupy a well defined position in the lattice, within a trigonal prism of sulphur atoms. Further pulse NMR measurements of the frequency

dependence of T_1 and T_2 (Silbernagel and Gamble, 1974) clearly established that only significant contributions to T_1 at room temperature were from the fluctuating dipolar magnetic field of neighbouring protons as a result of molecular motion, and that this motion is two-dimensional, resulting in a logarithmic variation of $1/T_1$ with frequency.

From the dynamic NMR studies it was concluded that the NH_3 molecules spin rapidly around the C_3 axis with an activation energy of 0.2 kcal $mole^{-1}$ and a rate of $\gtrsim 10^{12} s^{-1}$, much higher than the Larmour frequency, so that this motion does not contribute to T_1. The C_3 axis performs reorientations, mainly in the basal plane with a frequency of about $2 \times 10^{10} s^{-1}$ at 300K, and the translational jump frequency is about $4 \times 10^{9} s^{-1}$. Second moment measurements showed a strong line narrowing in a temperature range between 100 and 160K which is due to the freezing out of the reorientational and translational motions. It is not certain to what extent both of these motions contribute to the observed relaxation time, but an average activation energy of about 4.8(2) kcal $mole^{-1}$ was deduced, with a frequency of the motion of about $3.3 \times 10^{9} s^{-1}$ at 300K. Quasielastic incoherent neutron scattering experiments (Riekel et al, 1979) concluded that the activation energy for the preferred model with two dimensional hops of 3.32 Å to one of six adjacent lattice sites was 9.6(3) kcal $mole^{-1}$, and for reorientational motion $\gtrsim$ 1 kcal $mole^{-1}$. The discrepancy with the NMR measurement has remained unexplained.

Transition metal dichalcogenides may be intercalated with alkali metals by a variety of techniques, eg reaction with n-butyl

lithium or sodium naphthalide, or by electrointercalation (Dines, 1975a; Silbernagel and Whittingham, 1976a; Rouxel et al 1979). For lithium intercalated into TiS_2 a single crystalline phase Li_xTiS_2 with $0 < x < 1$ has been found (Whittingham, 1976). The c-lattice parameter increases monotonically with x from $c = 5.696$ Å at $x = 0$ to 6.195 Å at $x = 1.0$ (Whittingham and Gamble, 1975). This expansion of the lattice is somewhat unexpected as the vacant octahedral sites in the van der Waals gap in TiS_2 are about 0.7 Å in radius, almost identical to that of a fully ionised lithium ion. This expansion suggests then that lithium is not fully ionised, which is consistent with the observed decrease in free energy of intercalation with increasing x as shown by the Li/Li_xTiS_2 cell emf, Fig. 6.3. NMR studies showed lithium to be highly mobile with a continuously increasing ^7Li Knight shift with lithium content, and indicated that a large fraction of the lithium atom's 2s density was donated to the layers, but that this fraction decreased with increasing x (Silbernagel and Whittingham, 1976b). This behaviour is rationalised in terms of the progressive raising of the Fermi level in the TiS_2 conduction band as the lithium content increases, so decreasing the energy difference between this energy level and that in lithium metal. In addition, the intercalation energy must also be reduced by the electrostatic repulsive forces between lithium ions; these forces have been inferred from subtle anomalies in the voltage v composition curve to cause ordering of the lithium ions at room temperature (Thompson, 1978).

TiS_2 cells incorporating sodium have a lower voltage than those with lithium, reflecting the increased electronegativity of the

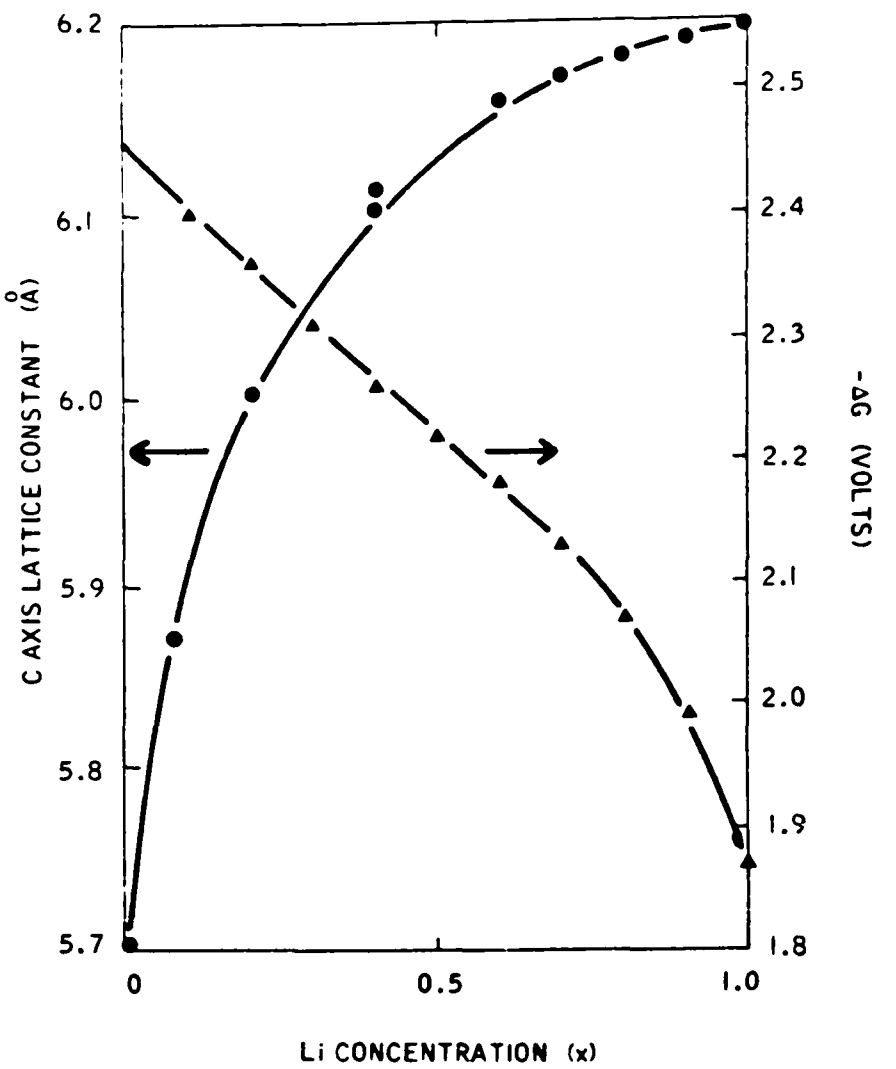


Fig. 6.3. Variation of the c axis lattice constant and partial molar free energy of formation for members of the Li_xTiS_2 series (Silbernagel and Whittingham, 1976b).

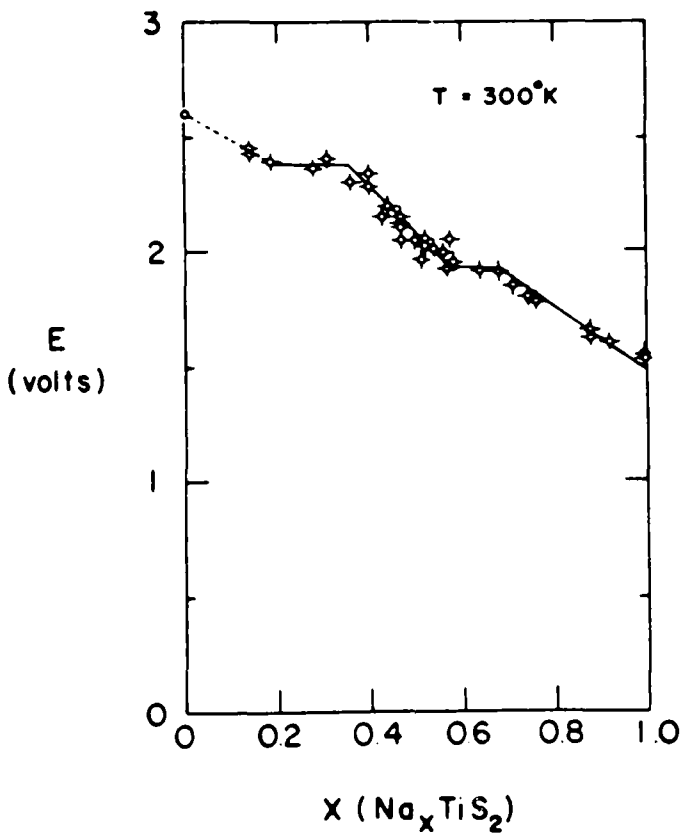


Fig. 6.4. Compositional variation of voltage with x in the Na_xTiS_2 electrode (Nagelberg and Worrel, 1979).

lithium ion bonding to the sulphur planes on intercalation. The emf v composition curves of Na_xTiS_2 show distinct discontinuities with two constant voltage plateaux for $0.25 < x < 0.35$ and for $0.6 < x < 0.7$, Fig. 6.4 (Nagelberg and Worrell, 1979). The first of these corresponds to a two-phase region where there is a transition from a Stage II compound, with sodium intercalated between every other interlayer gap, to a Stage I compound with sodium in every interlayer gap. In the second plateau region there is a change from trigonal prismatic to trigonal antiprismatic co-ordination of sodium. Similar two phase regions have been observed by powder X-ray diffraction (Rouxel, Danot and Bichon, 1971), and by NMR (Silbernagel and Whittingham, 1976a). However, the phase limits seem to vary quite substantially between these studies, reflecting perhaps the different methods of preparation employed. In any case, Winn, Shemilt and Steele (1976) have shown that the position of the discontinuity in the emf v composition curve is dependent on the stoichiometry of the host TiS_2.

In exactly the same way as they can accept foreign species into the interlayer gap, transition metal dichalcogenides incorporate atoms of their own type to form series of non-stoichiometric phases. For example Hahn and Ness (1957, 1959) report a homogeneity range for $ZrSe_2$ from $ZrSe_{1.7}$ to $ZrSe_2$, and the V-Te system shows a range of phases containing between 50 and 66.7 atomic % of Te (Lieth and Terhell, 1977). TaS_2 forms a wide range of metal or sulphur rich compounds with a variety of crystal structures and electronic properties. The preparation of stoichiometric 2H- and 1T-TaS_2 suitable for studies involving intercalation has been described by Gamble et al (1970). Titanium sulphide

forms only metal rich compounds (Winn and Steele, 1976), and polymorphs with compositions up to $Ti_{1.25}S_2$ have been reported (Tronc and Huber, 1973; Moret and Huber, 1976).

From X-ray diffraction studies on a single crystal with composition $Ti_{1.02}S_2$ grown by standard vapour phase transport techniques (Schäfer, 1964), Riekel and Schöllhorn (1975) concluded that within experimental error all the excess titanium was incorporated into the empty octahedral sites in the stoichiometric compound at 1b (0 0 1/2) in $P\bar{3}m1$. Magnetic susceptibility measurements by Thompson, Gamble and Symon (1975) suggest that the structural phase limit occurs with a 10% excess of titanium. The absence of a localised magnetic moment indicates that the excess Ti atoms have lost all four of their valence electrons to the conduction band (Klipstein et al, 1981; Wilson, 1978), which is supported by the form of the relationship between the electrical resistivity and the carrier concentration (Thompson, 1975).

The characteristics of the chemical reaction between titanium sulphide and lithium, ie reversibility, with a high free energy of reaction which changes only moderately over a wide range of x without severe structural rearrangements, accompanied by high ionic mobility of the guest ions, are considered to be those required by solid solution electrodes in solid state electrochemical cells (Whittingham, 1976, 1979). Serious attempts have been made to develop such solid state devices based on Li_xTiS_2 (Whittingham and Panella, 1981; Rao and Halbert, 1981). In these studies it has become clear that the amount of inter-

layer titanium has a very pronounced effect on the ionic mobility and the free energy and subsequent emf of the cell (Whittingham 1979). Winn, Shemilt and Steele (1976) have shown that for the Na/Na_yTiS_2 electrode a difference of up to 0.3V may occur between electrodes containing 0.2% and 2.0% excess titanium, Fig. 6.5. The sodium ion diffusion coefficient is two orders of magnitude less in the latter compound at $y \approx 0.4$. The small fraction of sites occupied by the excess titanium, now unavailable for the sodium, cannot by itself explain such a marked decrease in cation mobility and it has been suggested that strong covalent bonding must develop between the excess Ti and the adjoining layers, thus pinning the layers together and increasing the migration energy (Winn et al, 1976). Supporting evidence comes from Thompson et al (1975) who notice a very sharp decrease in the rate of ammonia intercalation into TiS_2 on increasing the Ti content, and also Whittingham and Gamble (1975) who report a sharp decrease in c with Ti content. As a result of these observations, it has been suggested that the discrepancy observed between the activation energy for diffusion of ammonia in TaS_2 as determined by NMR and quasielastic incoherent neutron scattering may be the result of a slightly non-stoichiometric sample in the latter (C. Riekel, private communication).

We have measured as a function of temperature the proton spin-lattice relaxation time, T_1, of ammonia intercalated into non-stoichiometric TiS_2, with 0.1%, 0.9% and 2.0% excess titanium. We hope to assess whether the mobility of the ammonia molecule is strongly influenced by the presence of interlayer titanium. If the excess Ti does indeed form strong covalent bonds with

the adjacent sulphur atoms then we might expect that it would be. We can also then say whether the presence of extra atoms in the interlayer gap might be responsible for the discrepancy observed between NMR and quasielastic neutron scattering measurements on $TaS_2(NH_3)$. We have chosen to study TiS_2 because the thermodynamic conditions required for precise control of stoichiometry have been published.

6.2. Sample preparation and characterisation

Winn and Steele (1976) have published precise thermodynamic measurements of the partial pressure and composition of sulphur vapour in equilibrium with non-stoichiometric $Ti_{1+x}S_2$ for $0 < x < 0.11$, at temperatures between 500 and 700°C. This allows us to calculate the exact quantities of titanium metal and sulphur required to form any desired composition of titanium sulphide. The nature of the material produced, however, is very dependent on the temperature of the reaction. Thompson et al (1975) have shown that stoichiometric TiS_2 prepared at 600°C contains substantially less than 0.1% of Ti atoms in the normally vacant octahedral sites in the van der Waals gap. Materials grown at higher temperatures contain substantially higher concentrations of interlayer Ti with compensating vacancies in the layers, which conforms with an earlier suggestion by Takeuchi and Katsuda (1970). Stoichiometric TiS_2 grown at 1000°C cannot be intercalated with ammonia.

For our experiment, 9 samples of $Ti_{1+x}S_2$ ($0 < x < 0.1$) were produced in batches of about 5g by sealing under vacuum the correct proportion of titanium sponge (Johnson Matthey "Specpure",

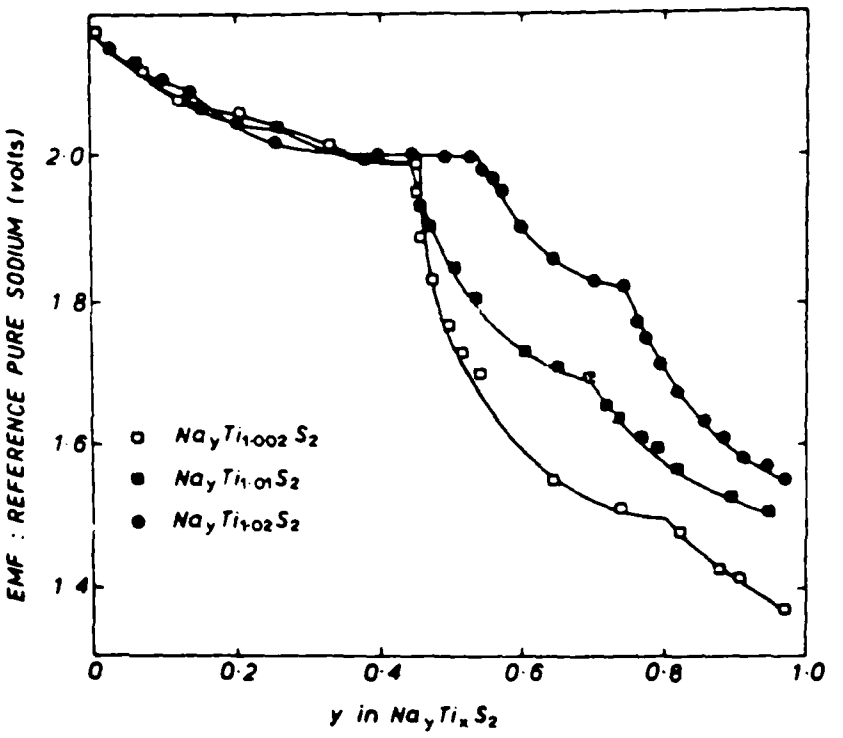


Fig.6.5. Emf vs composition curves for $Na_yTi_{1+x}S_2$ (Winn, Shemilt and Steele, 1976).

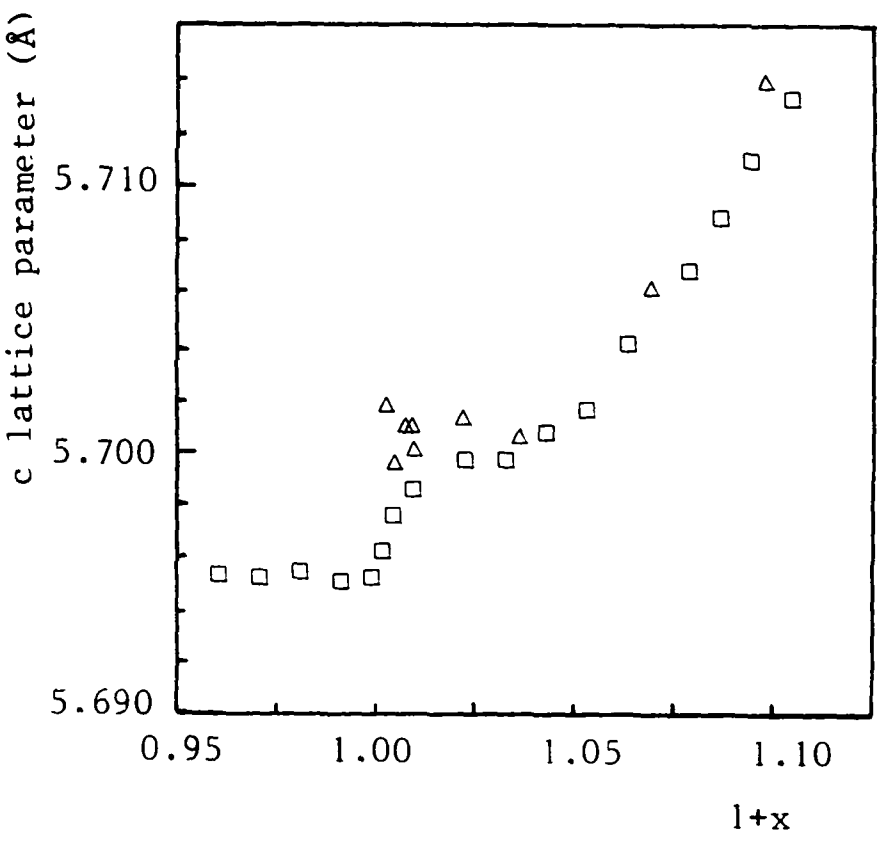


Fig.6.6. Variation of c lattice parameter with titanium content for $Ti_{1+x}S_2$; triangles, this work; squares, from Thompson, Gamble and Symon (1975).

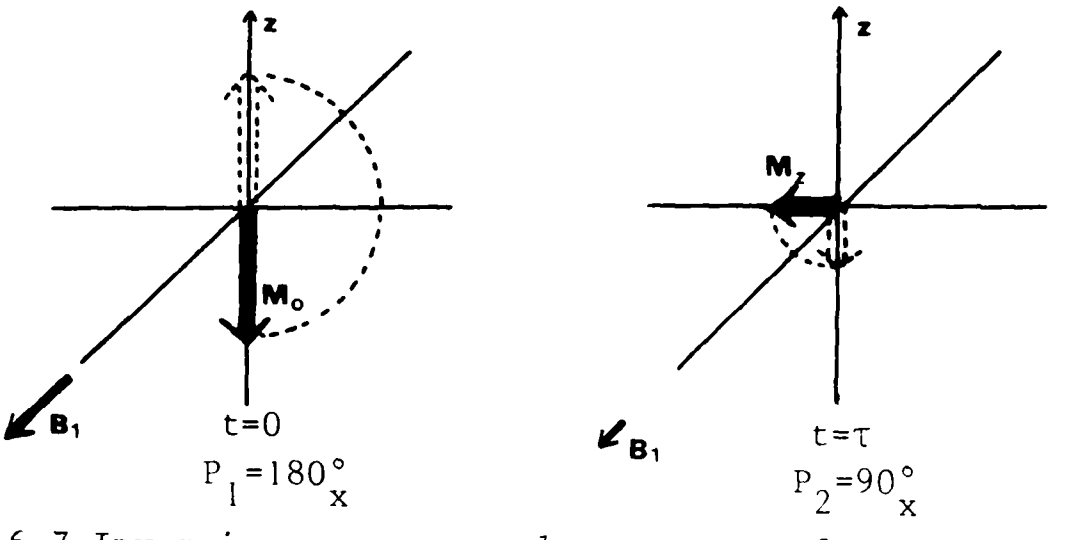


Fig.6.7. Inversion recovery pulse sequence for T_1.

99.9%) and sulphur powder (Koch Lite, 99.99%) in small dry quartz ampoules of about $10cm^3$ volume. The temperature of the ampoules was raised slowly over three days from room temperature to 550°C at which they were left to equilibrate for a week. If the temperature is raised too quickly, the high heat of formation of TiS_2 (400kJ $mole^{-1}$, Whittingham, 1978a) leads to a very rapid reaction, with the build-up of a very high sulphur pressure in the ampoule which then bursts. This can damage the brittle furnace heating elements. After a week at 550°C the ampoules were cooled, cracked open and the contents ground to a fine powder to ensure homogeneity, before being resealed in new tubes and annealed at 550°C for another week. The tubes were then quenched in cold water which causes the small amount of sulphur vapour in equilibrium with the product to condense and stick to the side of the tube. The mild conditions employed in this synthesis should have ensured that the number of titanium vacancies in the layers was at a minimum.

TiS_2 is stable in dry air, but reacts slowly in moist air to give TiO_2. The samples therefore were stored in a desiccator. The nominally stoichiometric compound was dark greenish gold, with progressive darkening of the other samples with increasing Ti content, as has been observed before (Lieth and Terhell, 1977). The titanium to sulphur ratio in each sample was determined from the weight change when about 0.5g of $Ti_{1+x}S_2$ was oxidised in air at 900°C, contained in a small platinum foil boat, to TiO_2 which is assumed to be stoichiometric. This method has been shown to give values for the composition of $Ti_{1+x}S_2$ in which x differs by less than 0.005 from the value as determined by wet chemical

analysis (Winn and Steele, 1976). Each sample was analysed twice and the values of x obtained were reproducible to within $x = 0.005$.

Powder X-ray diffraction studies were performed on a Philips diffractometer and indicated in each case the presence of a single phase. Lattice parameters were refined from the positions of about 20 peaks including α_1 and α_2 splittings. The nominally stoichiometric compound ($1+x = 1.001$ from the analysis) gave $a = 3.409(1)$ $c = 5.702(1)$ Å. Thompson et al (1975) report $a = 3.4073(2)$, $c = 5.6953(2)$ Å for stoichiometric TiS_2 which differs significantly from our values. They also show the variation of c with titanium content for typical samples of $Ti_{1+x}S_2$. Our values of c plotted against x are shown for comparison with those of Thompson et al in Fig. 6.6. Above $x = 0.02$ the two sets of data agree quite well, whereas below this value they diverge sharply. This may be because our samples contain higher proportions of interlayer titanium atoms, although the mild conditions of preparation should have kept this to a minimum. Our preparation used titanium sponge, whereas Thompson et al used higher purity (99.97%) titanium wire which will have a much smaller coating of surface oxide. The random substitution of small concentrations of oxygen for sulphur would lead to a net increase in the electronegativity of the sulphur planes, and hence greater repulsion between the layers. The method of analysis is almost 4 times less sensitive to replacement of sulphur atoms by oxygen than to the addition of extra titanium, so that up to

2% oxygen could be incorporated without affecting the accuracy of the result. The effect of these small amounts of oxygen incorporated into the lattice would become less significant at higher levels of non-stoichiometry where the increased number of intercalated titanium atoms in the van der Waals gap begins to dominate the binding between layers. Winn and Steele (1976), in their paper on the thermodynamics of $Ti_{1+x}S_2$ formation, state that their products were investigated both with a Philips X-ray diffractometer and a Guinier camera. They refer to the work of Thomson et al (1975), yet do not give the actual values they obtain for their lattice parameters.

Intercalation was effected by solidifying excess ammonia (Air Products, "ultra high pure", 99.999%) at liquid nitrogen temperature in a clean dry evacuated quartz ampoule containing about 1g of TiS_2. The ampoules were sealed off and left to warm to room temperature when the vapour pressure of ammonia is about 8 atmospheres. Quartz ampoules were preferred because they are much tougher than glass ampoules which tended to explode after a day or so, and are also much easier to seal off. The liquid ammonia in the ampoule turned blue or purple which is characteristic of a TiS_2 host (Chianelli et al, 1975), although the colour was progressively darker with increasing titanium content. Samples with a low titanium content reacted quickly, ie within a few hours as could be judged by a marked swelling of the powders, whereas other samples took much longer. Although we made no quantitative measurements, this would seem to be in broad agreement with the observations of Thompson et al (1975) and supports our view that, despite the discrepancy in the values of the c lattice

parameters, our samples do not contain large concentrations of interlayer titanium from vacancies in the layers. Samples with x greater than 0.03 would not intercalate ammonia even though they were left for several months. This may be associated with the added stability of the layers at $x \gtrsim 0.03$ as a result of the establishment of a superstructure along the c-axis (Thompson et al, 1975).

After reaction, the surviving ampoules were cooled to liquid nitrogen temperature to solidify the excess ammonia, then cracked open and left under a steam of dry nitrogen whilst the ammonia evaporated slowly. The intercalation compounds are moisture sensitive and must be protected from the air. TGA measurements showed that the layers were fully charged with approximately one molecule of ammonia per formula unit. X-ray diffractometer studies produced weak patterns with quite broad peaks which were however compatible with the assignment of a hexagonal unit cell with $a \gtrsim 3.43$, $c \gtrsim 8.91$ Å as reported by Chianelli et al (1975). The patterns became affected by moisture during the scan so that precise lattice parameters of the intercalation compounds as a function of titanium content could not be obtained, although any dependence appears to be unpronounced.

For the NMR studies, three samples of about 0.5g with titanium contents of $1+x = 1.001$, 1.009 and 1.020 were sealed in 10mm diameter flat bottomed pyrex tubes which had previously been flamed out under vacuum.

6.3. NMR Studies

Measurements of the proton spin-lattice relaxation time T_1, were made by the 180°_x - τ - 90°_x method on the three samples of

$Ti_{1+x}S_2(NH_3)$ at 60 MHz between room temperature and 160K. The pulse sequence is shown in Fig. 6.7. The first pulse of RF along x' rotates the equilibrium magnetisation M_o precessing around the field direction $\vec{z}$ into the $-\vec{z}$ direction. During the following time τ, the magnetisation recovers towards its equilibrium value exponentially,

$$\text{ie } M_z(\tau) = M_o\ (1-2\ \exp\ (-\tau/T_1)). \qquad 6.1$$

After time τ, a 90° pulse along x' rotates the magnetisation onto the y' axis where it is measured. After a wait of at least 6 x T_1, the pulse sequence can be repeated and the signals stored in the spectrometer's averager, to improve the signal to noise ratio. To determine T_1 about 10 measurements of $M_z(\tau)$ are made over the range $0 < \tau < 1.5T_1$. A plot of $\ln(M_o - M_z(\tau))$ versus τ has slope $-1/T_1$.

6.4. Results and Discussion

Kleinberg and Silbernagel (1980) have studied the variation of T_1 as a function of temperature and frequency for $TiS_2(NH_3)$ (presumably stoichiometric), and for $TaS_2(NH_3)_x$ where x = 0.8, 0.9 or 1.0. For $TiS_2(NH_3)$ a logarithmic variation of $1/T_1$ with frequency is observed on the high temperature side of the minimum in the T_1 v $1/T$ plot, (see Section 2.11). This sort of behaviour is characteristic of relaxation by magnetic dipolar fluctuations caused by two dimensional diffusion and has also been reported for $TaS_2(NH_3)$ by Silbernagel and Gamble (1974). At 295K a value of T_1 = 0.36s is given for $TiS_2(NH_3)$ which agrees very well with our value of 0.33s for stoichiometric $TiS_2(NH_3)$ at 294.5K.

Our measurements of T_1 v 1/T for the three compositions are shown in Fig. 6.8. The T_1 behaviour is so little different in each case that this is clear evidence for very little influence of the ammonia motion by the Ti^{4+} ions in the van der Waals gap, in contrast to lithium or sodium where there is a very strong effect. The shape of the curves show a marked deviation from the prediction of a symmetric minimum by BPP theory. The slope on the high temperature side of the minimum is twice that on the low temperature side. The results of Kleinberg and Silbernagel (1980) for T_1 of $TaS_2(NH_3)_{0.9}$ as a function of 1/T and frequency show qualitatively the same form. Abragam (1961) has pointed out that the main contributions to the magnetic relaxation of a spin in a diffusing system are different when $\omega\tau_c << 1$ (high temperature side) than when $\omega\tau_c >> 1$ (low temperature side). In the former case the relaxation is dominated by the motions of remote spins whose positions relative to the spin of interest change relatively more slowly with time, reflecting more the effect of molecular diffusion. For $\omega\tau_c >> 1$, however, the relaxation is controlled by the microscopic details of the molecular dynamics, ie the short time scale motions of nearby spins, and a random walk model may be more appropriate (Torrey, 1953). On this basis, the activation energy for diffusion in $TiS_2(NH_3)$, given by the slope ($=-E_A/R$) of the high temperature side of the plot, is estimated as 13.6(5) kJ $mole^{-1}$.

At 31MHz Kleinberg and Silbernagel (1980) observe no clear or consistent difference between the T_1 behaviour of their $TaS_2(NH_3)$ samples, Fig. 6.9, and consider that this may be indicative of th clustering of vacancies. Such a picture would be consistent with

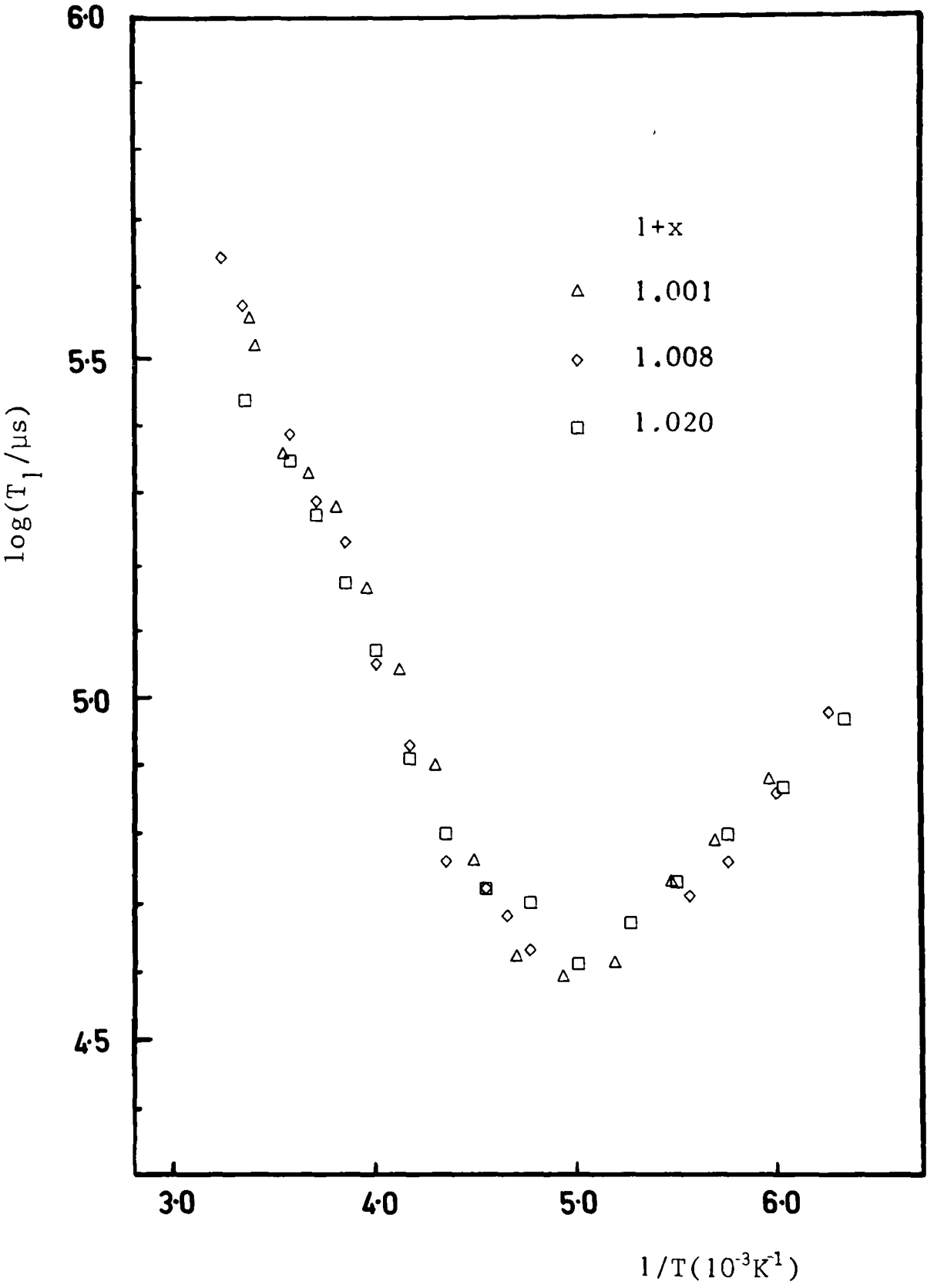


Fig. 6.8. Variation of the proton spin-lattice relaxation time T_1 with temperature for three different compositions of $Ti_{1+x}S_2(NH_3)$.

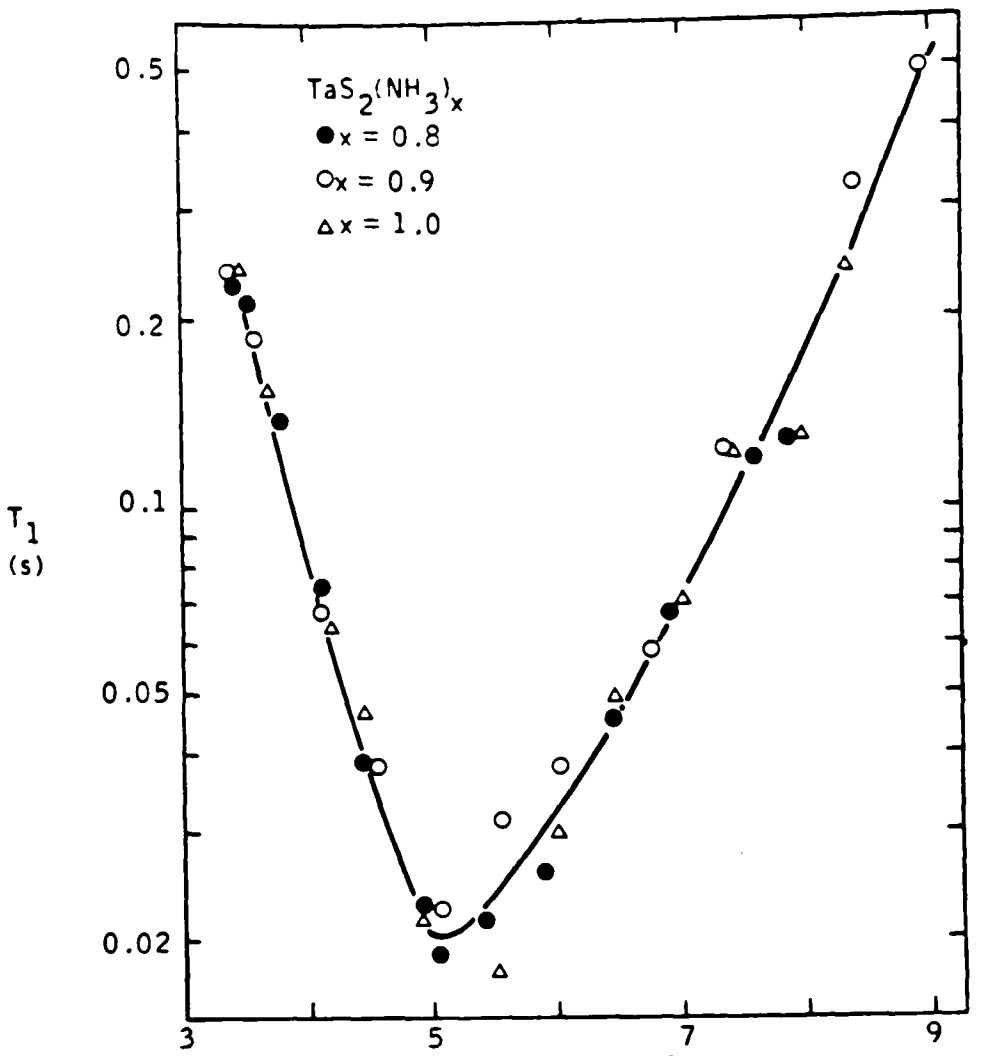


Fig. 6.9. Spin-lattice relaxation time T_1 data for $TaS_2(NH_3)_x$ from Kleinberg and Silbernagel (1980).

the work of Schöllhorn and Zagefka (1977) who have shown strong evidence that the intercalation of ammonia into TaS_2 is a redox process with the irreversible donation of charge from ammonia to the host layers, accompanied by the evolution of nitrogen. The resulting product is formulated as $[TaS_2]^{x-}(NH_4)^{+}_{x}(NH_3)_{1-x}$, where $x \approx 0.1$. The ammonium ions can be replaced by K^+. More recently, Schöllhom et al (1979) have shown that a similar mechanism is active for intercalation of pyridine into TaS_2 from, amongst other evidence, the extraction of about 10% 4 4'-dipyridine from the intercalated product. This model explains the perhaps surprising orientation of pyridine with its plane perpendicular to the layers, or ammonia with the C_3 axis parallel with the layers, and both with their nitrogen atom situated midway between the layers. With a ratio of NH_4^+/NH_3 of 1/9, each NH_4^+ is seen as acquiring a complete two dimensional solvation sphere of NH_3 which, by comparison with the crystal structures of ammonium halide-ammoniates (Olovson, 1960), must be arranged with the lone pair directed towards the positive charge centres.

Each NH_4^+ ion has six nearest neighbours at 3.43 Å, six next nearest neighbours at 5.94 Å and six more at 6.86 Å, which on average should include another NH_4^+ ion. Replacement of NH_4^+ by Ti^{4+} will have a very marked effect on the first solvation circle of ammonia molecules, but the effect must drop off very rapidly due to the screening of these molecules. On a very crude electrostatic basis with a $1/r^2$ fall off in potential, the second nearest neighbours of a Ti^{4+} are influenced by a potential only 1/3 more forceful than the nearest neighbours of an ammonium ion, and this neglects all screening effects. With such a small concen-

tration of additional titanium in the interlayer gap, it is clear that it can have little effect. Moreover, the c-axis expansion on intercalation of TiS_2 with ammonia is 3.2 Å, which is much larger than the diameter of Ti^{4+} (1.36 Å), so that the effect of the excess Ti^{4+} in pinning the layers together, which would affect interlayer mobility, is drastically reduced. It is not known whether the Ti^{4+} remains associated with one of the layers, or is midway between them co-ordinated by the surrounding ammonia. If the latter case were true, we might expect to see Ti^{4+} diffusing through the layers at about the same rate as ammonia.

For lithium intercalated into TiS_2, in the absence of any screening there has to be strong repulsion between the Ti^{4+} and the Li^{+}, which must reduce considerably the volume within the van der Waals gap easily accessible to the lithium. The c-axis expansion on intercalation is only 0.5 Å, so there is still a strong influence of the titanium pinning the layers together, and a marked decrease of c-lattice parameter with increasing titanium content for the fully charged lithium compound is observed (Whittingham and Gamble, 1975). In this case there is a sharp dependence of lithium mobility on titanium content.

CHAPTER 7

CONCLUSIONS AND SUGGESTIONS FOR FURTHER RESEARCH

The distribution of the hydrogen atoms over the available hydrogen bond sites in $DUO_2AsO_4.4D_2O$ has been determined. The observed distribution has been explained in terms of the presence of two types of dimeric water species, H_4O_2 and $[H_5O_2]^+$, whose dynamic interconversion provides a simple basic mechanism for the high proton mobility in this compound. It was not considered that the powder pattern contained sufficient information for the refinement of the separate details of these two species, although this might be possible from a single crystal study with a greater number of well-resolved reflections. The displacive phase transition at 301K to a poorly conducting antiferroelectric phase has been identified as involving the ordering of the hydrogen bonds over the formally disordered sites, and the formation of chains composed of the H_4O_2 and $[H_5O_2]^+$ units. Two such chains run in the direction of the b-axis of the triclinic unit cell, and one chain in the a-direction. The structure deduced appears compatible with the observed dynamic, optical and antiferroelectric properties of this phase. The replacement of 1/9 of the hydrogen ions in DUAs by Li^+, to form $LiUO_2AsO_4.4D_2O$, causes a rearrangement of the hydrogen bonded water squares of the former such that all hydrogen bond sites are now fully occupied. The unit cell is halved along c, and the water squares rotate about their four-fold axes so that four water oxygens of four separate squares are disposed tetrahedrally around the lithium ion which links the squares together. From a comparison

between the structures of DUAs and LiUAs, a possible structure and mechanism for sodium ion mobility in $NaUO_2PO_4.3H_2O$ has been proposed. Further powder diffraction studies would allow the validity of this model to be checked. For many other cation substituted compounds, which may be derived by cation exchange of HUAs or HUP, very little is known concerning the position and water co-ordination of the cation. Single crystal X-ray studies on the potassium and ammonium substituted compounds were inconclusive on this point. The work in this thesis indicates that this could be readily achieved by powder neutron diffraction. Indeed it might also be possible, considering the success of the multipattern program, to follow the structures evolving during cation exchange or during the loss of water from the crystals.

Na_2UCl_6 has been shown to be isostructural with the good ionic conductor Na_2UBr_6 in which half the octahedral sites in a close packed array of halide ions are filled with uranium or sodium ions in an ordered manner. The halide lattice contracts sharply around the highly polarizing uranium ion, to form distinctly molecular species which perform strong librational motion. Replacement of sodium ions by the smaller more polarising lithium ions leads to a reduction in the charge transfer from chloride to uranium, and a reduction in the libration and molecular nature of the $[UCl_6]$ octahedra. Lithium and uranium ions disorder over twice as many octahedral sites in an essentially ionic structure. Unambiguous assignment of the space group was not possible for this compound, although the extent of the disorder was clear. For K_2UCl_6 we could deduce very little about the

structures except that it was based on that of the antifluorite K_2PtCl_6, but with the $[UCl_6]$ octahedra tilted away from the crystal axes. This has been observed for other closely related compounds, and rationalised for K_2ReCl_6 and K_2SnCl_6 in terms of the rigid body libration of the $[MCl_6]$ octahedra, although none of the other models appeared to fit our data. Further powder work with Na_2UCl_6 and Li_2UCl_6, would be worthwhile to probe the high temperature phases of these compounds which, by analogy with Na_2UBr_6, might likewise become good ionic conductors. A single crystal study of Li_2UCl_6 at room temperature would be useful to describe more completely the nature of this disordered phase, although the method of producing a suitable single crystal is not obvious. Further work on K_2UCl_6 using neutrons of longer wavelength was discussed in Chapter 5.

Except in the case of K_2UCl_6, where in any case the very high absorption of this compound would preclude the use of X-rays, powder neutron diffraction coupled with profile analysis has proved a most valuable tool for investigation of the structures of some interesting compounds. In each case we have located light atoms, H, Li, or Na, in the presence of uranium, and have been able to give a clear chemical description of the structure, even when the structure is disordered as for Li_2UCl_6 or DUAs at room temperature. For the latter compound, this included a possible mechanism for the observed high proton mobility, with sufficient detail to provide models for the interpretation of NMR and quasielastic neutron scattering studies (which are in progress) designed to illuminate more directly the nature of the water motion and hydrogen diffusion. For $LiUO_2AsO_4.4D_2O$,

Na_2UCl_6 and DUAs at 4K, the structure has been solved completely without prior knowledge of the actual space group, although this would not have been possible without some knowledge of the symmetries of chemically related compounds. In the checking and comparison between various structural models proposed for a compound, the need for good responsive fast and efficient computing facilities cannot be over-emphasized. Much of the structural work described in this thesis would not have been possible without them. In particular, the large number of models tried for Li_2UCl_6, and the complexity of DUAs at 4K, both required considerable amounts of computer time. For DUAs at 4K, the redimensioned version of the Rietveld program, necessary to cope with the large number of reflections and parameters, used just over 100 K of core and required about 1 hour of CPU time for a three cycle refinement on the new DEC-10 computer at the Institut Laue-Langevin. This is probably the most complex structural determination attempted from powder diffraction data.

For such work, the quality of the data is as important as the facilities to fully analyse it, and the need for a high flux high resolution diffractometer such as D1A, to define with good statistics the extremely complicated profile, is obvious. Good data is also required to distinguish between subtly different structural models, eg between Na_2UCl_6 and Li_2UCl_6 which have very similar looking patterns, or between the various models proposed for DUAs at 4K. On an instrument of poorer quality, the manifestations of such differences are more likely to disappear into the statistical noise. In this respect, great care must be exercised in applying the notion that a structure is deemed

satisfactory if $R_{wp} < 2_{RE}$. As was seen for Li_2UCl_6, several different models may fit the data to within this limit. We should also be aware that in profile refinement problems the calculated errors on the various parameters may be somewhat underestimated, particularly if the pattern is very complex. In the examples studied in this thesis, this has at no time appeared a very serious problem and has not detracted from the essential chemical understanding of the structures. The modified Rietveld program which allows simultaneous refinement of more than one pattern contributing to a profile appears to be highly successful. Not only does it take very good account of the contaminating phases, the structural model obtained for ice is rather encouraging considering the most unfavourable situation of the data defining these parameters. The possibility of using the program for the examination of the structure of phase separate materials (as distinct from those containing an impurity) should be considered.

Finally, the measurements of the proton NMR spin-lattice relaxation time T_1 as a function of temperature for the ammonia intercalation compounds of non-stoichiometric TiS_2 showed that, within experimental error, there is no variation in the motion of the ammonia molecules with the titanium content of the host. This is probably because ammonia is a neutral polar molecule, which is much bigger than the excess Ti^{4+} ions with which it must co-exist in the van der Waals gap. Shielding, and the breaking of the interlayer bonding provided by the extra titanium ions, reduce the effect to a minimum.

BIBLIOGRAPHY

Aboagye, J.K. and Friauf, R.J. (1975), Phys. Rev. B, 11, 1654.

Abragam, A. (1961), "Principles of Nuclear Magnetism", p 461. Oxford: University Press.

Acton, F.S. (1970), "Numerical Methods that Work", p 254. New York: Harper International.

Babel, D. (1967), in "Structure and Bonding", (Eds C.K. Jørgensen et al), 3, p 1-87. Berlin: Springer-Verlag.

Bacon, G.E. (1975), "Neutron Diffraction", (3rd Edition), Oxford: Clarenden Press.

Bacon, G.E., Lisher, E.J. and Pawley, G.S. (1979), Acta Cryst. B35, 1400.

Balchin, A.A. (1976), in "Crystallography and Crystal Chemistry of Materials with Layered Structures", (Ed F. Levy), p 1. Dortrect: Reidel.

Barsis, E. and Taylor, A. (1966), J. Chem. Phys. 45, 1154.
(1968a), J. Chem. Phys. 48, 4357.
(1968b), J. Chem. Phys. 48, 4362.

Batra, A.P. and Slifkin, L.M. (1975), Phys. Rev. B, 12, 3473.

Beale, A.R. and Liang, W.Y. (1973), Philos. Mag. 27, 1397.
J. Phys. C, 6, L482.

Beintema, J. (1938), Recl. Trav. Chim. Pays-Bas Belg. 57, 155.

Bendall, P.J. (1980), D. Phil. Thesis, Oxford University.

Bendall, P.J. and Thomas, M.W. (1980), Harwell Report.

de Benyacar, M.A.R. and de Dussel, H.L. (1975), Ferroelectrics, 9, 241.
(1978), Ferroelectrics, 17, 469.

Bernard, L., Fitch, A.N., Wright, A.F., Howe, A.T. and Fender, B.E.F. (1981), Chem. Commun. p 784.

Bernard, L., Fitch, A.N., Wright, A.F., Fender, B.E.F. and Howe, A.T. (1981), Solid State Ionics, 5, 459.

Bloch, F. (1946), Phys. Rev. 70, 460.

Bloch, F., Hansen, W.W. and Packard, M. (1946), Phys. Rev. 70, 476.

Bloembergen, N., Purcell, E.M. and Pound, R.V. (1948), Phys. Rev. 73, 679.

Bode, H. and Wendt, W. (1952), Z. anorg. allgem. Chem. 269, 165.

Bogacz, A., Bros, J., Gaune-Escard, M., Hewat, A.W. and Taylor, J.C. (1980), J. Phys. C, 13, 5273.

Bogacz, A. and Trzebiatowski, W. (1964), Ann. Soc. Chim. Polonorum, 38, 729.

Boyce, J.B. and Hayes, T.M. (1979), in "Physics of Superionic Conductors", (Ed M.B. Salamon), Topics in Current Physics, 15, p 5. Berlin: Springer-Verlag

Boyce, J.B. and Huberman, B.A. (1977), Sol. State Comm. 21, 31.

Boysen, H. and Hewat, A.W. (1978), Acta Cryst. B34, 1412.

Boysen, H., Ihringer, J., Prandl, W. and Yelon, W. (1976), Sol. State Comm. 20, 1019.

Bray, P.J. and Sauer, G. (1972), Sol. State Comm. 11, 1239.

Brill, R. and Tippe, A. (1967), Acta Cryst. 23, 343.

Brinkmann, D. and Freudenreich, W. (1978), Sol. State Comm. 25, 625.

Brown, I.D. (1964), Can. J. Chem. 42, 2758.

Brown, I.D. and Lim, M.M. (1967), Can. J. Chem. 45, 678.

Brown, P.J., Forsyth, J.B. and Hewat, A.W. (1981), Submitted to Phase Transitions

Burley, G. (1963), J. Chem. Phys. 38, 2807.

Busey, R.H., Dearman, H.H. and Bevan, R.B. (1962), J. Phys. Chem. 66, 82.

Busing, W.R. and Levy, H.A. (1964), Acta Cryst. 17, 142.

Butt, N.M., Cheetham, A.K. and Willis, B.T.M. (1973), Acta Cryst. A29, 727.

Carr, H.Y. and Purcell, E.M. (1954), Phys. Rev. 94, 630.

Cava, R.J., Reidinger, F. and Wuensch, B.J. (1977), Sol. State Comm. 24, 411.

Chamberlain, J.S., Moore, F.H. and Fletcher, N.H. (1973), in "Physics and Chemistry of Ice", (Eds E. Whalley, S.J. Jones and L.W. Gold), p 283. Ottawa: Royal Society of Canada.

Cheetham, A.K., Fender, B.E.F., Steele, D., Taylor, R.J. and Willis, B.T.M. (1970), Sol. State Comm. 8, 171.

Cheetham, A.K. and Taylor, J.C. (1977), J. Solid State Chem. 21, 253.

Chianelli, R.R., Scanlon, J.C. and Thompson, A.H. (1975), Mat. Res. Bull. 10, 1379.

Chianelli, R.R., Scanlon, J.C., Whittingham, M.S. and Gamble, F.R. (1975), Inorg. Chem. 14, 1691.

Childs, P.E., Halstead, T.K., Howe, A.T. and Shilton, M.G. (1978), Mat. Res. Bull. 13, 609.

Clark, W.B. and Williams, P.M. (1977), Philos. Mag. 35, 883.

Cox, B. (1954), J. Chem. Soc. p 3251.

Cruickshank, D.W.J. (1959), in "International Tables for Crystallography", vol II, p 92. Birmingham: Kynoch Press.

Cruickshank, D.W.J. (1970), in "Crystallographic Computing", (Ed F.R. Ahmed), p 188. Copenhagen: Munksgaard.

Dickens, M.H., Hayes, W., Smith, C. and Hutchings, M.T. (1979a), in "Fast Ion Transport in Solids: Electrodes and Electrolytes", (Eds P. Vashishta, J.N. Mundy and G.K. Shenoy), p 225. New York: North Holland.

Dickens, M.H., Hayes, W., Hutchings, M.T. and Smith, C. (1979b), J. Phys. C, 12, L97.

Dines, M.B. (1975a), Science, 188, 1210.
(1975b), Mat. Res. Bull. 10, 287.

Farrar, T.C. and Becker, E.D. (1971), "Pulse and Fourier Transform NMR", New York: Academic Press.

Fouque, Y., Gaune-Escard, M., Szczepaniak, W. and Bogacz, A. (1978), J. Chemie Phys. 75, 360.

Friauf, R.J. (1977), Journal de Physique, 38, 1077.

Gamble, F.R., Di Salvo, F.J., Klemm, R.A. and Geballe, T.H. (1970), Science, 168, 568

Gamble, F.R. and Geballe, T.H. (1976), "Treatise on Solid State Chemistry", (Ed N.B. Hannay), 3, p 89. New York: Plenum.

Gamble, F.R., Osiecki, J.H. and Di Salvo, F.J. (1971), J. Chem. Phys. 55, 3525.

Gamble, F.R. and Silbernagel, B.G. (1975), J. Chem. Phys. 63, 2544.

Gamble, F.R. and Thompson, A.H. (1978), Sol. State Comm. 27, 379.

Hahn, H. and Ness, P. (1957), Naturwiss. 44, 534.
(1959), Z. anorg. allgem. Chem. 302, 37.

Hamilton, W.C. (1964), "Stastistics in Physical Science", New York: Ronald Press.
(1965), Acta Cryst. 18, 502.

Hartman, S.R. and Hahn, E.L. (1962), Phys. Rev. 128, 2042.

Hartwig, P., Weppner, W. and Wichelhaus, W. (1979), Mat. Res. Bull. 14, 493.

Hauser, J.J., Robbins, M. and Di Salvo, F.J. (1973), Phys. Rev. B, 8, 1038.

Hebecker, Ch. and Hoppe, R. (1966), Naturwiss, 53, 106.

Hebecker, Ch., von Schnering, H.G. and Hoppe, R. (1966), Naturwiss, 154, 53.

Hewat, A.W. (1973), Harwell Report, AERE-R7350.
(1975), Nucl. Inst. Meth. 127, 361.
(1978), "Powder Retrieval and Refinement System", ILL Report.
(1979), Acta Cryst. A35, 248.

Hewat, A.W. and Bailey, I. (1976), Nucl. Inst. Meth. 137, 463.

Hewat, A.W., Taylor, J.C., Gaune-Escard, M., Bros, J. and Bogacz, A. (1980), to be published.

Hoard, J.L. and Vincent, W.B. (1939), J. Am. Chem. Soc. 61, 2849.

Hoppe, R. and Dähne, W. (1960), Naturwiss. 47, 397.

Hoppe, R., Liebe, W. and Dähne, W. (1961), Z. anorg. allgem. Chem. 307, 276.

Howe, A.T. and Shilton, M.G. (1979), J. Solid State Chem. 28, 345.
(1980a), J. Solid State Chem. 31, 393.
(1980b), J. Solid State Chem. 34, 149.

Ihringer, J. (1977), Dissertation, University of Munich.
(1980), Acta Cryst. A36, 89.

Immirzi, A. (1980), Acta Cryst. B36, 2378.

Jacobs, P.W.M., Corish, J., Devlin, B.A. and Catlow, C.R.A. (1979), in "Fast Ion Transport in Solids: Electrodes and Electrolytes", (Eds P. Vashishta, J.N. Mundy and G.K. Shenoy), p 589. New York: North Holland.

Jellinek, F. (1962), J. Less-Common Met. 4, 9.

Johnson, C.M., Shilton, M.G. and Howe, A.T. (1981), J. Solid State Chem. 37, 37.

Känzig, W. (1957), in "Solid State Physics", (Eds F. Seitz and D. Turnbull), 4, p 124. New York: Academic Press.

Kennedy, C.D. and Peacock, R.D. (1963), J. Chem. Soc. p 3392.

Ketelaar and van Oosterhout (1943), Rec. Trav. Chim. Pays-Bas, 62, 197.

Kleinberg, R.L. and Silbernagel, B.G. (1980), Sol. State Comm. 33, 867.

Klipstein, P.C., Bagnall, A.G., Liang, W.Y., Marseglia, E.A. and Friend, R.H. (1981), J. Phys. C, 14, 4067.

Koerts, K. (1963), Acta Cryst. 16, 432.

Koshkin, V.M., Milner, A.P., Kukol, V.V., Zabrodskii, Yu.R., Dmitriev, Yu.N. and Brintsev, F.I. (1976), Sov. Phys. Sol. St. 18, 354.

Kuhs, W.F. and Lehmann, M.S. (1981), Nature, 294, 432.

Landau, L.D. (1937), Physik Z. Sowjetunion, 11, 545.

Landau, L.D. and Lifshitz, E. (1958), "Statistical Physics", Cambridge Mass: Addison-Wesley.

Lerbscher, J.A. and Trotter, J. (1976), Acta. Cryst. B32, 2671.

Lieth, R.M.A. and Terhell, C.J.M. (1977), in "Preparation and Crystal Growth of Materials with Layered Structures", (Ed R.M.A. Lieth), p 141. Dortrect: Reidel.

Lindner, A. and O'Keefe, M. (1975), J. Solid State Chem. 15, 171.

Lomer, W.M. and Low, G.G. (1965), in "Thermal Neutron Scattering", (Ed P.A. Egelstaff), London: Academic Press.

Lundgren, J.O. and Olovsson, I. (1967), Acta Cryst. 23, 966.

Lynn, J.W., Patterson, H.H., Shirane, G. and Wheeler, R.G. (1978), Sol. State Comm. 27, 859.

Marshall, W. and Lovesey, S.W. (1971), "Theory of Thermal Neutron Scattering", Oxford: University Press.

Meiboom, S. and Gill, D. (1958), Rev. Sci. Instrum. 29, 688.

Moret, R. and Huber, M. (1976), Acta Cryst. B32, 1302.

Morosin, B. (1978a), Acta Cryst. B34, 3732.
(1978b), Phys. Letts. A65, 53.

Morss, L.R. and Fuger, J. (1969), Inorg. Chem. 8, 1433.

Nagelberg, A.S. and Worrel, W.L. (1979), J. Solid State Chem. 29, 345.

Novotney, V., Martin, C.A., Armstrong, R.L. and Meincke, P.P.M. (1977), Phys. Rev. B , 15, 382.

Nuffield, E.W. and Milne, I.H. (1953), Am. Mineral. 38, 476.

O'Keefe, M. (1976), Sol. State Comm. 18, 47.

O'Leary, G.P. and Wheeler, R.G. (1970), Phys. Rev. B, 1, 4409.

Olovson, I. (1960), Acta Chem. Scand. 14, 1453 and 1466.

Parry, G.S., Scruby, C.B. and Williams, P.M. (1974), Philos. Mag. 29, 601.

Pawley, G.S. (1972),in "Advances in Structural Refinement by Diffraction Methods", (Eds W. Hoppe and R. Mason), 4, p 1. Oxford: Pergamon Press.

Pawley, G.S. (1980), J. Appl. Cryst. 13, 630.

Pawley, G.S., Mackenzie, G.A. and Dietrich, O.W. (1977), Acta Cryst. A33, 142.

Penneman, R.A., Ryan, R.R. and Rosenzweig, A. (1973), in "Structure and Bonding", (Eds J.D. Dunitz et al), 13, p 1. Berlin: Springer-Verlag.

Peterse, W.J.A.M. and Palm, J.H. (1966), Acta Cryst. 20, 147.

Peterson, S.W. and Levy, H.E. (1957), Acta Cryst. 10,70.

Pies, W. and Weiss, A. (1977). Landolt-Börnstein Numerical Data and Functional Relationships in Science and Technology: New Series, (Ed K.H. Hellwege), Vol 7, "Crystal Structure Data of Inorganic Compounds", Part a, and references therein. Berlin: Springer-Verlag.

Portier, J., Menil, F. and Grannec, J. (1969), Compt. Rendu. Acad. Sci. 269C, 327

Portier, J., Menil, F. and Hagenmuller, P. (1970), Bull. Soc. Chim. Fr. p 3486.

Portier, J., Tressaud, A., Menil, F., Claverie, R., de Pape, R. and Hagenmuller, P. (1969), J. Solid State Chem. 1, 100.

Prince, E. (1981), J. Appl. Cryst. 14, 157.

Prober, D.E., Beasley, M.R. and Schwall, R.E. (1977), Phys. Rev. B, 15, 5245.

Rao, B.M.L. and Halbert, T.R. (1981), Mat. Res. Bull. 16, 919.

Riekel, C., Heidemann, A., Fender, B.E.F. and Stirling, G. (1979), J. Chem. Phys. 71, 530.

Riekel, C. and Hohlwein, D. (1976), Chem. Commun. p 863.

Riekel, C. and Schöllhorn, R. (1975), Mat. Res. Bull. 10, 629.

Rietveld, H.M. (1967), Acta Cryst. 22, 151.
(1969), J. Appl. Cryst. 2, 65.

Rollet, J.S. (1965), "Computing Methods in Crystallography", Oxford: Pergamon Press.

Rollet, J.S. (1970), in "Crystallographic Computing", (Ed F.R. Ahmed), p 168. Copenhagen: Munksgaard.

Ross, M. and Evans, H.T. (1964), Am. Mineral. 49, 1578.

Ross, M., Evans, H.T. and Appleman, D.E. (1964), Am. Mineral. 49, 1603.

Rössler, K. and Winter, J. (1977), Chem. Phys. Lett. 46, 566.

Rouxel, J., Trichet, L., Chevalier, P., Colombet, P. and Abou Ghaloun, O. (1979), J. Solid State Chem. 29, 311.

Rouxel, J., Danot, M. and Bichon, J. (1971), Bull. Soc. Chim. Fr. P 3930.

Ruthardt, R., Schöllhorn, R. and Weiss, A. (1972), Z. Naturfor. 27b, 1275.

Sabine, T.M. and Clarke, P.J. (1977), J. Appl. Cryst. 10, 277.

Sakata, M. and Cooper, M.J. (1979), J. Appl. Cryst. 12, 554.

Schäfer, H. (1964), "Chemical Transport Reactions", New York: Academic Press.

Schöllhorn, R. and Zagefka, H.D. (1977), Angew. Chem. Int. Ed. Engl. 16, 199.

Schöllhorn, R., Zagefka, H.D., Butz, T. and Lerf, A. (1979), Mat. Res. Bull. 14, 369.

Shannon, R.D. and Prewitt, C.T. (1969), Acta Cryst. B25, 925.

Shilton, M.G. and Howe, A.T. (1977), Mat. Res. Bull. 12, 701.
(1979), Chem Commun. p 194.
(1980), J. Solid State Chem. 34, 137.

Schomaker, V. and Trueblood, K.N. (1968), Acta Cryst. B24, 63.

Siegel, S. (1952), Acta Cryst. 5, 683.
(1956), Acta Cryst. 9, 827.

Silbernagel, B.G. (1977), Sol. State Comm. 17, 361.

Silbernagel, B.G., Dines, M.B., Gamble, F.R., Gebhard, L.A. and Whittingham, M.S. (1976), J. Chem. Phys. 65, 1906.

Silbernagel, B.G. and Gamble, F.R. (1974), Phys. Rev. Lett. B32, 1436.
(1976), J. Chem. Phys. 65, 1914.

Silbernagel, B.G. and Whittingham, M.S. (1976a), Mat. Res. Bull. 11, 29.
(1976b), J. Chem. Phys. 64, 3670.

Squires, G.L. (1978), "Introduction to the Theory of Thermal Neutron Scattering", Cambridge: University Press.

Steichele, E. and Arnold, P. (1973), Phys. Lett. A44, 165.

Takeuchi, S. and Katsuda, H. (1970), J. Japan Inst. Met. 34, 758.

Taylor, J.C. and Wilson, P.W. (1974a), Acta Cryst. B30, 1216.
(1974b), Acta Cryst. B30, 1481.

Thomas, M.W. and Bendall, P.J. (1978), Acta Cryst. A34, S351.

Thomas, J.O, and Liminga, R. (1978), Acta Cryst. B34, 3686.

Thompson, A.H. (1975), Phys. Rev. Lett. 35, 1786.
(1978), Phys. Rev. Lett. 40, 1511.

Thompson, A.H., Gamble, F.R. and Koehler, R.F. (1972), Phys. Rev. B, 5, 2811.

Thompson, A.H., Gamble, F.R. and Symon, C.R. (1975), Mat. Res. Bull. 10, 915.

Tofield, B.C. and Wright, C.J. (1977), Sol. State Comm. 22, 715.

Torrey, H.C. (1953), Phys. Rev. 92, 962.

Tronc, E. and Huber, M. (1973), J. Phys. Chem. Sol. 34, 2045.

Van Driel, H.M., Armstrong, R.L. and McEnnan, M.M. (1975), Phys. Rev. B, 12, 488.

Verble, J.L. and Wietling, T.J. (1972), Sol. State Comm. 11, 941.

van Vleck, J.H. (1948), Phys. Rev. 74, 1168.

Von Dreele, R.B. and Cheetham, A.K. (1974), Proc. Roy. Soc. London, A338, 311.

Wagner, J.B. and Wagner, C. (1957), J. Chem. Phys. 26, 1597.

Waltersson, K., Werner, P.E. and Wilhelm, K.A. (1977), Cryst. Struct. Comm. 6, 231.

Waser, J. (1963), Acta Cryst. 16, 1091.

Weigel, F. and Hoffmann, G. (1976), J. Less-Common Met. 44, 99.

Wells, A.F. (1975),"Structural Inorganic Chemistry", (4th Edition), Oxford: Clarenden Press.

Whittingham, M.S. (1976), J. Electrochem. Soc. 123, 315.
(1978a), Progr. Solid State Chem. 12, 41.
(1978b), Mat. Res. Bull. 13, 775.
(1979), J. Solid State Chem. 29, 303.

Whittingham, M.S. and Gamble, F.R. (1975), Mat. Res. Bull. 10, 363.

Whittingham, M.S. and Panella, J.A. (1981), Mat. Res. Bull. 16, 37.

Willemsen, H.W., Armstrong, R.L. and Meincke, P.P.M. (1979), in "Fast Ion Transport in Solids: Electrodes and Electrolytes", (Eds P. Vashishta, J.N. Mundy and G.K. Shenoy), p 413. New York: North Holland.

Williams, R.J., Dillin, D.R. and Milligan, W.O. (1973), Acta Cryst. B29, 1369.

Willis, B.T.M. and Pryor, A.W. (1975), "Thermal Vibrations in Crystallography", Cambridge: University Press.

Wilson, J.A. (1978), Phys. Stat. Sol. B, 86, 11.

Windsor, C.G. (1973), in "Chemical Applications of Thermal Neutron Scattering", (Ed B.T.M. Willis), Oxford: University Press.

Winn, D.A., Shemilt, J.M. and Steele, B.C.H. (1976), Mat. Res. Bull. 11, 559.

Winn, D.A. and Steele, B.C.H. (1976), Mat. Res. Bull. 11, 551.

Wyckoff, R.W.G. (1963), "Crystal Structures", Vol 1, (2nd Edition), New York: Wiley.

Wyckoff, R.W.G. (1965), "Crystal Structures", Vol 3, (2nd Edition), New York: Wiley.

Young, R.A., Mackie, P.E. and Von Dreele, R.B. (1977), J. Appl. Cryst. 10, 262.

Zachariasen, W.H. (1948), Acta Cryst. 1, 285.

Zalkin, A., Forrester, J.D. and Templeton, D.H. (1964), Acta Cryst. 17, 1408.

Zheludev, I.S. (1971), in "Solid State Physics", (Eds H. Ehenreich, F. Seitz and D. Turnbull),26, p 454. New York: Academic Press.

ABSTRACT

THE STRUCTURE AND DYNAMICS OF COMPOUNDS RELATED TO FAST IONIC CONDUCTORS

A thesis submitted for the degree of Doctor of Philosophy in the University of Oxford by

A. N. FITCH

St. Catherine's College, Hilary, 1982

Powder neutron diffraction studies have been performed on the deuterated form of the proton conductor $HUO_2AsO_4.4H_2O$ both above and below the transition at 301K to a poorly conducting antiferroelectric phase. The observed structures have been rationalised in terms of the presence of two types of water dimer, H_4O_2 and $[H_5O_2]^+$, whose dynamic interchange above the transition, in a scheme of hydrogen disorder, provides a simple mechanism for the high hydrogen mobility. Further diffraction studies on cation substituted $LiUO_2AsO_4.4D_2O$ show a change to a structure which is completely ordered with adjacent water squares linked together via tetrahedral co-ordination about the lithium ion. Comparison of this structure with that of some similar cation substituted compounds allows the proposal of a mechanism for sodium mobility in $NaUO_2PO_4.3H_2O$.

The series of compounds Li_2UCl_6, Na_2UCl_6 and K_2UCl_6 have been investigated at room temperature by powder neutron diffraction, with the aim of assessing the importance of the light cation in the structures of such compounds. The decrease in polarising power of the cation through the series leads to structures in which the $[UCl_6]^{2-}$ octahedron exhibits progressively greater molecular character as the charge transfer from chloride to uranium increases.

Measurements of the proton NMR spin-lattice relaxation time T_1 as a function of temperature have been performed on the ammonia intercalation compounds $TiS_2(NH_3)$ for three different stoichiometries of TiS_2, ranging from 0.1-2.0% excess titanium. There appears to be no influence of excess titanium on the mobility of the ammonia molecules in contrast to $LiTiS_2$ and $NaTiS_2$, where ther is a very marked decrease with increasing titanium content.